Laser-Assisted Deposition of Thin Films from Gas-Phase and Surface-Adsorbed Molecules

IRVING P. HERMAN

Department of Applied Physics, Columbia University, New York, New York 10027

Received January 6, 1989 (Revised Manuscript Received June 6, 1989)

Contents

I.	Scope	1323
II.	Basic Mechanisms and Features	1324
III.	Deposited Materials	1327
	A. Metals	1327
	B. Semiconductors	1336
	C. Compound Insulators	1343
IV.	Growth Models	1345
	A. Pyrolytic Deposition	1346
	B. Photolytic Deposition	1348
	C. Nucleation and Other Surface Effects	1349
V.	Spatial Localization of Deposits	1350
VI.	Optical Spectroscopy	1351
	A. Reactant Absorption	1351
	B. Optical Diagnostics of Deposition	1351
VII.	Applications	1351
VIII.	Conclusions	1352

I. Scope

Laser chemical modification of surfaces entails a wide range of processes that can be subdivided into photoassisted deposition, chemical etching, ablative etching, doping, and thin–film transformations such as oxidation. In these processes the laser may be used as a localized heat source, a source of photons for dissociation, or in some cases as both. The species reacting with the solid surface may be a gas, liquid, or predeposited thin film. Much of the burgeoning research in this field is closely tied to the potential processing applications in microelectronics, optoelectronics, and materials production, because in some instances laser techniques may offer processing advantages that may not be available with conventional fabrication methods, such as low-temperature fabrication, localization of interaction, discretionary material modification, process compatibility, repair capabilities, fast turnaround for prototype development, and semicustomization. This article reviews one subset of laser chemical processing, laser-assisted deposition from gas-phase and adsorbed molecules. Emphasis is placed on the important chemical and physical interactions in the many examples of laser-assisted deposition that have potential significance in microelectronics processing. The reader is referred to other recent reviews covering other aspects of laser-assisted processing that are not considered here, such as laser etching and doping and deposition by laser-assisted evaporation or ablation of targets.[1-18]

Research on the deposition of thin films with lasers has been aided by fundamental studies in reaction kinetics, spectroscopy, and reagent synthesis and also, notably, by applied research in other areas of thin-film deposition. In some cases, these related studies have been, in fact, directly motivated by the potential applications of laser deposition. Laser spectroscopy of solids, gases, and surface-adsorbed species is needed to characterize the fundamental initiation steps in laser deposition and can also help serve as an in situ optical diagnostic probe of the deposition process. An understanding of the modes of excitation and energy relaxation during laser heating of solids and gases is clearly necessary to explain how lasers promote deposition. The fundamental chemistry in homogeneous and heterogeneous pyrolytic decomposition of precursor molecules is very important in both laser and non-laser methods of film deposition. Photolytic decomposition reactions can also be important in laser deposition, as they are in UV lamp assisted deposition of thin films. Furthermore, mass transfer in the gas phase and surface events, such as adatom migration, desorption, and nucleation, can be significant in the overall kinetics of laser-assisted deposition as well as in conventional

Irving P. Herman was born in Brooklyn, NY, in 1951. He received the S.B. and Ph.D. degrees in physics at the Massachusetts Institute of Technology in 1972 and 1977, respectively. While doing his doctoral research involving laser chemistry and spectroscopy, he was a Fannie and John Hertz Foundation fellow. During his stay at M.I.T., he was also involved with the early efforts on optically pumped infrared lasers and Dicke superradiance. In 1977 he joined the Lawrence Livermore National Laboratory, where he later became a section leader, and worked on laser isotope separation of deuterium and tritium, laser microchemical processing of surfaces and its applications in microelectronics, and Raman microprobe analysis. In 1986 he joined Columbia University as an Associate Professor of Applied Physics. His current research interests include optical diagnostics of thin-film processing, laser processing of microelectronics materials, laser spectroscopy of semiconductor microstructures, modeling the interaction of lasers with materials, and the physics of semiconductors under high pressure. He is also affiliated with the Columbia Radiation Laboratory and the Microelectronics Sciences Laboratories.

0009-2665/89/0789-1323$06.50/0 © 1989 American Chemical Society

physical and chemical vapor deposition. When particularly relevant to progress in laser-assisted deposition, this related research is also cited in this review, as is the extremely relevant work on conventional thermal chemical vapor deposition and UV lamp assisted deposition.

The basic features of laser-assisted deposition are described in section II. This includes a general discussion of how lasers can influence deposition chemistry and the different ways that lasers can be geometrically coupled to the reactor in the deposition process. After a brief discussion of the requirements of the precursor molecules used in laser-assisted deposition, section III covers the demonstrated examples of laser-assisted deposition. For convenience, this section is divided into the deposition of metal, semiconductor, and insulator thin films. The subsection on metal deposition is subdivided according to the type of precursor reagent used for laser-assisted deposition, with an additional section on metal silicides, while the latter two subsections are subdivided according to material type. The twin goals of this section are to provide a fairly comprehensive listing of the demonstrated methods of laser deposition and to discuss the current, and often quite limited, understanding of the chemistry involved in laser-assisted deposition. As will be seen, much of the process physics and chemistry transcend this specific classification by type of material and precursor. Section IV discusses linking the chemical mechanism of deposition with the other elements of this process, to model laser-assisted growth of thin films. Nucleation is also discussed in this section. Spatial localization in laser-assisted deposition is described in section V. The use of optical spectroscopy to evaluate potential reagent molecules is examined in section VI, along with the utilization of optical diagnostics to probe the thin-film and gas-phase chemistry in situ during deposition. Applications of laser-assisted deposition are discussed briefly in section VII.

The emphasis of this review is on the chemical and physical processes involved in laser deposition. The physical and electronic properties of the deposited films, such as crystallinity, epitaxy, morphology, and electrical conductivity, and other processing features of laser deposition, such as the quest for fast growth rates and minimum feature sizes, are not reviewed in great detail though they are discussed in some contexts. The other reviews and the original papers cited here delve into these other matters in some detail. An attempt has been made to provide a comprehensive review of the current literature.

II. Basic Mechanisms and Features

Though the overall reaction mechanisms in laser deposition are in general complex, the basic types of laser interactions and reactions are readily classified. The laser can be used to heat the substrate and induce thermal reactions on the surface where deposition occurs. Such pyrolytic, thermochemical, or laser chemical vapor deposition reactions are analogues of heterogeneous chemical vapor deposition (CVD) of thin films by conduction heating. When metalloorganic compounds are used as reactants, CVD is usually called metalloorganic chemical vapor deposition (MOCVD). In these laser-assisted pyrolytic reactions, the gas-phase and surface-adsorbed reactants are transparent to the laser wavelength and the laser is absorbed by the substrate or by some film overlaying it. Alternately, the laser can be absorbed by the reactant or reactant mixture, which is initially excited into nondissociative states. After energy relaxation, the reactant gas can get hot and then a thin film can form, as in conventional homogeneous chemical vapor deposition; this is also classified as a pyrolytic process. Clearly, in some instances the substrate and the gas can be heated simultaneously by the laser. Furthermore, when the laser directly heats the substrate only, gas near the surface can be heated by diffusion and convection in some cases, and homogeneous pyrolysis can also occur. Both laser-assisted heterogeneous and homogeneous chemical vapor deposition are often called laser CVD.

In a complementary arrangement, the laser is used to dissociate gas-phase or surface-adsorbed molecules to form deposit atoms or intermediates containing these atoms, without heating the surface appreciably or, quite often, at all. The substrate is transparent to the laser and the laser is absorbed directly by the reactant. If this occurs without significant heating of the gas, the method is known as photolytic or photochemical deposition, or photodeposition. Laser excitation could occur by stimulating electronic transitions by the absorption of one ultraviolet photon or, alternately, by the absorption of several visible or ultraviolet photons; in this latter case, absorption may occur either in a concerted manner as in multiphoton absorption or in a sequential manner, which may, in fact, involve photon absorption by intermediate products as well. Unimolecular infrared laser multiple-photon dissociation can also produce deposit atoms or intermediates for photodeposition. In some cases, the photodissociation products must be decomposed further by conventional heating of the substrate in order to obtain pure deposits.

Several other deposition processes do not fit cleanly into these so-defined pyrolytic/photolytic classifications. For instance, a low-intensity laser, to which the reagents are transparent, can be absorbed by the surface and lead to a negligible temperature rise, and yet stimulate a reaction at the surface. This has been shown to occur on semiconductor surfaces because of the creation of electron–hole pairs near the surface. To date, this decidedly nonthermal mechanism has been found to be more important in laser-etching reactions than in laser deposition.[4]

Furthermore, the predominant deposition mechanism can change during the course of deposition. For example, at the start of deposition the laser may photodissociate the reactant and not heat the surface of the initially transparent substrate, as in photolytic deposition. However, if the deposited thin film itself absorbs the laser wavelength, pyrolytic deposition may begin after the initial stage of photodeposition, and the overall rate of deposition can be accelerated much beyond the photodeposition rate.[19,20] This hybrid deposition process combines the non-substrate-specific versatility of photodeposition with the typically faster rates of pyrolytic deposition.

The selection of either a pyrolytic or a photolytic process to deposit a given film on a specific substrate is dictated by many factors, including the properties of the available reactants containing the deposit atoms of

interest, such as their absorption spectrum, volatility, and routes to dissociation; the available lasers; substrate properties, such as absorption spectrum and thermal conductivity; process compatibility with existing features on and within the substrate; and the desired deposition rates, deposit impurity levels, crystallinity, and morphology. For example, surface pyrolytic processes are not dependent on the spectroscopy of the reactant, but on the broad-band absorption features in solids, and can often be promoted by visible lasers, such as argon ion lasers. However, the kinetics of surface-initiated pyrolytic deposition are often very sensitive to the optical and thermal properties of the substrate and of the time-varying deposit. When true, this is a severe liability, which will lead to either self-limited, greatly accelerated, or oscillating rates of deposition, unless there is feedback control of the laser power.

One advantage of pyrolytic deposition is that any reactant used in conventional CVD can be used in laser-assisted pyrolytic deposition; however, many of these precursors are unsuitable for photolytic deposition because of mismatch between available lasers (excimer lasers, frequency-doubled argon ion lasers, etc.) and the dissociative absorption transitions of the reactants. Though the choice of wavelength for photolysis is typically more restrictive (and is usually limited to the ultraviolet), the kinetics of photodeposition are relatively insensitive to changes in surface properties during the course of deposition, in contrast to pyrolysis. In general, the rates of pyrolytic deposition are faster and the resulting pyrolytic deposits are purer than for photodeposition. Both of these factors are very important in applications. However, when high surface temperatures are necessary to induce deposition, the pyrolytic process can lead to more structural damage from these high temperatures and thermally induced stresses[21] than the damage caused by the ultraviolet radiation used in photolytic deposition. This is also a very important concern in microelectronics applications.

To understand laser deposition, the many interlocking component processes in deposition must be addressed individually and then they must be linked. Any of these components may limit the rate of deposition or may lead to inferior material properties of the deposit. The laser interaction with the substrate, gas-phase reactants, adsorbed reactants, intermediate products, deposit atoms, and the deposited film must be well characterized. These interactions may change during the course of deposition. The laser can also transform already deposited films by annealing or recrystallization. Clearly, the chemistry in the gas and on the surface must be followed. It may be much more complex than a simple nascent chemical step may suggest. Thermal decomposition of photolytically produced intermediates can be crucial in "photodeposition", while laser-related nonthermal effects, such as the creation of electron–hole pairs or photoabsorption by intermediates, can be important in "pyrolytic deposition". Surface diffusion, desorption, and nucleation can affect both laser pyrolytic and photolytic deposition. Gas-phase transport of reactants to the surface and products from the surface is frequently the rate-limiting step in laser-assisted deposition. For most of the laser irradiation configurations described herein, the spatial dependence of each of these components of the overall process must be followed. Moreover, much can be learned about laser CVD and photodeposition from published studies of the analogous thermal CVD and UV lamp assisted deposition processes, respectively. Unfortunately, the reaction pathways for most examples of CVD and lamp deposition of interest here are still poorly understood and are in fact under active investigation themselves.

There are several common themes for the entire range of precursors, deposited materials, and laser excitation mechanisms in laser-assisted deposition. For instance, the underlying questions about dynamics and kinetics are very similar. Consider, the deposition of an elemental thin film A from a precursor AX_m, which is representative of metal alkyls, carbonyls, halides, and hydrides. In gas-phase-initiated processing, does the pyrolytic or photolytic decomposition of AX_m remove all the X ligands, producing A, which deposits on the surface? If so, is there aggregation of these atoms to form clusters before deposition? If not, will the partially decomposed precursor AX_{m-i} produce the atom A after impinging on the heated surface? Similarly, in the processing of molecules adsorbed on the surface, is the pyrolytic or photolytic decomposition of these precursors complete? Since in some cases, decomposition of both gas-phase and surface-adsorbed species can occur, are the respective processes coupled and which process deposits material faster, and with superior properties?

When compound AB is deposited from precursors AX_m and BY_n, additional issues arise. Both pyrolytic and photolytic deposition can proceed either by the direct dissociation of both compounds, followed by combination in the gas or on the surface, as

$$AX_m \rightarrow A + mX \quad (1a)$$

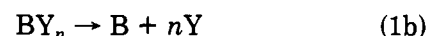

$$BY_n \rightarrow B + nY \quad (1b)$$

$$A + B \rightarrow AB \quad (1c)$$

or by the initial dissociation of only one precursor, followed by cross reactions, such as represented schematically in the net reactions

$$AX_m \rightarrow A + mX \quad (1a')$$

$$X + BY_n \rightarrow B + XY_n \quad (1d)$$

$$A + B \rightarrow AB \quad (1c')$$

The real situation is much more complex than this. For example, in gas-phase deposition some steps occur in the gas, while others can occur on the surface. One important illustration of this is when the final product AB (or A) is not the species reaching the surface, but instead an $A_aB_bX_xY_y$ (or A_aX_x) complex is formed in the gas, migrates to the surface, and decomposes on it. Moreover, in many important cases X and Y are not atoms, but ligands such as CO and CH_3, which can decompose and produce impurities in the deposit during gas-phase or surface deposition. Finally, sometimes the composition of a surface has been found to be as crucial to the progress of a heterogeneous reaction as is the local temperature; this can be very important in both laser and non-laser deposition. Several examples of these representative types of deposition mechanisms will be given in section III.

Three general types of irradiation geometries can be used in laser-assisted deposition, represented by geom-

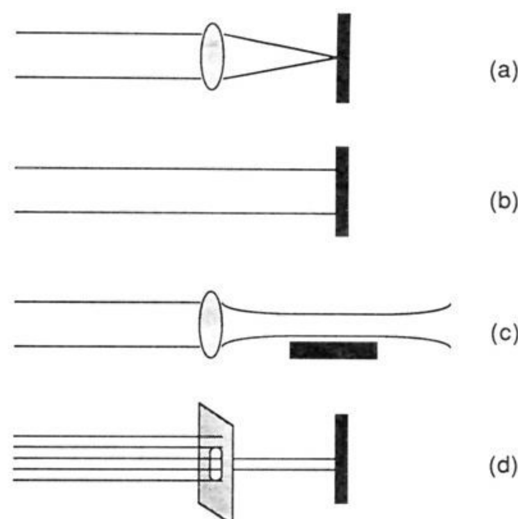

Figure 1. Schematic of laser configurations used in laser-assisted deposition: (a) localized deposition with the laser focused to a spot for direct writing; (b) large-area processing with an unfocused or weakly focused beam impinging the surface; (c) large-area deposition with the laser focused to a line above and parallel to the surface with a cylindrical lens; (d) large-area patterned processing with the laser passing through a mask.

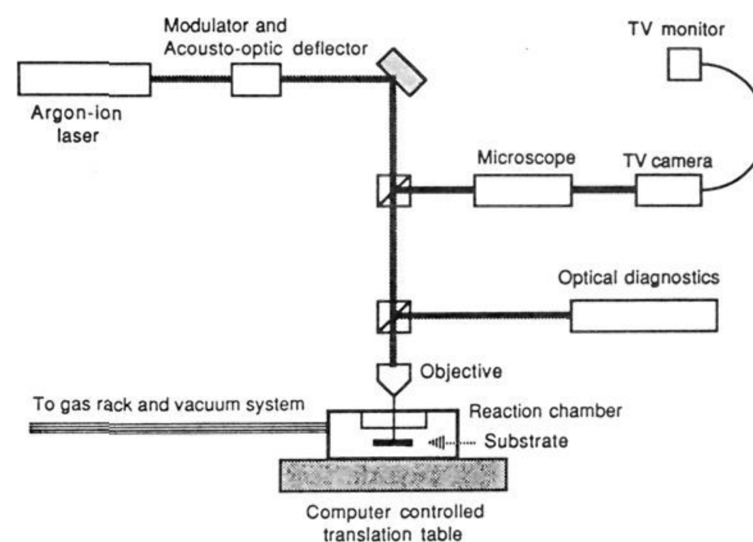

Figure 2. Experimental setup for direct laser writing. The laser can be scanned relative to the surface by scanning the substrate via the translation table or by deflection of the laser beam, possibly by acoustooptic deflection. (Adapted from ref 23–25.)

etries a, b,c, and d of Figure 1. In all three, the laser is responsible for inducing thin-film deposition. Moreover, in the first and third configurations, the laser is also used to produce a spatially patterned deposit. Consequently, when used in the second configuration during integrated circuit fabrication, the laser thin-film deposition process replaces only one step, namely, the analogous conventional thin-film process, whereas when used in the first or third configuration, it replaces the masking (patterning) steps as well.

In one irradiation geometry used in laser deposition, a nearly diffraction-limited laser beam is focused onto a substrate which is bathed within the reactant (Figure 1a). This type of laser processing is often referred to as direct laser writing (or laser direct writing). Deposition occurs by the decomposition of gas-phase molecules near the surface or of molecules adsorbed on the surface. If the laser and the substrate are stationary, a disk-like microstructure is deposited (static conditions), while if either the laser or the substrate is laterally translated, lines are formed (scanning conditions). The minimum deposit dimension depends on the diameter of the laser beam at the focus and several features specific to deposition, such as the dependence of deposition rate on laser intensity or laser-induced temperature rise and the possible diffusion of intermediates containing the product atoms in the gas phase or on the surface. If a beam with a TEM_{00} mode, having the Gaussian intensity profile

$$I(r) = I_0 \exp(-r^2/w^2) \tag{2}$$

where w is the beam radius, is focused by a lens with focal length f, the diameter of the beam at the focus is d:

$$d = 0.64\lambda\left(\frac{f}{2w}\right) \tag{3}$$

where λ is the laser wavelength. Submicron-dimension deposits have been demonstrated using direct laser writing, as would be expected from eq 3.[17,22] Because of the serial nature of this localized laser processing method, direct writing techniques are usually at a competitive disadvantage in most microelectronics applications, because even the relatively fast demonstrated deposition rates (sometimes $\gtrsim$1 mm/s) are usually much too slow. However, direct laser writing is competitive for circuit and mask repair operations, for which slower deposition rates may be acceptable. CW lasers are usually used in direct writing because of their superior beam quality and the high laser duty cycle needed in writing line-type features. When the focal spot is small, the modest laser powers available from CW lasers are sufficient to attain laser intensities high enough to drive a localized reaction. When very high peak intensities are required, pulsed lasers must be used. Figure 2 is a schematic layout of the experimental apparatus typically used in direct writing.[23-25]

Another type of irradiation geometry used in laser deposition involves unfocused or weakly focused beams and, consequently, requires high-intensity pulsed lasers. In one configuration, the beam impinges on the surface at nearly normal incidence (Figure 1b), while in one variation the laser is focused to a line by a cylindrical lens and either the substrate or the beam is translated laterally, perpendicular to the line. In either case, a large, unpatterned film is formed by a laser-initiated homogeneous reaction above the surface or a reaction at the surface, or by a combination of both routes. Alternately, the laser can be focused to a line by a cylindrical lens and travel parallel to and just above the substrate (Figure 1c). In this case, the laser initiates chemistry in the gas only and not on the surface; this eliminates possible laser heating of the substrate surface. Since these configurations represent parallel processing in which the laser interacts with the entire surface at one time, with no spatially selective patterning, these studies have a single goal: to see if films can be formed faster, at lower substrate temperature, and with fewer defects by these laser-assisted techniques than by non-laser methods. Other aims of these studies include the possibility of monolayer control of deposits and compatibility with multistep in situ processing.

The third type of laser irradiation geometry again involves broad-area illumination; however, in this case the illumination passes through a mask before impinging on the surface (Figure 1d). The mask may be on the surface (contact printing) or very near the surface (proximity printing), or it may project patterned light onto the surface in an arrangement using a lens (projection printing). In projection printing, which is

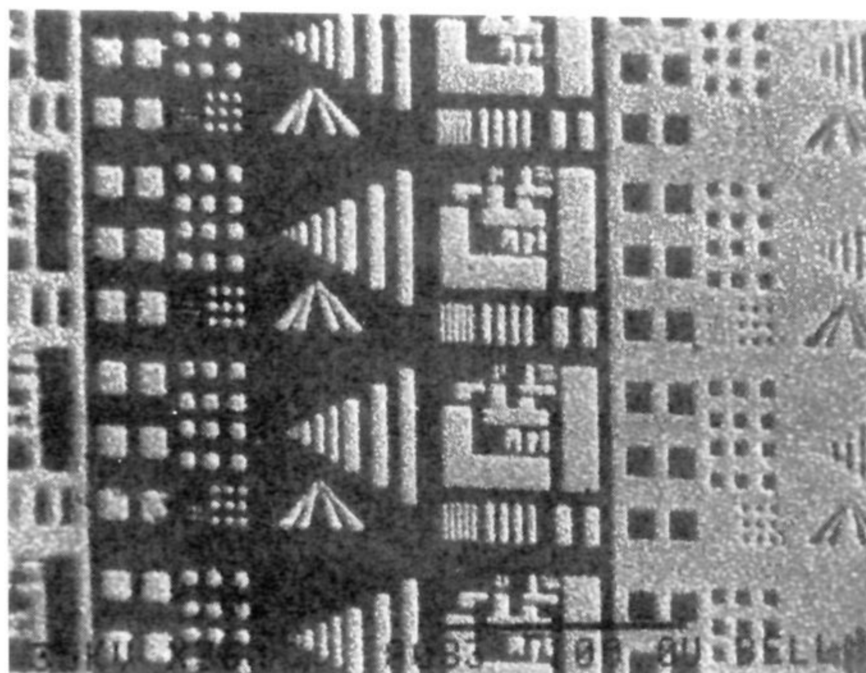

100 μm

Figure 3. Scanning electron micrograph of projection printed pattern of aluminum, made by first nucleating the hydroxylated oxide surface in selected regions by KrF laser (248 nm) photodissociation of TIBA, followed by CVD growth of Al in those nucleated regions using TIBA. (From ref 27.)

usually preferred to contact and proximity arrangements because of superior resolution and freedom from defects, an objective is placed between the mask and the substrate shown in Figure 1d.[26] These techniques retain the effective overall speed of parallel processing, while having the one-step pattern generation capability of direct writing. When gas-phase photochemistry dominates deposition, diffusion in the large volume of gas excited in this mode of deposition hinders spatial selectivity. The spatial features of the mask will be transferred to the deposit only if surface chemistry dominates, as in the photodecomposition of adsorbed molecules. Projection printing was used as the first step in the fabrication of the aluminum patterns seen in Figure 3.[27]

Another way to achieve spatially selective deposition is to combine direct laser writing or projection printing with a large-area deposition process that is not spatially selective but is instead chemically selective. Laser deposition is first used to deposit locally a thin nucleation layer on the substrate. Then a large-area deposition process, such as thermal CVD, is used which selectively deposits material on the nucleated areas but not on the bare substrate. The Al pattern in Figure 3 was produced in this manner. The nucleation layer deposit need not always be composed of the same material as the final thin-film layer. In some cases the localized "nucleation" layer can serve as a localized catalyst.[28]

Most early work on laser-patterned deposition centered on direct laser writing. However, because the effective deposition rates needed in practical microelectronics fabrication can be attained only by large-area patterned projection, most research has shifted to this area. Still, direct laser writing is the method of choice for repairs and circuit restructuring and also in testing and semicustomization of gate arrays when it is too time-consuming or expensive to make new masks. As more and more devices are put on a given chip in future years, circuit repair and restructuring may become ever more necessary to maintain high yields of working chips.

III. Deposited Materials

Gas-phase reactants containing metal and semiconductor deposit atoms usually fall within one of a number of classes: hydrides, halides, alkyls, carbonyls, and the AcAc's. With few exceptions, most metals have suitable precursors in only one or two of these classes. Ideal precursors should either decompose at relatively low temperature or photodecompose at low intensities at available laser wavelengths to form impurity-free films. These reactants and their volatile products should be relatively unreactive, and they should have large enough vapor pressures to permit fast deposition rates. As will be seen below, many of the best precursors used to date still have several disadvantages. Consequently, the search for new suitable precursor gases is very important for laser-assisted deposition, as it is important as well for CVD and UV lamp assisted deposition of thin films. For example, dimethylaluminum hydride[29] and (trimethylamine)aluminum hydride[30] have recently been synthesized for use in CVD and laser CVD of aluminum thin films as alternatives to trimethylaluminum, because they produce purer deposits, and divinylmercury has been synthesized as a source of Hg for the photolytic deposition of HgTe epilayers in place of dimethylmercury, because it has a much larger absorption cross section.[31]

Most research on laser-assisted deposition has concentrated on the materials currently used in the fabrication of integrated circuits, including the metals Al and Cu, the semiconductors Si and GaAs, and the insulators SiO_2 and Si_3N_4. The need for materials in other applications, such as the production of solar cells and infrared detectors, has also motivated some of these studies. For example, much of the work on depositing II–VI semiconductors is driven by the need for good infrared detector material.

A. Metals

Metal Alkyls

The metal alkyls were among the first compounds used in laser deposition[32–34] because many of these molecules photodissociate at 257 nm, thereby permitting photodeposition to be studied in detail using this wavelength from a frequency-doubled 514.5-nm argon ion laser line. This is exemplified by the $Cd(CH_3)_2$ spectrum in Figure 4, which shows significant, though weak, absorption at this wavelength.[35] Many metals have been deposited from these alkyls by either photolytic or pyrolytic direct laser writing, including Cd from $Cd(CH_3)_2$ [DMCd],[32,33,36–40] Zn from $Zn(CH_3)_2$ and $Zn(C_2H_5)_2$ [DMZn and DEZn],[37,41] Al from $Al(CH_3)_3$ [TMAl] (which forms $Al_2(CH_3)_6$ dimers in the gas phase),[32,36,37,42–44] $AlH(CH_3)_2$ [DMAH],[29] $Al(i\text{-}C_4H_9)_3$ (triisobutylaluminum (TIBA)),[45] Pb from $Pb(C_2H_5)_4$,[46] Ga from $Ga(CH_3)_3$,[47,48] In from $In(CH_3)_3$,[49] and Sn from $Sn(CH_3)_4$.[32,50–52] Large-area thin-film photodeposition of aluminum has been studied with a KrF laser at 248 nm and with an ArF laser at 193 nm using TMAl,[53–59] DMAH,[60] and TIBA[26,61,62] reactants; in the last case, a nucleation layer was first formed by photodeposition with the laser projected through a mask, and growth was then continued using CVD (Figure 3). Most of these studies concentrated on the material properties of the deposits. The relatively few investigations de-

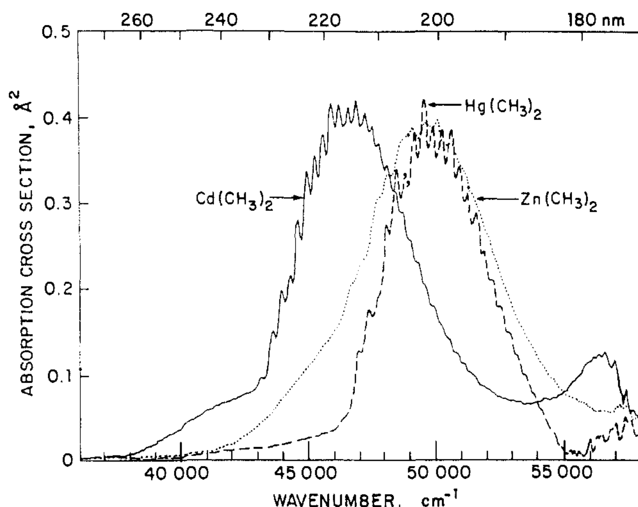

Figure 4. UV absorption spectra of DMCd, DMHg, and DMZn. (Reprinted from ref 35; copyright 1984 American Institute of Physics.)

tailing the chemistry of deposition will be discussed below.

Photodissociation of gas-phase dimethylalkyls is relatively well understood. ΔH°_{298} for DMCd and DMZn to the respective metal atom and two methyl radicals is ~72 and ~88 kcal/mol, respectively,[35,63,64] which is much smaller than the 111 kcal/mol in one 257-nm photon. The bond energies for removing the first and second methyl groups from these molecules are ~59 and ~13 kcal/mol for DMCd and ~66 and ~22 kcal/mol for DMZn, respectively,[64] though this exact partition of bond energies is not certain.[64a,d] This cited DMCd second bond energy is significantly larger than the ~6 kcal/mol value cited and used in ref 35.

Photolytic dissociation of a dimethylmetal molecule to a metal atom and $2CH_3$ appears to occur by the absorption of a single ultraviolet photon by the following route for $M(CH_3)_2$ for M = Cd, Zn, or Hg:[35,65]

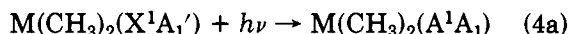

$$M(CH_3)_2(X^1A_1') + h\nu \rightarrow M(CH_3)_2(A^1A_1) \quad (4a)$$

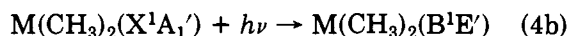

$$M(CH_3)_2(X^1A_1') + h\nu \rightarrow M(CH_3)_2(B^1E') \quad (4b)$$

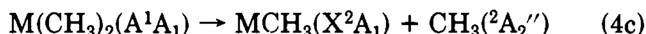

$$M(CH_3)_2(A^1A_1) \rightarrow MCH_3(X^2A_1) + CH_3(^2A_2'') \quad (4c)$$

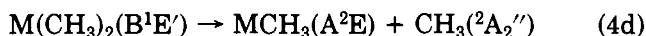

$$M(CH_3)_2(B^1E') \rightarrow MCH_3(A^2E) + CH_3(^2A_2'') \quad (4d)$$

$$MCH_3 \rightarrow M + CH_3 \quad (4e)$$

For $\lambda > 230$ nm, DMCd is excited only to the bent A state (reaction 4a), while for shorter λ, both the A and linear B states (reaction 4b) are excited. In both cases, highly excited $CdCH_3$ is formed (reactions 4c and 4d), which is some cases is electronically excited (reaction 4d) and fluoresces. For either route, with the photolysis wavelengths used in deposition the internal energy of $CdCH_3$ is expected to greatly exceed ΔH°_{298} for monomethylcadmium, ~13 kcal/mol,[64] so reaction 4e occurs; this decomposition to Cd + CH_3 is expected to be particularly fast for the $CdCH_3$ product from reaction 4c. Therefore, both methyl groups are removed in CW or pulsed laser ultraviolet dissociation of dimethylmetals. This dissociation pathway is consistent with the anisotropic UV photodissociation of DMCd,[66] the product translational distribution, fluorescence, and absorption of the products of 193-nm excited DMCd and DMZn,[63] and the high levels of vibrational excitation of the methyl radical symmetric bend and asymmetric C–H stretch in 248-nm photolysis of dimethylmercury.[67] As is not unexpected from reactions 4, metals photodeposited from gas-phase dimethylmetals are relatively pure. For example, Zn photodeposited on GaAs from DMZn has <4% C.[41b]

If the photolyzing laser does not hit the substrate, as in Figure 1c, only gas-phase dissociation of dimethylmetals need be considered. However, if the laser hits the substrate, as in Figure 1a,b,d, photolytic deposition from both gas-phase and surface-adsorbed metal alkyls must be examined. This has been done for CW laser photodeposition of two dimethylmetals: DMCd[68] and DEZn.[41] Sometimes the difference in the ultraviolet absorption spectra of gas-phase, physisorbed, and chemisorbed metal alkyls is significant in photolysis. For example, the fine structure in the gas-phase DMCd absorption spectrum is absent in the physisorbed spectrum,[40,69] while the spectrum of DEZn chemisorbed on fused silica (which probably had adsorbed water or hydroxyl groups) is weaker and blue-shifted relative to the physisorbed and gas-phase spectra.[41] At lower reactant pressures, surface photolysis is most important, producing films with relatively good morphology and high electrical conductivity. At relatively high pressures, the rate of deposition can be much faster because of the dominating contribution of gas-phase photolysis; however, the material properties of these deposits are usually poor.

The photochemistry of adsorbed dimethylmetals could be very different from that of gas-phase molecules because of surface relaxation, different accessible decomposition pathways, and the aforementioned difference in absorption spectra. Other than measurements of the net deposition rate and analysis of deposit quality in regimes where the photolysis of either gas-phase or surface-adsorbed species dominates, there has been far too little work in this area, with careful examination of the mechanistic differences beginning only recently. Preliminary studies suggest that under pulsed irradiation, surface-adsorbed DMCd and DMZn decompose at 193 nm (ArF laser) but not at 248 nm (KrF laser), even though there is absorption at this wavelength.[70] Furthermore, though the absorption cross sections of gas-phase and surface-adsorbed species are approximately equal at 193 nm (for each of these dimethylmetals), the photodissociation cross section of each of these dimethylmetals at this wavelength is ~$^1/_{20}$ of the gas-phase absorption cross section, suggesting that surface energy relaxation is very important.[70] These observations have not been explained well enough to date; much more work is needed in this area.

Because of its low resistivity and widespread use in microelectronics, laser-assisted deposition of Al has been investigated by many groups. In the majority of these studies, and especially in the earlier work, TMAl was used as the Al precursor. Unfortunately, TMAl has been shown to produce very impure films usually, and is now regarded as an unsatisfactory precursor.

The photodissociation of trimethylaluminum in the gas phase appears to require the sequential absorption of several photons to produce pure Al deposits. In one series of studies[54-56] it was hypothesized that gaseous TMAl is photodecomposed by 248-nm KrF laser radiation via the steps

$$Al_2(CH_3)_6 + h\nu \rightarrow 2Al(CH_3)_3 \quad (5a)$$

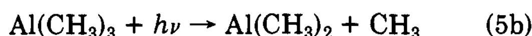

$$Al(CH_3)_3 + h\nu \rightarrow Al(CH_3)_2 + CH_3 \quad (5b)$$

$$Al(CH_3)_2 + h\nu \rightarrow AlCH_3 + CH_3 \quad (5c)$$

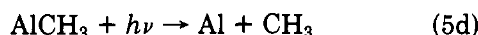

$$AlCH_3 + h\nu \rightarrow Al + CH_3 \quad (5d)$$

First the dimer is dissociated and then one methyl group is removed for each subsequent photon absorbed.

The $Al_2(CH_3)_6$ dimer bond energy is ~20 kcal/mol, while the average Al–CH_3 bond energy is ~67 kcal/mol;[64] the individual Al–CH_3 bond energies are apparently not known. Energetically, at least four 248-nm photons are needed per $Al_2(CH_3)_6$ to produce free aluminum atoms and methyl radicals. The internal energy of TMAl produced in reaction 5a can be as high as ~47 kcal/mol. Consequently, after this excited TMAl absorbs another 248-nm photon, there may be enough energy to break two Al–CH_3 bonds. Then five 248-nm photons would be consumed per dimer, instead of the seven photons needed in the route proposed in reactions 5. This proposed four-step mechanism conflicts with the observed linear dependence of Al 4s $^2S \rightarrow$ 3p ^2P fluorescence on laser intensity, unless three of the four steps in reaction 4 are heavily saturated. On the basis of other studies of metal alkyl photolysis, this seems unlikely. CH radical A $^2\Delta \rightarrow$ X $^2\Pi$ fluorescence is also produced promptly in this photolysis, suggesting that it may be produced after $AlCH_3$ absorbs a photon in a pathway alternate to reaction 5d. CH production may account for part of the carbon contamination in the aluminum films formed by TMAl photolysis.[56] No CH fluorescence was observed in the photolysis of triethylaluminum (TEAl) in this same study,[56] which is consistent with the observation of less carbon contamination in Al films produced from TEAl vis-à-vis TMAl. (As discussed below, the availability of β-hydride elimination in TEAl but not in TMAl dissociation also helps explain the purity of Al films made from these two precursors.)

The yields of Al, AlH, and $AlCH_3$ were measured recently by using laser mass spectrometry during the low-intensity 193- and 248-nm photolysis of gas-phase TMAl, TEAl, DMAH, and TIBA.[71] (These three products were inferred from the observed Al^+, AlH^+, and $AlCH_3^+$ yields, respectively. The photolysis of other metal alkyls, such as DMGa, DEGa, DMTe, DETe, DMDTe ($(TeCH_3)_2$), and DMDSe were also investigated in this study.) This technique is particularly useful in identifying certain specific products and in determining relative rates of different reaction pathways. For 193-nm photolysis, the relative yield of Al atoms was found to be greatest for the TMAl reactant and least for TIBA, with the specific order TMAl $\gg$ TEAl > DMAH > TIBA. The ratio of the $AlCH_3$ to Al product densities followed the same order, with TMAl having the highest fractional yield of $AlCH_3$ and TIBA having the least, and, in fact, no detectable $AlCH_3$. This $AlCH_3$/Al ratio follows the same order as the resistivity of the aluminum films deposited from these reactants. The AlH/Al ratio decreased in the order TIBA ~ DMAH > TEAl > TMAl.

The absence of $AlCH_3$ in TIBA photolysis in these experiments[71] may be explained by β-hydride elimination in TIBA:

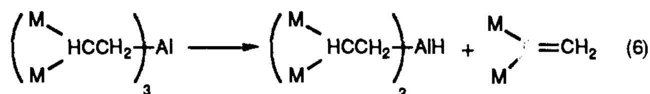

$$\left(\begin{matrix}M\\M\end{matrix}\!\!>\!HCCH_2\right)_3\!\!-\!Al \longrightarrow \left(\begin{matrix}M\\M\end{matrix}\!\!>\!HCCH_2\right)_2\!\!-\!AlH + \begin{matrix}M\\M\end{matrix}\!\!>\!=CH_2 \quad (6)$$

(where M is a methyl group), which cannot occur in TMAl and DMAH. The lower $AlCH_3$/Al ratio with TEAl vs TMAl is due to the availability of β-hydride elimination as a dissociation pathway in TEAl, in addition to bond breakage to form C_2H_5. DMAH photolysis leads to a smaller $AlCH_3$/Al ratio than does TMAl photolysis, because the Al–H bond is stronger than the Al–CH_3 bond and is selectively broken in DMAH photolysis (leaving AlH after two Al–CH_3 bonds are broken). In analogous experiments with dimethylaluminum chloride (DMACl), the product distribution was AlCl > AlH > $AlCH_3$, which is the same order as the relative average Al bond strengths. These experiments explain the large levels of carbon contamination and high resistivities of Al films deposited by TMAl photolysis and the purer films produced with the other precursors.

At 248 nm, the Al yields were found to be lower for TMAl, TEAl, and TIBA than at 193 nm in these experiments, and the $AlCH_3$/Al ratio was relatively low for TMAl photolysis.[71] Curiously, the Al, AlH, and $AlCH_3$ yields varied linearly with laser fluence for the photolysis of each reactant at 193 and 248 nm, which is consistent with the observations in ref 56. Since these products cannot form after the absorption of a single photon because of energy considerations, it appears that a multiple-step process must occur, which is partially saturated even at relatively low laser intensities. This is still not well understood.

Though it is clear that stepwise absorption is important in gas-phase photodissociation of these Al precursors, the specific steps have not been determined yet. It should be noted that in one study of 193-nm deposition of Al films from TMAl, conducted with an electric field present,[57] there was indirect evidence presented for the formation of positive Al ions during deposition. These ions were probably produced by multiphoton ionization.

The relatively few detailed studies of the photolysis of surface-adsorbed aluminum alkyls have been conducted only recently. One study of 193-nm photodecomposition of TMAl adsorbed on aluminum at ambient temperature[72] used time-of-flight measurement and suggests a multistep mechanism similar to that outlined above (eq 5) for the photolysis of TMAl in the gas phase. Apparently, TMAl on the surface is found in the form of dimers,[73] as in the gas phase. During photolysis, TMAl monomers come off the surface with a temperature only slightly higher than that of the substrate, while DMAl, MAl, and methyl radicals leave the surface much hotter, with temperatures ranging from 900 to 1300 K under the conditions of this study. All observed Al atoms were attributed to the fractionation of Al-containing radicals in the mass analyzer. Sequential absorption of photons by the Al-containing adsorbates is suggested by the measurement of successively higher laser intensity thresholds for the appearance of successively smaller $Al(CH_3)_x$ fragments in the gas. More work is needed to confirm this proposed mechanism.

In earlier studies,[74] this same group noted that the fractional carbon content in Al films produced by the

193-nm photolysis of TMAl on Si increased linearly with laser intensity, suggesting that secondary photolysis or a two-photon process is responsible for the carbon impurities in these Al films. In a different study of photolysis of TMAl adsorbed on Si(100),[73] using XPS, UPS, and HREELS, surface photolysis was observed at 193 nm but not at 248 nm. Methyl groups were found to leave the surface upon 193-nm excitation of the adsorbed TMAl; however, carbidic and polymeric carbon were found to remain on the surface even at high intensity and with continued laser exposure. Photolysis of TMAl at 193 nm on both Al and Si surfaces probably involves the sequential absorption of several photons and is certainly incomplete, with carbon impurities always remaining.

Analogous experiments of 193-nm photolysis of TMAl chemisorbed on hydroxylated oxides (Al_2O_3, SiO_2, SiO_2/Si) have also been performed. In this case, methyl radicals were observed to leave the surface subthermally (150 K),[58] in contrast to the hot methyl radicals observed in similar experiments on aluminum cited above. Optoacoustic surface infrared spectroscopy has also been utilized in this series of investigations to monitor C–H bonds of TMAl adsorbed on these hydroxylated oxides both before and after laser irradiation.[75–77] There was no observable change in the strength of the C–H stretching bands after 248-nm irradiation; however, after irradiation at 193 nm, all C–H bands disappeared, indicating photolysis.

To help explain these photolysis experiments, this group calculated the electronic structure of molecules, such as AlH_3 (by the general valence bond method (GVB)) and $AlH_2(CH_3)$ (configuration interaction (CI)),[59] to serve as models of Al complexes adsorbed on these surfaces. These calculations suggested to the authors that optical excitation of adsorbed TMAl does not directly lead to the dissociation of the adsorbate to produce CH_3. Instead, an electronically excited metastable bound state or unbound state is thought to be formed in which the product has little energy available for translation. Furthermore, most of the available energy probably accommodates with the surface. Because these model molecules only crudely approximate the real physical system, much more work is needed for a definitive understanding.

The desorbed products of excimer laser photolysis of TMAl, TEAl, and TIBA adsorbed on quartz and silicon covered with native oxide have also been examined by laser mass spectrometry.[71] Al, AlH, and $AlCH_3$ products were detected from laser photolysis of these adsorbed alkyls at 193, 248, and 308 nm. These three products were also observed in the 193- and 248-nm gas-phase photolysis of these aluminum alkyls in this same study; however, at 308 nm no products were observed in gas-phase photolysis. Moreover, large $AlCH_3$/Al ratios were measured during 248-nm photolysis of adsorbed TMAl, while much smaller product ratios were measured for the similar photolysis of gas-phase TMAl. This indicates that a large amount of carbon impurities will be found in Al films deposited by photolysis of either gas-phase or surface-adsorbed TMAl. Note that in this study,[71] 248 nm light photolyzed TMAl on oxide surfaces, while in the similar studies reported in ref 75–77, no products were measured at 248 nm.

As with photolytically produced material, metals deposited pyrolytically from dimethylmetals are relatively free of carbon. However, aluminum films from pyrolysis and photolysis of TMAl are contaminated with carbon. Specifically, films thermally deposited from TMAl have the approximate stoichiometry Al_4C_3.[78a] This explains the ever increasing use of alternative metal alkyl sources of aluminum, such as TIBA, in conventional and laser-assisted deposition of Al films. The attraction of TIBA as a precursor stems from studies of Al deposition by CVD using this precursor, which have shown that pure Al films are deposited,[78a,b] and that the chemical decomposition of TIBA can be surface selective.

Conventional thermal deposition of Al films from TIBA on Al(100) and Al(111) produces carbon-free deposits for $470 < T < 600$ K, while carbon impurities appear for $T > 600$ K.[79] The rate-limiting step is the decomposition of surface butyl ligands. Up to 600 K, this occurs by β-hydride elimination (reaction 6), producing volatile isobutylene and hydrogen, with no C remaining on the surface. Above 600 K, β-methyl elimination can also occur, which leaves residual carbon on the surface. On Si substrates, Al deposition from TIBA is slow to 650 K; above 750 K, carbon-contaminated Al deposits are formed. As mentioned earlier, β-hydride elimination cannot occur in TMAl decomposition and therefore this route to carbon-free Al deposits is not available in laser pyrolytic deposition using TMAl. Recent work on thermal dissociation of TMAl may be found in the references.[78c]

Thermal decomposition of TIBA on oxide surfaces produces an aluminum oxide–carbon layer which does not promote further growth of aluminum.[26,62] Consequently, after the spatially selective deposition of Al nucleation sites (containing Al, C, and O)[62] on oxides by direct laser writing[45] or projection printing,[26] the spatially selective growth of thicker Al layers can be continued by using this chemically selective thermal deposition of TIBA (Figure 3).[62]

The most important metal in microelectronics available from an alkyl precursor is aluminum. Since TMAl has many disadvantages as a precursor, much recent research on laser-assisted Al deposition has employed other reactants, such as TIBA and DMAH, instead of this intensively studied molecule. As has been seen, with proper choice of reactants and conditions, pure and indeed spatially selective aluminum thin films can be fabricated by laser-assisted deposition. Discussion of the laser decomposition of those metal alkyls usually used as precursors in III–V and II–VI semiconductor deposition, such as TMGa and DETe, is delayed to section III.B.

Metal Carbonyls

Direct writing of several metals has been demonstrated by using focused CW laser deposition from their respective metal carbonyls, including Ni from $Ni(CO)_4$ pyrolytically,[24,80–85] Fe from $Fe(CO)_5$ pyrolytically[86,87] or photolytically,[88] and several refractory metals photolytically (W from $W(CO)_6$,[19,52,88–93] Cr from $Cr(CO)_6$,[88,91–96a] and Mo from $Mo(CO)_6$[19,91–93]) or pyrolytically (W,[52,86,96b] Cr,[96b] and Mo[96b,97]). In one of these examples,[19] a hybrid deposition technique was used in which deposition began photolytically using the 350–

360-nm lines from an argon ion laser on a transparent substrate and then growth was continued pyrolytically after the initial deposition of an absorbing thin film.

Large-area deposits of metal films have been formed by excimer laser deposition of the carbonyls: Fe,[98,99] W,[100,101] Cr,[100–103] and Mo.[100,101] In these examples, the excimer laser was either parallel to the substrate, in which case deposition by only gas-phase photolysis was important and impurity-ridden films were formed, or the laser impinged the surface, so that mixed photolysis/pyrolysis of gas-phase and/or surface-adsorbed molecules contributed and relatively more pure (but still $\lesssim$7% O, ~1% C),[100] shiny films were deposited. Ni has also been deposited over large areas by CO_2 laser induced breakdown of gaseous nickel carbonyl.[104]

In photolytic deposition using the tungsten, molybdenum, and chromium carbonyls, transitions to dissociative metal–ligand charge-transfer states ${}^1A_{1g} \rightarrow {}^1T_{1u}{}^{(1)}$ and ${}^1A_{1g} \rightarrow {}^1T_{1u}{}^{(2)}$ are excited. These absorption bands are quite broad and peak roughly near 2850 and 2250 Å, respectively.[101,105] The lifetimes of the excited states of $Fe(CO)_5$ near 305 and 280 nm are less than 2 and 0.6 ps, respectively.[106]

Conventional pyrolytic deposition of many of these carbonyls has been studied: $Ni(CO)_4$,[107] $Fe(CO)_5$,[108,109] $Cr(CO)_6$,[109] $Mo(CO)_6$,[109] and $W(CO)_6$.[109] ΔH°_{298} for these five metal carbonyls to their respective metal atom and gas-phase CO molecules is 140, 140, 154, 218, and 256 kcal/mol, respectively, corresponding to an average energy per metal–CO bond of 35, 28, 26, 36, and 43 kcal/mol, respectively.[93,109] For comparison, ΔH°_{298} for the first metal–CO bond dissociation in these five carbonyls is 25, ~41.5, 36.8, 40.5, and 46.0 kcal/mol, respectively.[109]

The nascent product distribution in the gas-phase, excimer laser photodissociation of several of these carbonyls has been deduced by using PF_3 as a scavenger.[110–112] The laser intensity in these experiments was kept low enough so that only one photon was apparently absorbed per reactant molecule, with no secondary photolysis. In the photolysis of $Fe(CO)_5$ (ΔH°_{298} = 140 kcal/mol), the branching ratios to $Fe(CO)_4$, $Fe(CO)_3$, $Fe(CO)_2$, and $Fe(CO)$ were measured to be 0.23, 0.46, 0.31, and 0.00, respectively, at 352 nm (tripled Nd^{3+}:YAG laser, 81 kcal/mol), 0.10, 0.35, 0.55, and 0.00 at 248 nm (KrF laser, 115 kcal/mol), and 0.09, 0.09, 0.81, and $\lesssim$0.012 at 193 nm (ArF laser, 148 kcal/mol).[110,111] Gas-phase photodissociation of $Fe(CO)_5$ to Fe + 5CO is energetically allowed at 193 nm but apparently does not occur. In the photolysis of $Cr(CO)_6$ (ΔH°_{298} = 154 kcal/mol) at 248 nm, the branching ratios to the nascent products $Cr(CO)_5$, $Cr(CO)_4$, $Cr(CO)_3$, and $Cr(CO)_2$ were found to be 0.03, 0.73, 0.14, and 0.10.[112] Similar measurements have been made for the photolysis of iron pentacarbonyl and the metal hexacarbonyls by using transient infrared absorption spectroscopy of the CO and $M(CO)_x$ products[113] and VUV laser-induced fluorescence (LIF) of the CO products.[114]

Photodissociation of $Fe(CO)_5$ in a collisionless molecular beam with 193 nm from an ArF laser has been examined more recently.[115a] Time-of-flight measurements indicate that $Fe(CO)_2$ accounts for >99% of all Fe-containing photoproducts after the absorption of one photon, with the three CO eliminated sequentially with no correlation. This nascent product distribution, produced by the following mechanism, is the only route predicted statistically:

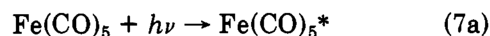

$$Fe(CO)_5 + h\nu \rightarrow Fe(CO)_5^* \quad (7a)$$

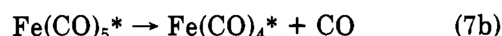

$$Fe(CO)_5^* \rightarrow Fe(CO)_4^* + CO \quad (7b)$$

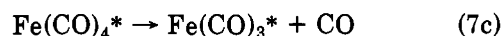

$$Fe(CO)_4^* \rightarrow Fe(CO)_3^* + CO \quad (7c)$$

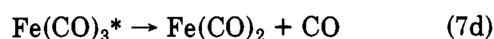

$$Fe(CO)_3^* \rightarrow Fe(CO)_2 + CO \quad (7d)$$

where the asterisk denotes internal excitation. The earlier studies with a PF_3 scavenger[110,111] found that $Fe(CO)_2$ accounts for only 81% of the Fe-containing products, a somewhat smaller fraction than measured under collision-free conditions. Note, however, that because of the collisional relaxation and reactivity that probably occurred in the scavenger studies, those earlier experiments more closely mimic the conditions during laser photodeposition of films than do the molecular beam experiments. Still, note that the VUV LIF measurement of CO products formed in $Fe(CO)_5$ photolysis at 193 nm,[114] also conducted in a collisionless molecular beam, arrived at a different final state $Fe(CO)_x$ distribution than did ref 115 (and also ref 110 and 111). In the molecular beam studies conducted at higher laser intensities, a second 193-nm photon was absorbed by the $Fe(CO)_2$ photoproduct, leading to the sequential elimination of the two remaining CO ligands to produce Fe atoms.[115a] Also, the values of the five $Fe(CO)_5$ bond energies were obtained in these studies[115b] by adjusting the model fit to the measured velocity distribution in (one photon) 193-nm and (one and two photon) 248-nm photolysis of $Fe(CO)_5$, using a modified form of the separate statistical ensemble theory. The first through fifth bond energies were found to be 41, 10, 25, >27, and <39 kcal/mol, respectively.

After the transition metal hexacarbonyls absorb one 248-nm photon in a collisionless molecular beam[115c] two or three CO are eliminated [$Cr(CO)_6$ to $Cr(CO)_4$ (0.38) + $Cr(CO)_3$ (0.62); $Mo(CO)_6$ to $Mo(CO)_4$ (0.85) + $Mo(CO)_3$ (0.15); $W(CO)_6$ to $W(CO)_4$ (1.0)], the first CO nonstatistically and the others statistically.[113f,115c] Free Mo and W atoms are formed only after the absorption of three 248-nm photons.[115c]

Though energetically allowable in some instances, in no case is the carbonyl fully stripped of all CO after the absorption of only one photon at these laser wavelengths.[116] One such example is $Fe(CO)_5$ photolysis, where two 193-nm photons are needed to produce a free Fe atom, though energetically, only one 193-nm photon is needed. This explains the many observations of very large C and O impurities in photolytically deposited metals from the gas-phase carbonyls, particularly in CW photolysis where laser intensities are so low that only one photon is absorbed.

In CW 257-nm deposition of Cr from gas-phase $Cr(CO)_6$, the Cr atomic fraction in the film has been found to be about 0.3, with most of the impurity being O (0.5–0.7) and the remainder C (0.1).[91,93,96] In these experiments, deposition occurs from the photolysis of both gas-phase and surface-adsorbed species. In one of these studies,[96] the deposits within the laser-irradiated areas were found to have the approximate stoichiometry CrCO, while those outside the laser irradiation region had the approximate composition $Cr(CO)_2$. Though products from gas-phase and surface-adsorbed molecules contributed to the first observation, while prob-

ably only gas-phase dissociation contributed to the latter, it is hard to obtain dynamical information from these observations, other than the incompleteness of photolysis. It should be noted that the adsorption of metal carbonyls to surfaces is generally fairly weak at the ambient temperatures used in this study, but can be significant at lower temperature. Also, adsorption is quite dependent on surface preparation, so the relative contribution to deposition from photolyzed gas-phase and adsorbed metal carbonyls depends critically on the experimental conditions.[91,93] Similar experiments involving molybdenum and tungsten carbonyls gave only slightly purer metal films (0.4–0.6 metal, 0.3–0.4 O, and 0.1–0.3 C).[91,93] The high impurity level in these metal films produced by low-intensity photodeposition is expected from the photolysis studies cited earlier.

Definitive studies of photodissociation of the metal carbonyls adsorbed on surfaces cleaned in UHV, with no gas phase present, suggest that the decomposition to pure metal is also incomplete in most cases.[91,117-122] Many of these studies were conducted at temperatures below ambient because of the weak adsorption of carbonyls on substrates, such as Si at 300 K. In one series of studies, the deposition of Mo, W, and Fe was examined by low-intensity CW laser irradiation of the respective carbonyls on Si(111) 7 × 7.[91,118-120,123] At 90 K substrate temperature $Mo(CO)_6$ and $W(CO)_6$ adsorbed molecularly, while $Fe(CO)_5$ adsorbed partly molecularly and partly dissociatively. Low-power UV radiation (257 nm) was shown to remove some, but definitely not all, of the CO ligands for each of the three carbonyls, with the adsorbed $Mo(CO)_6$ decomposing to form (possibly) $Mo(CO)_3$ on the surface. Only ~10% of the photoexcited $Mo(CO)_6$ molecules were found to release at least one CO ligand.[119] The residual C and O apparently remain only as CO ligands. In contrast, low-power visible radiation (514.5 nm) led to no dissociation at all in any of the three carbonyls, though it did lead to structural changes in adsorbed $W(CO)_6$ and $Fe(CO)_5$.[119] These experiments demonstrate that adsorbate absorption of photons, and not the creation of electron–hole pairs in the substrate, is important in photodecomposition, even though electron–hole pairs may influence the structure of the adsorbate. At high power, 514.5-nm radiation induced thermal desorption of only intact metal carbonyl molecules. Figure 5 shows EELS spectra from ref 120, which demonstrate the influence of photons on adsorbed $Mo(CO)_6$.

Analogous studies have been performed for excimer laser photolysis of several metal carbonyls adsorbed on surfaces under UHV conditions. Photolysis of $W(CO)_6$ adsorbed on Si(111) at 120 K using 248 (KrF laser) and 308 nm (XeCl laser) also led to incomplete decomposition.[121,122] In the 248-nm photolysis of $Mo(CO)_6$ adsorbed on UHV-prepared Si(100) at 150 K, the photochemical decomposition cross section was measured to be about 5×10^{-17} cm^2, which falls within the range of measurements of the gas-phase absorption cross section ($(0.5-8) \times 10^{-17}$ cm^2).[117] In that study, the remaining film had stoichiometry $MoCO_{0.3}$. The flux of CO desorption due to photodissociation of $Mo(CO)_6$ adsorbed on Si(111) at 90 K has been shown to follow the absorption coefficient of the carbonyl, increasing rapidly from zero as the photolysis wavelength is decreased from about 360 nm.[123] As with the previously cited

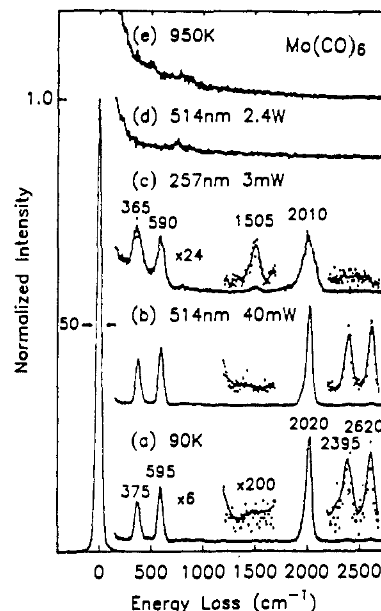

Figure 5. EELS (electron energy loss spectroscopy) spectra of 1.5 L of $Mo(CO)_6$ on Si(111) 7 × 7 (a) at 90 K, (b) after 514.5-nm laser irradiation of 40 mW/cm^2 for 20 min, (c) after 257-nm laser irradiation of 3.8 mW/cm^2 for 20 min, (d) after 514.5-nm laser irradiation of 2.4 W/cm^2 for 5 min, and (e) after resistive heating to 950 K. (Reprinted from ref 120; copyright 1988 Gordon & Breach Science Publishers Ltd.)

studies of adsorbed carbonyls,[119] temperature-programmed desorption showed that unphotolyzed carbonyl adsorbates and visible laser irradiated adsorbates both desorb intact.

There is evidence of complete removal of all CO groups in one study of photolysis of adsorbed metal carbonyls, the 248-nm photolysis of $Fe(CO)_5$ adsorbed on UHV-prepared Si(111) 7 × 7.[121,124] Infrared absorption measurements after photolysis indicated no bound CO molecules, and furthermore, Auger analysis found no elemental C and O as well. Because the photon energy 115 kcal/mol for one 248-nm photon is less than $\Delta H°_{298}$ for $Fe(CO)_5$, 140 kcal/mol, each molecule must be absorbing more than one photon. The dependence of yield vs laser fluence in this experiment did not give a conclusive indication of the number of photons absorbed per $Fe(CO)_5$ molecule. In this study, the photochemical decomposition cross section (~1.2×10^{-16} cm^2) was found to be comparable to the gas-phase absorption cross section (0.27×10^{-16} cm^2).

In addition to the incomplete photolysis of adsorbates, dissociative chemisorption of product CO is a source of the impurities found on the surface after the photolysis of metal carbonyls.[91] Even though there is evidence that the CO ligands remaining after photolysis are intact,[119] it should be remembered that each of these cited studies of UV photodecomposition of adsorbed metal carbonyls was conducted at low surface coverage. At higher coverages and in the actual growth of thin films, large C and O impurities are not unexpected for Fe, W, Cr, and Mo deposition because of dissociative chemisorption of the CO products,[125] which are initially released to the gas and can later reappear at the surface during the course of photodeposition.

Laser CVD of Ni from nickel carbonyl by heating amorphous silicon films with focused visible krypton and argon ion lasers produces very pure material with a resistivity 2–3× bulk.[24,82] The measured effective

activation energy for deposition is 22 ± 3 kcal/mol,[84] which is consistent with that for conventional CVD, 22 kcal/mol.[107] A recent study of laser CVD of W, Cr, and Mo from their carbonyls[96b] has shown that very pure deposits of each of these metals can be produced. A focused argon ion laser (514.5 nm) was used to heat silicon (with native oxide) in the presence of the metal carbonyl at its room temperature vapor pressure. Under UHV base pressure conditions ($\sim 10^{-9}$–10^{-8} Torr), very pure deposits of each of these metals were deposited, sometimes with trace quantities of C or O. These deposits are purer than those usually obtained by conventional CVD. With poorer base pressure conditions ($\sim 10^{-4}$–10^{-3} Torr), the W and Mo deposits were still very pure, but Cr_2O_3 deposits were produced when $Cr(CO)_6$ was the precursor.

Since CO adsorbs molecularly on nickel surfaces,[125] it is not surprising that pure nickel films can be deposited pyrolytically with lasers, as has been shown to be true also for conventional thermal decomposition of nickel carbonyl.[107] However, because of dissociative chemisorption of CO on W, Cr, and Mo at room temperature,[125] it is somewhat surprising that laser CVD can produce pure deposits of each of these metals.[96b] Perhaps, at the elevated temperatures used in these laser CVD experiments dissociative chemisorption of CO is relatively unimportant in the overall process kinetics.

Laser-assisted photolytic deposition of metals from the carbonyls produces films that are laden with carbon and oxygen impurities in most cases. This is definitely true for the photodeposition of refractory metals from gas-phase and adsorbed carbonyls at low laser fluences, an area that has been studied intensively. Formation of pure deposits of nickel and the refractory metals appears to be possible by laser pyrolytic deposition from metal carbonyls.

Metal Halides

An alternate source of tungsten is the highly volatile metal halide WF_6. This compound can be used to form tungsten films thermally in several ways.[126-130] The detailed mechanisms of several of these thermal modes of deposition are still uncertain and, in fact, are under intensive scrutiny at present. The important net reactions of interest in pyrolytic laser deposition of tungsten are given here, with some of the mechanistic details, when available. In each case of W deposition by WF_6 reduction, the highly corrosive reactant is replaced by another corrosive gas product.

At temperatures below 750 °C, tungsten can be deposited by hydrogen reduction, with apparent net reaction

$$WF_6 + 3H_2 \rightarrow W + 6HF \quad (8a)$$

Kinetic studies[127] have shown that when the growth rate is not transport limited, there are two regimes of this type of deposition, depending on the nature of reactant flow, both having $E_{act} \sim 17$ kcal/mol. In one regime, characterized by relatively more streamlined flow, the reaction orders with respect to WF_6 and H_2 are 0 and $^1/_2$, respectively, while in the second regime, characterized by more turbulent flow and more heating of the gas by the heated substrate, these reaction orders are 2 and 2.

From a Langmuir–Hinshelwood type analysis, the rate-limiting step in this first regime appears to be H_2 dissociation on the surface.[127] The measured E_{act} is consistent with measured values of H_2 migration on tungsten surfaces, which is thought to be a key step in dissociation by bringing H_2 to sites where one of the H atoms can jump to a neighboring site. Homogeneous reactions appear to be important in the second regime,[127] with hypothesized reaction schemes

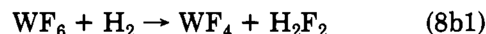

$$WF_6 + H_2 \rightarrow WF_4 + H_2F_2 \quad (8b1)$$

$$WF_6 + WF_4 \rightarrow W_2F_{10} \quad (8b2)$$

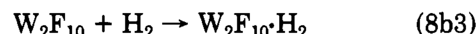

$$W_2F_{10} + H_2 \rightarrow W_2F_{10}{\cdot}H_2 \quad (8b3)$$

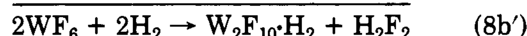

$$2WF_6 + 2H_2 \rightarrow W_2F_{10}{\cdot}H_2 + H_2F_2 \quad (8b')$$

and

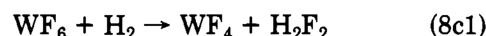

$$WF_6 + H_2 \rightarrow WF_4 + H_2F_2 \quad (8c1)$$

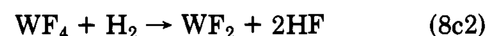

$$WF_4 + H_2 \rightarrow WF_2 + 2HF \quad (8c2)$$

$$WF_6 + WF_2 \rightarrow W_2F_8 \quad (8c3)$$

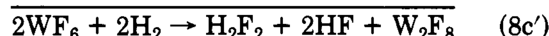

$$2WF_6 + 2H_2 \rightarrow H_2F_2 + 2HF + W_2F_8 \quad (8c')$$

These possible steps are questionable, in part because of the inclusion of the unknown molecule H_2F_2. The kinetic details in this second regime remain unresolved.

WF_6 can also be reduced by a Si substrate, in which the near-surface layers of Si are replaced by W.[128,129] For $T > 450$ °C, the dominant gas product is SiF_4

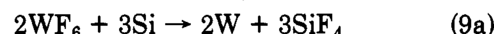

$$2WF_6 + 3Si \rightarrow 2W + 3SiF_4 \quad (9a)$$

while for $T < 450$ °C, SiF_2 is the main gas product

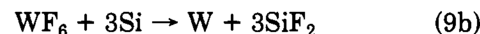

$$WF_6 + 3Si \rightarrow W + 3SiF_2 \quad (9b)$$

Initially, these reactions occur on the bare silicon surface, onto which WF_6 has a sticking coefficient of ~ 0.3 for T = 200–700 °C (Si(100)). As the reaction proceeds, Si atoms from the bulk diffuse through the deposited W to the surface and react with WF_6. Apparently, the sticking coefficient of WF_6 on "Si on W" is higher, $\sim$ 0.48. Both the SiF_2 and SiF_4 products have prompt components (as the WF_6 sticks to the surface) and slow components (several tens of seconds), possibly due to regrouping of adsorbed F atoms on the Si surface to form volatile products.[128] This type of growth is self-limiting to ~500-Å-thick tungsten films.[127] Currently, there is no detailed kinetic model to account for reactions 9.

Yet another route for conventional thermal tungsten deposition has been investigated recently, WF_6 reduction by silane at relatively low temperatures (300 °C). The net overall reaction is[130]

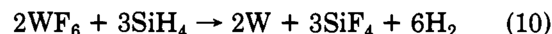

$$2WF_6 + 3SiH_4 \rightarrow 2W + 3SiF_4 + 6H_2 \quad (10)$$

which is 23 kcal/mol exothermic. For $T < 600$ °C, no HF is formed. Recent studies[130] indicate that the net reaction 10 represents one cycle that is continually repeated. First, WF_6 fluorinates the W surface; then silane reacts with the fluorinated surface to form SiF_4 and H_2, leaving silicon and silicon subfluorides on the surface; WF_6 then reacts with this surface to form SiF_4 and regenerates the fluorinated tungsten surface for the next cycle.

Another mode of tungsten CVD has been reported[126] for temperatures above 750 °C in a nonreducing atmosphere, in which WF_6 apparently decomposes on an

inert substrate by the net reaction

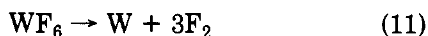

$$WF_6 \rightarrow W + 3F_2 \quad (11)$$

This has not been studied in detail.

Laser-assisted analogues of most of these thermal modes of tungsten deposition have been demonstrated. In two cases, the deposition is surface specific: for WF_6 reduction by a silicon surface (reactions 9) and for heterogeneous WF_6 reduction by H_2 (reaction 8a), which requires a surface that can dissociate H_2, such as tungsten.

Direct writing of tungsten has been studied by using focused argon ion or CO_2 lasers to heat a surface locally to induce hydrogen reduction of WF_6 (reaction 8)[23,83,86,131-135] or the reduction of WF_6 by crystalline or amorphous silicon surfaces (reactions 9a,b).[136-138] In the latter process, the maximum film thicknesses are self-limited to 500–1000 Å, as in conventional thermal processing, because of the need for tungsten species to diffuse through the deposited film to the underlying W/Si interface. These laser-deposited tungsten features are very pure and generally have good morphology.

The kinetics of local laser CVD of tungsten on native oxide atop Si using WF_6/H_2 mixtures has been studied recently.[135] In this investigation, the reaction orders of the deposition rate with respect to WF_6 and H_2 were determined to be $^1/_6$ and $^1/_2$, respectively. On the basis of the analysis in ref 127c, this suggests that the rate-limiting step in laser CVD of tungsten is HF desorption from the surface. This is surprising since in the analogous CVD experiments, the reaction orders were 0 and $^1/_2$, respectively, when surface decomposition dominated, which suggested instead that H_2 dissociation was the rate-limiting step. The reason for this difference is not clear.

Recently, direct writing of pure tungsten lines at fast scanning speeds has been demonstrated by using WF_6/SiH_4 mixtures (reaction 10).[139] Only low laser-induced temperature rises (to 150 °C) are needed to drive this highly exothermic reaction. With a relatively larger reactant fraction of silane, tungsten silicide can be formed instead of tungsten (which is sometimes undesirable in applications because of its relatively higher resistivity). WF_6/SiH_4 mixtures can be explosive. This danger is alleviated by operating at lower total reactant pressures and silane partial pressures (5/1 reactant ratio, total reactant partial pressure of 10 Torr, buffered to 350 Torr) and with suitably fast flow of reagents and products through the reaction zone.

Large-area deposition of tungsten films by hydrogen reduction of tungsten hexafluoride has been investigated by using an ArF laser (193 nm) passed above a heated substrate to assist the reaction photolytically by dissociating WF_6.[140-142] The activation energy of reaction 8 without laser photolysis, ~17 kcal/mol, is decreased to 9.7 kcal/mol[140] (or 8.2 kcal/mol[142]) with laser photolysis, showing that surface chemistry is still important in laser photodeposition and, concomitantly, that the substrate temperature is still a significant parameter during this "photolytic" process.[140] It has been hypothesized that the 193-nm radiation releases one or more F atoms from WF_6 molecules during photodeposition of tungsten;[140,142] this has not yet been proven. The reaction order during laser photolysis was shown to be $^1/_2$ with respect to WF_6 and 1 with respect to H_2,[142] which is very different from that in thermal CVD,[127] where the orders with respect to WF_6 and H_2 are 0 and $^1/_2$, and 2 and 2, respectively, in the two regimes described earlier.[127] There is currently no satisfactory description of the kinetics during this type of laser-assisted deposition.

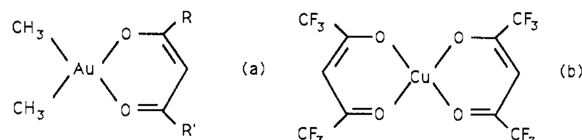

Figure 6. Structure of some of the AcAc's used in laser deposition: (a) $Me_2Au(AcAc)$ with $R = R' = CH_3$; $Me_2Au(TFAc)$ with $R = CH_3$, $R' = CF_3$; $Me_2Au(HFAc)$ with $R = R' = CF_3$; (b) $Cu(HFAc)_2$. (Adapted from ref 147 and 148.)

Though the corrosiveness of tungsten hexafluoride and its volatile products can lead to processing problems, this molecule is still a very useful, and certainly the best available, source for laser-assisted deposition of pure tungsten films. Another potential metal halide source of tungsten is WCl_6; however, its low vapor pressure makes it a much less attractive precursor than WF_6.

It should also be noted that the volatile metal halides are also a good source of titanium. Direct writing of Ti lines has been demonstrated by photodeposition from $TiCl_4$ at 257 nm.[143] Also, films of the complex Ti:Cl:Al:CH_3 have been photodeposited from coadsorbed $TiCl_4$ and $Al_2(CH_3)_6$.[28,144]

Finally, In, Tl, and Al films have also been deposited by laser photoionization of their corresponding iodide or bromide in the presence of a uniform electric field.[145,146]

Metal Acetylacetonates

Since most noble metals do not form stable, volatile alkyls, carbonyls, or halides, other precursor molecules are needed to achieve laser-assisted deposition, or even conventional CVD, of these metals. The 2,4-pentanedionates, also known as β-diketonates or acetylacetonates, and commonly referred to as AcAc's, permit pyrolytic and photolytic deposition of these metals.[147,148] Typical AcAc structures are shown in Figure 6. Though they generally have relatively low vapor pressures, from 8 to 700 mTorr at ambient temperature,[2] their vapors decompose at relatively low temperatures (~200 °C) and have photodissociation bands in the near-ultraviolet (~250–350 nm), making them good candidates for laser-assisted pyrolytic and photolytic deposition.

Both localized and large-area films of Cu, Au, and Pt have been deposited by pyrolysis and photolysis, and of Pd by photolysis; there has been limited work on infrared-laser-assisted deposition. Copper deposition has been achieved by using $Cu(HFAc)_2$ [bis(1,1,1,5,5,5-hexafluoro-2,4-pentanedionate)copper(II)] (Figure 4);[149-153] gold deposition has employed $Me_2Au(AcAc)$ [dimethylgold(III) acetylacetonate] and its two more volatile fluorinated derivatives $Me_2Au(TFAc)$ [dimethylgold trifluoroacetylacetonate] and $Me_2Au(HFAc)$ [dimethylgold hexafluoroacetylacetonate] (Figure 4);[148,154-159] platinum deposition has involved $Pt(AcAc)_2$ [platinum acetylacetonate][160] and $Pt(HFAcAc)_2$ [platinum bis(hexafluoroacetylacetonate)];[19,51,161,162] iridium deposition has used Ir-

(AcAc)$_3$ [iridium acetylacetonate];[160] and palladium deposition has employed Pd(HFAcAc)$_2$ (and films of PdAcAc and PdAc).[163] In this last study, spatially localized Pd thin films deposited on polyimide using 351 nm from an argon ion laser served as sites for further growth of copper by electroless deposition. In another AcAc study, Pt films were deposited from Pt(HFAcAc)$_2$ in a hybrid mode, with only photodeposition occurring initially on the transparent substrate and then with pyrolytic deposition beginning only after the photodeposition of a thin, absorbing Pt film.[20] Furthermore, in a related study[162b] it was shown that with a small increase in the laser-induced temperature rise, by a few tens of degrees, photolytic deposition of Pt went from being dominated by the photolysis of surface-adsorbed species to the photolysis of gas-phase Pt(HFAcAc)$_2$ molecules.

In most cases, laser pyrolytic deposition from the AcAc's produces very pure metal films ($\gg$95%),[148] while purely photolytically deposited films are highly laden with carbon ($\sim$10–90%),[147,149] oxygen, and, when present in the precursor, fluorine impurities.[147,152,162a]

Very little research was performed on the photolysis of gas-phase AcAc's before this recent interest in laser-assisted metal deposition; however, extensive studies had been conducted earlier of the photolysis of AcAc's in solution.[147] Only the ultraviolet absorption bands in AcAc's can be used for photolytic decomposition. For example, Cu(HFAc)$_2$ dissociates when the strong absorption peak near 250 nm is excited, but the close analogue Cu(AcAc)$_2$ is stable when it is excited within its visible absorption band near 600 nm; this is presumably true also for Cu(HFAc)$_2$.[149,164] Absorption in the ultraviolet in the AcAc's is due to ligand-centered n–π^* and π–π^* excitations near 300 nm, and charge transfer to metal (CTTM) and to ligand (CTTL) transitions from 200 to 300 nm.[147]

In laser photolysis of gas-phase Cu(HFAc)$_2$, adding ethanol and increasing the light intensity both increase the ratio of Cu/contaminants, presumably by helping form more volatile products.[147,149,152] In fact, ethanol is necessary to form any deposits at all using the low-intensity levels in Hg lamp assisted deposition. Apparently, at low light intensities ethanol serves as a coreductant and, as in solution, gives two electrons to reduce Cu^{2+} to metallic Cu.[149] There is proportionately less O and F than C contamination in the photodeposited Cu film vis-à-vis the Cu(HFAc)$_2$ reactant, suggesting that the volatile products are relatively rich in O and F.[147] Film purity is not affected by reactant pressure or temperature during photodecomposition.[147]

Free Cu atoms have been identified by laser-induced fluorescence promptly after the KrF laser (248 nm) photolysis of Cu(HFAc)$_2$.[151] The importance of collisions in forming the Cu atoms was not ruled out in these experiments, and the possibility of absorption by photoproducts was also not considered. Since these experiments were conducted at laser intensities much higher than those commonly used during CW laser photodeposition (of impurity-laden Cu films), the relevance of this observation of free Cu atoms (which would be expected to give pure copper films) to the photodecomposition experiments cited above is not clear. Furthermore, Cu films deposited by 248-nm (KrF laser) or 193-nm (ArF laser) photolysis of Cu(HFAc)$_2$ have been shown to have significant levels of C, O, and F impurities.[149] This suggests that while some free Cu atoms may form, other incompletely photolyzed molecules may also be present, which help produce the deposit.

The laser-induced increase in surface temperature needed for the decomposition of the AcAc's is very low relative to that required for the other metal precursors. For example, Cu(HFAc)$_2$ decomposes above 220 °C, while Me$_2$Au(AcAc) decomposes above 165 °C. Since pyrolytically deposited films are pure, the ligands apparently desorb intact. Few fundamental studies have been done to understand this process. One such study utilized modulated relaxation spectrometry to examine the gas-phase products during gold deposition by decomposition of Me$_2$Au(HFAc) on laser-heated substrates.[157] Two gas-phase products were identified from the mass spectrum, $C_5H_4O_2F_3$ and C_2H_6. This first product may be formed after the recombination of CH_3 and HFAc ligands to produce a complex that then fragments to form this product and CF_3. The detailed mechanism of this formation is currently unknown.

Laser pyrolytic deposition of Au, Cu, Pt, and Pd using AcAc precursors produces highly pure films and requires relatively low temperatures for deposition, which is good for overall compatibility in microelectronics processing. However, the maximum deposition rates are fairly slow because of the low vapor pressure of the reagents. The vapor pressure can be increased, thereby improving deposition rates, by using the more volatile fluorinated AcAc's and by operating the reaction chamber at above-ambient temperatures.

Other Metal Precursors

Alternative gas-phase precursors for the deposition of several metals are under current scrutiny because of some of the disadvantages of the compounds discussed above. For example, (trimethylamine)aluminum hydride (TMAAH) has recently been used as a precursor for Al in pyrolytic direct writing using 514.5 nm from an argon ion laser.[30] This compound produces deposits that are purer (>97% Al) than those produced with TMAl or TEAl, and has a vapor pressure of 2 Torr at 25 °C and, as such, is much more volatile than TIBA. Both TMAAH and the other recently tested aluminum-containing reagent, DMAH, will be the subject of much future investigation.

There has been very little laser-assisted deposition research using precursors outside of the reactant groups already discussed here. Some alternate volatile precursors have been employed to help deposit noble metals in lieu of the AcAc's. Specifically, these have been used to deposit copper and platinum films: Cu from (triethylphosphine)(cyclopentadienyl)copper(I)[165] and Pt from Pt(PF$_3$)$_4$[166] and CpPt(CH$_3$)$_3$.[167] Pt was photodeposited from this last precursor using 308 nm from a XeCl laser and the 351- and 364-nm UV lines from an argon ion laser. Shiny deposits were produced that are >96.5% Pt and <3.5% C when H_2 was present during photolysis, and black deposits were formed with about 20% C when no H_2 was present. Apparently, this study was partly motivated by work on non-laser CVD of Pt films using CpPt(CH$_3$)$_3$.[168,169]

Photodecomposition of Ni and Fe films has also been demonstrated using nickelocene and ferrocene vapor as

an alternative to deposition by their carbonyls.[170] By tuning the laser wavelength, variable-stoichiometry Fe/Ni alloys have been formed using ferrocene/nickelocene mixtures.[171]

Metal Silicide Deposition

Relatively little research has been devoted to laser-assisted deposition of metal silicides. The processes used in this deposition sometimes parallel the photochemistry of metal deposition. For example, in the silicon substrate reduction of WF_6 (reactions 9a,b) to form tungsten lines, there is evidence from Raman microprobe spectroscopy that the center of the line is tungsten silicide.[172,173]

Large-area titanium silicide films have been formed by irradiating $TiCl_4/SiH_4$ reagent mixtures with either a CW CO_2 laser[174,175] or pulsed ArF laser[175,176] directed parallel to the substrate. In the CO_2-laser-driven reaction, the 10P(20) line at 944 cm^{-1} is absorbed by silane, which is pressure broadened by the addition of an argon buffer, leading to gas-phase thermal reactions. In the ArF-laser-driven reaction, the $TiCl_4$ strongly absorbs the 193-nm light and photolyzes, while SiH_4 absorption and photodissociation occur at a much slower rate. The $TiCl_4$ photodissociation products probably react directly with undissociated SiH_4.

B. Semiconductors

Group IV Elements

Silicon Deposition. The deposition of silicon films is essential to the fabrication of many types of integrated circuits and to related electronics applications such as the production of solar cells. Consequently, there have been numerous investigations of the deposition of Si thin films by CVD, plasma CVD, Hg-sensitized photo-CVD, deep UV lamp assisted deposition, and, more recently, laser-assisted CVD, making it, perhaps, the most studied thin-film deposition process in microelectronics research. Despite these extensive investigations, the details of the kinetics of most of these silicon thin-film depositions remain poorly understood. In particular, the mechanism of conventional Si CVD has been the subject of much debate in recent years.

Silicon films have been deposited with lasers by laser heating of surfaces in the presence of gas-phase precursors and by gas-phase photolytic and pyrolytic decomposition of these precursors. Crystalline, polycrystalline, and amorphous films, undoped and doped, have been grown by using these methods. Most earlier studies used SiH_4 as the silicon precursor. For reasons cited below, Si_2H_6 has also been used in many recent studies.

Direct laser writing of micron-dimension structures of polycrystalline and crystalline silicon by localized laser chemical vapor deposition of silane has been investigated by several groups.[24,136,177-189] In most of these experiments, a visible line of the argon ion laser (such as 514.5 nm) is transmitted through the nonabsorbing silane gas and is focused onto an absorbing substrate.

To understand local laser CVD of silicon, the dynamics and kinetics of conventional CVD must be examined. The kinetics of Si CVD, using silane in static and flow reactors, has been the subject of controversy for many years,[190-192] with the relative importance of heterogeneous and homogeneous chemistry still not totally resolved. A large range of effective activation energies E_{act} for deposition, ~15–60 kcal/mol, have been measured,[190-192] depending on the specific experimental conditions. Recent careful experiments have made several essential features of Si CVD clear, which are also vital in understanding laser CVD.

At very low SiH_4 partial pressures (≪1 Torr), surface dissociation of silane molecules is clearly responsible for deposition by

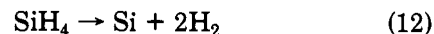

$$SiH_4 \rightarrow Si + 2H_2 \quad (12)$$

This reaction has $E_{act} \sim 17$ kcal/mol;[190] there may be a short-lived intermediate species, SiH_2.[190]

In a CVD reactor, this heterogeneous reaction always occurs and is most important at relatively low silane partial pressures and for fast flow rates (short reactor residence times). Surface reactivity is saturated at higher SiH_4 pressures, with hydrogen desorption probably being the rate-limiting step, leading to an effective overall E_{act} ~37.5 kcal/mol.[191,192]

At higher silane pressures and for slower flows (longer residence times), homogeneous decomposition can become faster than surface decomposition of silane. The primary step is

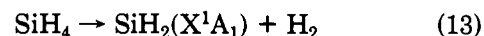

$$SiH_4 \rightarrow SiH_2(X^1A_1) + H_2 \quad (13)$$

which has $E_{act} \sim 52$ kcal/mol;[192] the precise value of this activation energy is still much in doubt. This is followed by complex chemistry involving the production of higher order silanes, such as by

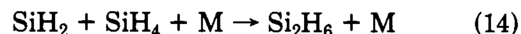

$$SiH_2 + SiH_4 + M \rightarrow Si_2H_6 + M \quad (14)$$

(where M is any third body), the decomposition of these silanes, and the diffusion of these silanes and silylene to the heated surface, which is followed by further decomposition to form Si. In a 2-cm-radius cylindrical reactor, the homogeneous decomposition rate of SiH_4 exceeds the heterogeneous rate for silane partial pressures above 100 Torr at 600 K, and for pressures above 3 Torr at 800 K.[191b]

Given the questions remaining in large-area, conventional CVD of Si using silane, the exact processes occurring in local, surface-heated laser CVD of silicon are not expected to be clear. In two of these studies of laser direct writing silicon, activation energies (E_{act}) were determined from the observed deposition rates and by the measured or estimated laser-produced temperatures, giving about 44[179] and 38 kcal/mol.[188] In one of these cited studies (ref 179), the measured E_{act} was cited as being within the range of activation energies that were thought at the time to represent both heterogeneous and homogeneous deposition. However, current understanding of Si CVD suggests that heterogeneous CVD is probably dominant in most regimes studied in laser CVD, with hydrogen desorption from the surface or the transport of silane molecules to the surface being the rate-limiting step.

Further evidence that this laser CVD is surface dominated comes from heat conduction calculations,[193] which show that gas-phase reactants near the laser-heated area on the surface are not expected to get very hot. Moreover, silane molecules that gain energy after colliding with the heated surface are much more likely

to relax collisionally outside the local reaction volume at low reactant pressures than to collide with each other within this volume to promote homogeneous decomposition. Furthermore, because of the small microreaction volume in local laser CVD, any higher order silane formed near the site of deposition will rapidly be diluted by three-dimensional gas transport and will also rapidly be displaced from the new site of laser heating and deposition when the scanning is suitably fast. Consequently, local CVD occurs in an experimental regime equivalent to the short residence time/fast flow regime in conventional CVD, where surface deposition dominates. It should be noted that for slow scan rates and high reactant pressure, explosive-type reactions leading to unlocalized deposits can occur during heterogeneous localized laser CVD of silicon and other materials.[187] This nonlocal deposition may be triggered by homogeneous reactions that may occur in specific experimental regimes.

There is also some evidence that silicon deposition promoted by visible laser heating of a substrate may not always be a purely thermal reaction.[187-189] For example, when deposition occurs on a silicon substrate, the laser both heats the surface and creates electron–hole pairs. These free carriers may modify the reaction, nucleation conditions, or hydrogen desorption from the surface.[187-189] More work is needed to substantiate this possibility.

Large-area silicon films have been deposited by laser CVD of silane using pulsed and CW CO_2 lasers impinging on an absorbing substrate[194-198] and CW CO_2 lasers propagating parallel to the surface.[199-203] In the latter case, and sometimes in the former, the laser directly heats the silane. These processes are analogous to heterogeneous and homogeneous CVD, respectively. For instance, homogeneous CVD will occur by dissociation of the ground electronic state of silane, as in eq 13, after the net excitation of silane molecules by about 23 CO_2 laser photons. This can occur either by collisional multiple-photon absorption and dissociation[201] or by excitation by collisional transfer from absorbing molecules.[192]

In one study of the deposition of large-area Si films by CW CO_2 laser heating of gas-phase silane, the steady-state gas temperature was estimated by balancing energy input and heat flow.[201] An effective $E_{act} = 46 \pm 5$ kcal/mol was obtained from the silicon deposition rate and the gas temperature that was determined. This value is consistent with the activation energy obtained in conventional gas-phase pyrolysis of silane, $\sim$52 kcal/mol (reaction 13),[192] given the uncertainties in both measurements.

Similarly, ArF excimer lasers (193 nm) have been used to deposit silicon in both perpendicular[204-206] and parallel[204] geometries, and F_2 excimer lasers (157 nm) have also been used to deposit amorphous silicon from silane.[207] With parallel illumination (193 nm), the deposits are amorphous unless the surface is heated.

Silane has a very small linear absorption cross section at 193 nm, reported to be 1.2×10^{-21} cm^2,[208] so the photolytic deposition rate using ArF lasers is very slow. Recent work suggests that even this small cited linear cross section may be an overestimate and that the measured absorption at 193 nm is likely due to two-photon absorption with cross section roughly 6×10^{-44} cm^4 s.[209] Consequently, these cited studies of 193-nm deposition of Si actually involve two-photon absorption by SiH_4. One-photon absorption becomes important in SiH_4 for $\lambda \lesssim 155$ nm. At 157 nm (F_2 excimer laser) the single-photon cross section of silane is relatively large, about 2×10^{-18} cm^2.[210]

After the absorption of one photon with wavelength $\lesssim$155 nm or of two or more photons of longer wavelength, there are several routes of SiH bond rupture, leading to Si, SiH, SiH_2, or SiH_3 in different electronic states.[211] Nine primary dissociation channels are available thermodynamically, though not necessarily kinetically, after the absorption of one F_2 laser photon (157 nm, 182 kcal/mol). Two reactions seem to be important in the 147-nm photolysis of silane:[212]

$$SiH_4 + h\nu \rightarrow SiH_2(^1A_1) + 2H \qquad (15a)$$

$$\rightarrow SiH_3(^2A_1) + H \qquad (15b)$$

with respective quantum yields of 0.83 and 0.17 at this wavelength. $\Delta H°_{298}$ for these two reactions are $\sim$159 and $\sim$90 kcal/mol, respectively,[211] making both routes energetically available at 157 nm as well. Though the latter pathway is energetically open after the absorption of a single ArF laser photon at 193 nm (148 kcal/mol), there is no one-photon absorption at this wavelength. Many dissociation channels to neutral and ionized species are accessible after the absorption of two 193-nm photons.[211]

Doped polysilicon has also been formed in several of these cited cases of laser pyrolytic and photolytic deposition by adding to the silane reactant a hydride that contains a dopant atom, such as B_2H_6 to get boron atoms for p-type doping and PH_3 to get phosphorus atoms for n-type doping.[24,136,178,184,185,196,200,202,204,205] In several of these pyrolytic studies, the addition of diborane to the silane gas mixture was shown to enhance the silicon deposition rate, while the addition of phosphine was found to decrease the rate. These trends are consistent with those observed in conventional CVD.[213,214]

Alternative silicon sources have also been used in the laser-assisted deposition of silicon films. The silicon deposition rate using silane has been shown to be accelerated by adding a higher order silane, such as disilane, to the reactant mixture or instead (and preferably) by using a higher order silane alone, such as disilane or trisilane.[23,206,207,215-222] These higher order silanes have two potential advantages over silane. They decompose at much lower temperatures than does silane,[223] which is important in pyrolytic deposition,[23,218] and one-photon absorption begins at much longer wavelengths for these higher order silanes than for SiH_4, which is important in photolytic deposition. For example, Si_2H_6 absorbs strongly for $\lambda \lesssim 220$ nm,[211] while silane absorbs strongly only for shorter wavelengths. Notably, the linear absorption coefficients at 193 nm for these higher order silanes are much larger than that of silane, which is favorable for photolytic deposition using ArF lasers.[207,215-217,219,220] For Si_2H_6 and Si_3H_8 the reported absorption cross sections are about 2×10^{-18} and 3×10^{-17} cm^2, respectively, at 193 nm.[210] The absorption coefficients for disilane and trisilane are also significantly larger at 157 nm (F_2 excimer laser), 5×10^{-17} and 9×10^{-17} cm^2, respectively, than for silane (2×10^{-18} cm^2).

The primary dissociation pathways in photodissociation of disilane are uncertain at present. Under low-intensity 193-nm irradiation, disilane absorbs one photon, probably exciting the 4s ← $2a_{1g}$ Rydberg transition.[210] Twenty dissociation pathways are energetically allowed after the absorption of one 193-nm photon, while 38 routes are allowed after the absorption of two photons.[211,224] Earlier work has concluded that three primary steps are important in the 147-nm photolysis of disilane:[225]

$$Si_2H_6 + h\nu \rightarrow SiH_2 + SiH_3 + H \quad (16a)$$

$$\rightarrow SiH_3SiH + 2H \quad (16b)$$

$$\rightarrow Si_2H_5 + H \quad (16c)$$

with respective quantum yields of 0.61, 0.18, and 0.21 at this wavelength. $\Delta H°_{298}$ for these three reactions are 149.5, 165.5, and 88 kcal/mol, respectively[211] (or 142, 155, and 78 kcal/mol, respectively).[217] Therefore, only the third reaction is energetically accessible after the absorption of one 193-nm photon, while each route is open at 157 nm. Because the electronic energy surfaces reached after 193- and 147-nm absorption are different, these results are probably of little value toward understanding 193-nm photolysis of disilane.

It has been suggested that the first step in 193-nm photolysis of disilane is[220]

$$Si_2H_6 + h\nu \rightarrow SiH_3SiH + H_2 \quad (16d)$$

analogous to the ultraviolet photolysis of ethane. Recent studies of disilane photolysis at 193 nm[224] using time-resolved spectroscopic probes of products and reactants immediately after photolysis suggest that the absorption transition in disilane is not totally dissociative, having a quantum yield of 0.7 for the loss of Si_2H_6, while the quantum yield for SiH_4 production is only 0.1. Since the diode laser absorption studies[224] showed that <20% of the primary products are silylenes and silylidynes, most of the silicon-bearing products are probably stable silicon monoradicals and/or unsaturated silicon hydride species. The primary dissociation pathways of disilane at 193 nm are still very uncertain.

In contrast, the first step in pyrolytic growth of silicon using disilane is thought to be

$$Si_2H_6 \rightarrow SiH_4 + SiH_2 \quad (17a)$$

which has the lowest activation energy of all disilane decomposition routes, $E_{act} \cong \Delta H°_{298} = 57.8$ kcal/mol.[211] The activation energy for the next available channel

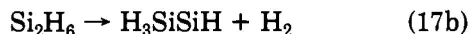

$$Si_2H_6 \rightarrow H_3SiSiH + H_2 \quad (17b)$$

is $E_{act} \cong \Delta H°_{298} = 61.3$ kcal/mol.[211] If the intermediate H_3SiSiH converts into H_2SiSiH_2 rapidly (barrier ~3 kcal/mol), then the lowest energy products of disilane dissociation

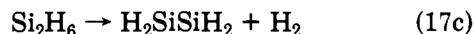

$$Si_2H_6 \rightarrow H_2SiSiH_2 + H_2 \quad (17c)$$

($\Delta H°_{298} = 38.0$ kcal/mol)[211] are formed with $E_{act} \sim 64$ kcal/mol.

In both laser-assisted photolytic and pyrolytic deposition of silicon thin films, a series of reactions take place after these nascent steps, which eventually leads to the production of higher order silicon hydrides $(SiH_2)_n$ that decompose further on the heated substrate. Study of the growth of amorphous silicon films onto a heated substrate by 193-nm photolysis of Si_2H_6 has shown that the deposition rate depends on $T_{substrate}$ very weakly, with an effective activation energy of ~2 kcal/mol,[220] which is much smaller than E_{act} for thermal CVD growth with no laser present, 37.5 kcal/mol.[191,192]

Multilayer superlattice structures of amorphous silicon with amorphous Ge or silicon nitride have been grown by alternating disilane reactant with the reactants for the other film (GeH_4 or SiH_4/NH_3 mixtures, respectively) during laser deposition.[221] Monolayer control of silicon film thickness was demonstrated in this study and in ref 222, which also showed that layer-by-layer epitaxial growth occurs during the initial stages of 193-nm photolysis of disilane on sapphire.

In analogy with common practice in conventional CVD, silicon chlorides have also been used as the gas-phase precursor in laser-assisted silicon deposition: $SiHCl_3$,[226] SiH_2Cl_2,[227] and $SiCl_4$.[228]

Germanium Deposition. Because of its lesser role in microelectronics, there has been less research on laser-assisted deposition of germanium than on the deposition of silicon. Germanium microstructures have been deposited from GeH_4 by pyrolytic laser writing using an argon ion laser (514.5 nm) focused on absorbing substrates.[229] Conventional thermal decomposition of germane has been found to produce Ge films for temperatures above ~280 °C.[230] Activation energies for heterogeneous and homogeneous growth are thought to be ~17 and 28 kcal/mol, respectively.[230]

Photodeposition of large-area Ge films has been studied by 248-[231,232] and 193-nm photolysis of GeH_4.[221,231a,233-236] The earlier studies were conducted with the laser incident on the substrate, while the later experiments were conducted with the laser collimated to a line propagating above and parallel to the substrate surface. The details of the kinetics of this photodeposition process are highly uncertain, with even the initial photolysis step in question. In both 193- and 248-nm laser-assisted deposition, digermane is thought to form and to play a major role.[234c]

Optical measurements suggest and energetics require that each GeH_4 molecule absorb (at least) two 248-nm photons in Ge deposition at this wavelength.[205,232] The absorption cross section of germane at 248 nm is 6×10^{-23} cm^2.[232] It has been hypothesized that GeH_2 is formed initially by two-photon dissociation,[232] but this is still very uncertain. In the 248-nm laser-assisted deposition,[231b] the deposition rate is only very weakly dependent on substrate temperature with $E_{act} \sim 2$ kcal/mol, as in the laser-assisted deposition of amorphous silicon from disilane.[220,221]

An insertion reaction analogous to that expected in silane pyrolysis (reaction 14) may then occur after initial photolysis:

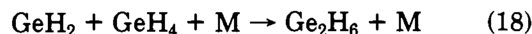

$$GeH_2 + GeH_4 + M \rightarrow Ge_2H_6 + M \quad (18)$$

where M is any third body. Optical detection of Ge and GeH during 248-nm photolysis of germane[232] suggests that there may be free H atoms, which can then promote the fast hydrogen abstraction reaction:

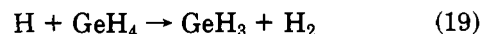

$$H + GeH_4 \rightarrow GeH_3 + H_2 \quad (19)$$

Digermane can then also form by germyl radical recombination:

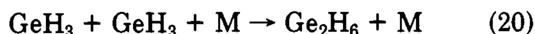

$$GeH_3 + GeH_3 + M \rightarrow Ge_2H_6 + M \quad (20)$$

Because the activation energy measured in this experiment is so small, 2 kcal/mol, digermane cannot be the final product decomposed on the surface in 248-nm laser-assisted deposition; further chemistry must occur in the gas phase after the production of digermane.

The absorption cross section of GeH_4 at 193 nm is much larger, 3×10^{-20} cm^2,[237] than at 248 nm. Also in contrast to 248-nm photolysis, the substrate temperature is an important parameter in the photolytic deposition of Ge films at 193 nm. For $T_{substrate} > 280$ °C, growth can occur without the laser and has an effective activation energy of about 21 kcal/mol,[233] in rough agreement with the non-laser thermal studies.[230] Without the laser present, growth does not occur for $T < 280$ °C on quartz. However, at these lower temperatures (150–280 °C) the laser can initiate growth, which will continue without the laser present, at a rate characterized by the same 21 kcal/mol effective E_{act} found for higher T.[233] Alternately, at these lower substrate temperatures growth can occur even faster with sustained laser irradiation. In this case, the effective E_{act} is only about 10 kcal/mol.[233] In the laser-initiated or triggered growth, it has been argued that Ge_2H_6 is formed by the laser, which then decomposes at even low temperatures on quartz. With the laser off, deposition then continues by conventional GeH_4 pyrolysis on the deposited Ge film, which can occur for $T < 280$ °C on Ge but not on quartz. In laser-sustained growth, digermane is continuously formed by the laser, leading to a smaller effective E_{act} for deposition than for CVD using germane. In fact, the role of the ArF laser in this example of Ge photodeposition may be only to convert GeH_4 to Ge_2H_6.[236]

In 193-nm photolysis of germane, the first step is thought to be the absorption of a single photon to give GeH_3;[233] again even this first step is uncertain. Germyl radicals may then recombine as in reaction 20 to form digermane.

The deposition of Ge from 193-nm photolysis of GeH_4 is greatly accelerated with the addition of NH_3.[235] Since no N is measured (<1%) in these deposited Ge films, the NH_3 acts solely as a sensitizer. It has been hypothesized that H atoms from NH_3 photolysis abstract a H from germane, as in reaction 19, to produce GeH_3. The germyl radicals recombine to produce digermane, as in reaction 20, and the digermane then decomposes on the surface.

Recent work using digermane as a precursor in 193-nm photolysis, instead of germane, has produced crystalline films for $380 < T_{substrate} < 600$ °C and amorphous films at lower temperatures.[238] However, above about 330 °C the reaction is primarily a thermal reaction induced by conventional substrate heating. At lower temperatures, the rate is controlled by gas-phase photolysis. The properties of the laser-deposited thin film are sensitive to the deposition rate and to the surface temperature, as is exemplified by the refractive index, showing that the reaction is still partly surface controlled in this regime.

Large-area germanium films have also been pyrolytically deposited by CW CO_2 laser heating of several germanium precursors: germane (10P(30) line), ethylgermane (10R(26)), diethylgermane (9R(14)), and triethylgermane (9R(14)).[239] Ge/Cd and Ge/Al films were also deposited by CO_2 laser pyrolysis of GeH_4/DMCd and GeH_4/TMAl mixtures.[239]

Ge–Si Alloy Deposition. Germanium–silicon alloy microstructures have been deposited by localized laser heating of substrates in the presence of germane/silane mixtures.[229] The laser-assisted decomposition probability of GeH_4 to form Ge was found to be about 6 times larger than that of SiH_4 to form Si in the deposited film; this is not unexpected because germane is thermally less stable than silane.

Large-area Ge–Si alloy thin films have been deposited photolytically by the 193-nm photolysis of GeH_4/Si_2H_6 mixtures.[240] Even though the absorption cross section at 193 nm is roughly 70 times larger for disilane (2×10^{-18} cm^2)[210] than for germane (3×10^{-20} cm^2),[237] the Si/Ge elemental ratio in the films was only 3 times the ratio of the Si_2H_6 and GeH_4 partial pressures (or 1.5 times the Si/Ge atomic ratio in the reactants). This suggests that disilane photolysis may initiate complex cross chemistry in the gas phase to produce $Si_nGe_mH_{2n+2m}$ species that then migrate to the surface and decompose on it. If SiH_2 is formed in the 193-nm photolysis of disilane, then in analogy with the silylene/silane insertion reaction (reaction 14)

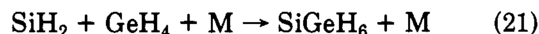

$$SiH_2 + GeH_4 + M \rightarrow SiGeH_6 + M \quad (21)$$

can occur as part of this cross chemistry. Furthermore, H atoms formed in disilane photolysis can react with germane, as in reaction 19, to form germyl radicals as part of the cross chemistry.

Ge/Si superlattices with alternating very thin layers of amorphous Ge and Si ("ordered" Ge–Si alloys) have also been grown by 193-nm photolysis, with alternately germane and then disilane in the reaction chamber.[221]

Carbon Deposition. Carbon microstructures have been deposited by focused argon ion laser heating of absorbing substrates, with C_2H_4, CH_4, and, most preferably, C_2H_2 as reactants.[241–243] With the acetylene reactant, the apparent E_{act} for the deposition of pyrolytic carbon is about 51 kcal/mol,[242] which is consistent with that measured in the conventional thermal decomposition. At high laser power, high reactant pressure, and slow lateral scanning of the substrate, carbon deposits are also observed in the attempted etching of GaAs by laser heating of the substrate in the presence of CCl_4.[244] Large-area carbon deposits have been formed by using pulsed CO_2 laser multiple-photon dissociation of several compounds, such as C_2H_4, C_2H_5Cl, and C_3H_4.[245]

Also, amorphous carbon films have been deposited by 193-nm photolysis of either C_2H_3Cl or CCl_4.[246] Initial reports[247] suggested that diamond-like films were formed by ArF laser photolysis of acetylene diluted in hydrogen, probably by a multiple-photon process; however, more recent analysis[248] has shown that heat-treated carbon black, a graphitic structure, was actually produced by laser deposition.

Silicon Carbide Deposition. Localized silicon carbide features have been formed by CO_2 laser heating of a hot-pressed SiC substrate in the presence of a SiH_4/CH_4 mixture.[249] Epitaxial SiC films have been grown on sapphire and α-Al_2O_3(0001) substrates (1150 °C) by 193-nm photolysis of Si_2H_6/C_2H_2 mixtures.[250] Purely epitaxial growth occurred only when the laser was incident on the substrate; in the parallel irradiation ge-

ometry, the films were polycrystalline. Both reactants absorb at this wavelength.

III–V Semiconductors

Films of most III–V semiconductors have been formed by using mixtures of the methyl or ethyl alkyls or the hydrides of the group III and V elements. Purely thermal growth of these compound semiconductors with the metalloorganic reagents by CVD is known as MOCVD at relatively high pressures (on the order of 1 Torr and higher) where both homogeneous and heterogeneous chemistry can be important. At lower pressures (on the order of 10^{-5} Torr and lower) where heterogeneous chemistry dominates, it is known as MOMBE (metalloorganic molecular beam epitaxy) or CBE (chemical beam epitaxy). The final goal in many of these studies of laser-assisted deposition is low-temperature growth of epitaxial thin films.

Deposition of GaAs and Related Ternary Compounds. The kinetics of conventional MOCVD of thin films of GaAs and related compounds is under intensive study.[251a] It is very complex and poorly understood. In GaAs deposition from TMGa and AsH_3, the arsine is thought to decompose heterogeneously by adsorption and loss of H to the surface. Though TMGa can decompose homogeneously by DMGa–CH_3 bond scission, one recent model suggests that TMGa decomposition on the surface is probably more important in determining the growth rate under common growth conditions, though these gas-phase processes may contribute to the observed carbon contamination in the GaAs films.[251a] Use of alternate reactants for GaAs and other III–V semiconductor MOCVD is under active investigation. Use of the ethyl compounds TEGa and TEAl instead of methyl compounds for $Al_xGa_{1-x}As$ growth produces less carbon contamination in the films because of the possibility of β-hydride elimination (as with TEGa $\rightarrow$ DEGaH + C_2H_4) in addition to bond scission (producing C_2H_5).[251b–d] The use of arsenic precursors other than arsine, such as TMAs, TEAs, and *tert*-butylarsine ($H_2AsC_4H_9$ (TBAs)), is under study for safety reasons.[251c,d] There is some evidence that after β-hydride elimination, TBAs converts to arsine in the deposition reactor.

Laser pyrolytic deposition of GaAs has been demonstrated by focused argon ion laser heating of Si or GaAs substrates using $Ga(CH_3)_3$ [TMGa] or $Ga(C_2H_5)_3$ [TEGa] as the source of Ga and AsH_3 as the As source.[252–260] In one case p-type-doped GaAs was grown by adding DMZn or DEZn to the reaction mixture to provide the Zn dopant.[260] Similarly, GaP has been deposited locally by pyrolysis of TMGa/*tert*-butylphosphine mixtures.[261] Ternary III–V semiconductors have also been grown by adding a third reactant to the GaAs reactant mixture: PH_3 for GaAsP,[254,255] $In(C_2H_5)_3$ for InGaAs,[255] or TMAl for AlGaAs.[259] In most of these cited studies, the III–V semiconductor film was deposited epitaxially on the substrate.

To date, these laser-assisted processes have not been modeled. Heterogeneous processes are expected to dominate the kinetics of these surface-heated depositions.

Stepwise monolayer growth of alternately Ga and As has been achieved in laser-assisted atomic layer epitaxy (ALE) of GaAs within a reasonably wide range of operating conditions.[256–258] Alternating gas pulses of TMGa or TEGa, and then AsH_3, enter the reactor in this process. In one series of studies performed in a low-pressure reactor,[256,257] ALE was observed only when the laser was chopped, impinging the surface only during the TMGa (or TEGa) cycle. Apparently, during the laser cycle $Ga(CH_3)_n$ reacts selectively with the exposed As surface sites to form one Ga monolayer, which reacts rapidly with AsH_3 during the next part of the cycle. In contrast to the low-pressure studies, in an atmospheric reactor,[258] ALE was observed with the laser on during either the Ga or As cycle; this has not been fully explained. Because growth in each cycle is limited to one monolayer, even with a large variation of experimental parameters, such as temperature ($T_{substrate} + \Delta T_{laser}$) and reactant flux, flat-topped structures can be grown even when the temperature rise caused by laser heating is not uniform across the substrate. It has been suggested that laser-assisted ALE of GaAs is not a purely thermal effect. In one study,[257] ALE was observed with 355- or 514.5-nm photons from an argon ion laser, but not with 1.06-μm photons from a Nd^{3+}:YAG laser or with conventional heating. The mechanistic origin of this observation is still under investigation.

Large-area GaAs polycrystalline and epitaxial crystalline thin films have been grown by using 193-nm radiation from an ArF laser directed parallel to or normal to the substrate; in the latter arrangement growth proceeds photolytically at low intensities, as in the former geometry. The gas-phase sources of Ga have been TMGa, TEGa, or triisobutylgallium (TIBGa), while arsine or trimethylarsenic (TMAs) has usually been the source of As;[262–271] CO_2 lasers have also been used to promote deposition.[272] In ArF laser assisted deposition, the addition of TMAl to the TMGa and AsH_3 reactants has produced AlGaAs.[263] GaAs, AlAs, and AlGaAs thin films have also been photodeposited by 193- and 248-nm irradiation of gas-phase TMGa–TMAs and TMAl–TMAs Lewis acid–base adducts.[273] Photolysis in the parallel geometry produced films with the same composition of group III and V elements as the adducts. Perpendicular irradiation of the substrate did not yield stoichiometric films, probably because of desorption.

Gas-phase photolysis of TMGa/TMAs mixtures at 193 nm to form Ga and As atoms can occur by the following hypothesized steps:

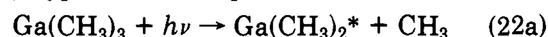

$$Ga(CH_3)_3 + h\nu \rightarrow Ga(CH_3)_2{}^* + CH_3 \quad (22a)$$

$$Ga(CH_3)_2{}^* \rightarrow GaCH_3 + CH_3 \quad (22b)$$

$$Ga(CH_3)_2{}^* + h\nu \rightarrow GaCH_3{}^* + CH_3 \quad (22c)$$

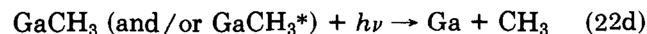

$$GaCH_3 \text{ (and/or } GaCH_3{}^*) + h\nu \rightarrow Ga + CH_3 \quad (22d)$$

$$GaCH_3{}^* \rightarrow Ga + CH_3 \quad (22e)$$

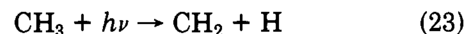

$$CH_3 + h\nu \rightarrow CH_2 + H \quad (23)$$

with analogous reactions for $As(CH_3)_3$, where the asterisk denotes internal excitation.

The energies needed to break the first, second, and third Ga–CH_3 bonds in TMGa are ~61, ~35, and ~76 kcal/mol, respectively, while the first bond energy in TMAs is ~67 kcal/mol and the average As–CH_3 bond energy is ~58 kcal/mol.[64] Therefore, a minimum of two 193-nm photons is required to strip the three methyl radicals from both TMGa and TMAs. Since one

193-nm photon has enough energy to break the first two Ga–CH_3 bonds in TMGa, with ~52 kcal/mol excess energy, it is quite likely that reactions 22a,b occur rapidly sequentially, followed quickly by the absorption of a second photon in reaction 22d.[267] Since the second bond energy in TMAs is probably the weakest of the three (in analogy with other trimethylmetals), the energetics suggest that this sequence is probably also true for TMAs. Electronically excited Ga is formed during deposition, presumably due to reaction 22d, which fluoresces with an intensity varying quadratically with laser intensity.[267] In the absence of saturation, this implies a two-photon process with rapid thermal dissociation of DMGa by reaction 22b, and not a three-photon process, which would include photolysis of DMGa in reaction 22c. No statistical analysis of CH_3 group removal from DMGa or DMAs has been performed, as has been done for the 193-nm photolysis of $Fe(CO)_5$,[115] to assess the importance of reaction 22b. Note that ref 71 reports that $GaCH_3$ and $Ga(CH_3)_2$ were detected by laser ionization mass spectrometry after 248- and 193-nm photolysis of TMGa. Since DMGa was produced in low abundance at 193 nm and higher abundance at 248 nm, while relatively more $GaCH_3$ was seen at 193 nm than at 248 nm, DMGa was hypothesized to be an intermediate transient fragment.[71d] Also, ref 274 reported that $GaCH_3$ is formed when TMGa is photolyzed at 222 nm (KrCl laser) at low fluence, possibly by reactions 22a and 22b. Both 193- and 222-nm photons have enough energy to break the first two Ga–CH_3 bonds, but not the third. Ionic fragmentation can occur at higher fluence (222 nm).

The absorption cross sections at 193 nm are 1.7×10^{-17} and 3.9×10^{-17} cm^2 for the TMGa and TMAs photodissociation step, respectively (eq 22a). The model used in ref 267 suggests that $GaCH_3$ and $AsCH_3$ have comparable absorption cross sections, $\sim 4 \times 10^{-17}$ cm^2, while the upper limit of the measured methyl photolysis cross section at 193 nm is an order of magnitude smaller, $<3 \times 10^{-18}$ cm^2.

Recently, laser-assisted MOMBE of GaAs and AlGaAs has been investigated by using 193-nm ArF laser radiation within an otherwise conventional MOMBE chamber.[275] For GaAs epitaxial deposition, the reactants were TEGa and As_4. On GaAs substrates the growth rate was spatially selectively enhanced over normal rates for MOMBE growth only when the substrate temperature was below ~450 °C. The laser apparently pyrolyzed surface-adsorbed TEGa. In fact, the laser was found to depress the growth of GaAs on $(Ca,Sr)F_2$, probably because Ga atoms, which are weakly bound on this surface, desorb when the surface is heated by the laser.

In related studies, the levels and nature of surface-bound carbon were measured by XPS for either TMGa or TEGa adsorbed on GaAs(100) prepared in UHV. Without laser irradiation, these adsorbates were found to be dissociatively chemisorbed. After laser irradiation at 193 nm, the carbon levels were remeasured to determine the laser-assisted rate of carbon removal from the surface.[276] At low laser fluence, the removal rate is slow and increases faster than linearly with fluence, suggesting a two-photon photodissociation mechanism. At higher fluences, the carbon removal rate increases even more rapidly with fluence and is independent of wavelength (i.e., it was the same at 193 and 351 nm for ~200 mJ/cm^2 fluence), suggesting pyrolytic decomposition of the chemisorbed species, as was hypothesized in the laser MOMBE investigations.[275] Photodecomposition of chemisorbed TMGa and TEGa is similar, except TMGa decomposes about 20 times slower.

Laser-assisted MOMBE has also been investigated for AlAs and Al growth using TIBA as the aluminum source and As_4 as the arsenic source, with an ArF laser (193 nm) incident on the substrate.[277] At 350 °C substrate temperature, Al deposition was observed only at the site of laser irradiation, and the growth of stoichiometric AlAs was about 20 times faster with laser irradiation.

The influence of excimer laser radiation on epitaxial growth of GaAs using a heated Ga metal reservoir as the source of Ga atoms along with $AsCl_3$ and H_2 was examined with 222 (KrCl laser), 248 (KrF), 308 (XeCl), and 351 nm (XeF) radiation.[278] It was found that 248-nm radiation incident on the substrate accelerated the growth rate, while the other laser lines had no effect. When the Ga atom source was instead irradiated with one of the lasers, 248-nm radiation decreased the growth rate markedly; the only other laser to have any effect on the growth rate was the 222-nm line, which slightly decreased the growth rate. It was thought that the rate enhancement with substrate irradiation may be due to excitation of GaCl or $GaCl_2$, while the rate decrease with Ga source irradiation may be due to photoinduced reduction of $AsCl_3$ by H_2. These hypotheses have not been proven.

InP and InSb Deposition. Much less work has been done on laser deposition of In-based III–V semiconductor thin films. InP films have been grown by 193-nm photolysis of $P(CH_3)_3$ [TMP] or PH_3 with the gaseous adduct $(CH_3)_3InP(CH_3)_3$, which decomposes to $In(CH_3)_3$ [TMIn] and $P(CH_3)_3$ at the temperatures used in these studies.[49,279-281] In the presence of small amounts of water vapor and oxygen indium oxide films are grown with stoichiometries close to In_2O_3.[279]

The energy of the first P–CH_3 bond in TMP is ~72 kcal/mol, while the average bond energy is ~69 kcal/mol.[64] At least two 193-nm photons must be absorbed by TMP to produce P + $3CH_3$. Since one 193-nm photon has enough energy to break two P–CH_3 bonds in $P(CH_3)_3$ (if the second P–CH_3 bond is relatively weak, as is expected), photolysis of this reactant may follow that of TMGa in reactions 22, with PCH_3 formed after the absorption of the first photon and free P atoms, probably electronically excited, produced after the absorption of the second photon.

The first, second, and third In–CH_3 bond energies in TMIn are ~49, ~29, and ~39 kcal/mol, respectively.[64] Because one 193-nm photon can break all three In–CH_3 bonds in $In(CH_3)_3$, In atoms may be produced after the absorption of only a single photon, perhaps by[1]

$$In(CH_3)_3 + h\nu \rightarrow In(CH_3)_2^* + CH_3 \quad (24a)$$

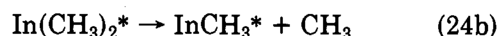

$$In(CH_3)_2^* \rightarrow InCH_3^* + CH_3 \quad (24b)$$

$$InCH_3^* \rightarrow In + CH_3 \quad (24c)$$

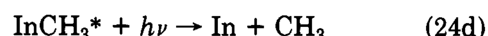

$$InCH_3^* + h\nu \rightarrow In + CH_3 \quad (24d)$$

This hypothesized mechanism includes the possibility of photolyzing $InCH_3^*$. If one-photon dissociation of TMIn were dominant, the production rates of In and

P atoms would have different fluence dependences, and the stoichiometry of laser-deposited InP films would be expected to depend on fluence; this has been confirmed.[1]

InSb deposition has been studied by 193- and 248-nm irradiation of a GaAs substrate in the presence of TMIn and TMSb (trimethylantimony) reactants.[282] These two reagents have roughly the same absorption cross sections at each of these two wavelengths, $\sim 10^{-17}$ cm^2 at 193 and $\sim 10^{-18}$ cm^2 at 248 nm. In the reported preliminary study, the photolytically grown films were stoichiometric InSb and were polycrystalline. With 193-nm photolysis, only one photon is energetically needed to dissociate TMIn to In + 3CH_3. The first bond energy of TMSb is ~61 kcal/mol and the average bond energy is ~54 kcal/mol, so two photons must be absorbed to form Sb atoms,[64] probably as in TMGa photolysis (reactions 22). One 248-nm photon has approximately the same energy as the sum of the three In–CH_3 bond energies, within experimental uncertainty. Therefore, two 248-nm photons are probably needed to photolyze TMIn to form In atoms, as is likely also true for TMSb photolysis to form Sb.

II–VI Compound Semiconductors

Recent work in epitaxial photochemical deposition of II–VI semiconductors has been reviewed recently, covering laser- and lamp-assisted and Hg-sensitized deposition.[283] The key issue in the deposition of small-band-gap II–VI semiconductors, such as HgCdTe and HgTe, is maintaining sharp interfaces. This is accomplished by operating at low substrate temperatures to prevent atomic diffusion. By using a laser or some other light source to dissociate one of the reactants, deposition can be conducted at a lower substrate temperature than by thermal CVD. Only the recent work in laser-assisted deposition is discussed here; deposition studies employing ultraviolet lamps are mentioned in the citations of the laser studies. In the laser studies of thin-film growth, the excimer laser is parallel to the surface, photolyzing only gas-phase reactants.

Epitaxial HgCdTe films have been grown on CdTe substrates by ArF laser (193 nm) photolysis of DMHg/DMCd/DMTe mixtures, with the laser directed parallel to the heated substrate (150 °C), as stated above.[284] In this work, the decomposition of each of the reactants (M = Hg, Cd, or Te) was reported to be by

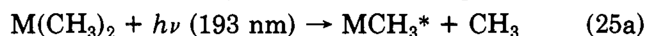

$$M(CH_3)_2 + h\nu \text{ (193 nm)} \rightarrow MCH_3^* + CH_3 \quad (25a)$$

$$MCH_3^* \rightarrow M + CH_3 \quad (25b)$$

as given in reaction 4. This mechanism is certainly reasonable for the photodecomposition of the Hg and Cd precursors, which have first and second bond energies ~59 and ~3 kcal/mol for DMHg and ~59 and ~13 kcal/mol for DMCd, respectively.[64] There is relatively little information about the bond energies for DMTe. Recent measurements suggest that the first bond energy in DMTe is ~46 kcal/mol[285] and that free Te atoms (+2CH_3) are formed[286] in (the low fluence) 248-nm photolysis of DMTe.[283e] If true, DMTe also decomposes by reactions 25. ($TeCH_3$ has been detected in the 248-nm photolysis of DMTe,[71] but it may be a transient species.)

Similarly, epitaxial growth of CdTe on GaAs at 165 °C has been demonstrated by laser-assisted MOCVD via KrF laser (248 nm) and ArF laser (193 nm) photolysis of DMCd/DETe mixtures.[31,286,287] From about $T_{substrate}$ = 150–300 °C, the photolytic deposition rate in these experiments was approximately constant and was significantly faster than the rate with equivalent substrate heating and no laser present. Since DMCd readily dissociates at these substrate temperatures, the rate-limiting step is DETe photodissociation. In these studies, the photolysis of DETe at 248 nm was shown to produce the $^3P_2$ ground state of Te, while 193-nm photolysis yielded Te atoms distributed among the $^3P_2/^3P_1/^3P_0$ states in the ratio 13/2/1.[288] Apparently, in 248-nm photolysis (115 kcal/mol) cleaving of both Te–ethyl bonds occurs, with the photon energy barely exceeding the estimated value of $\Delta H°_{298}$ for DETe into Te + 2C_2H_5 (~112 kcal/mol).[283d] The production rate of Te was observed to be linear with laser intensity at 248 nm by using laser-induced fluorescence, showing that photolysis of DETe is probably due to a one-photon process, though this is not certain.

CdTe film quality was observed to be about the same at 193 and 248 nm in these experiments. Photolysis at shorter wavelengths, such as 193 nm, is usually avoided in photodeposition when dissociative absorption bands are suitably strong at longer wavelengths, such as 248 nm in this case. Though the absorption coefficient is sometimes larger at shorter wavelengths, there is a greater probability of secondary photolysis of volatile radicals and molecules. This can lead to the introduction of impurities into the film, such as carbon.

Also, HgTe films have been deposited on GaAs at $T_{substrate}$ = 165 °C using 248 nm to photolyze the Te source DETe and either DMHg or divinylmercury [$(CH_2CH)_2Hg$ (DVHg)] as the Hg source.[31] DVHg was synthesized for the first time in the cited study and was used instead of the more readily available precursor DMHg because it decomposes at a relatively lower temperature (200 vs 350 °C) and because it has a relatively larger absorption cross section at 248 nm ($\sim 4.4 \times 10^{-19}$ vs $\sim 1.5 \times 10^{-19}$ cm^2). Stoichiometric HgTe films were obtained by using a DVHg/DETe partial pressure ratio of 1.3/1, while even much higher DMHg/DETe reactant ratios (27/1) still produced mercury telluride that was 20% deficient in Hg.

Because 248-nm photons appear to have barely enough energy to remove both ethyl groups from DETe, photolysis at longer wavelengths, such as by 254 nm from Hg lamps, requires either the absorption of two photons or other processes to help form free Te atoms. This may be the reason why 254-nm irradiation of neat, flowing DETe (absorption cross section $\sim 1.5 \times 10^{-18}$ cm^2) does not produce Te films locally, but downstream from the site of initial irradiation.[283] This has been explained by the following mechanism:[283]

$$Te(C_2H_5)_2 + h\nu \rightarrow TeC_2H_5 + C_2H_5 \quad (26a)$$

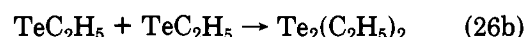

$$TeC_2H_5 + TeC_2H_5 \rightarrow Te_2(C_2H_5)_2 \quad (26b)$$

$$Te_2(C_2H_5)_2 + h\nu \rightarrow Te(C_2H_5)_2 + Te \quad (26c)$$

At these longer wavelengths, the TeC_2H_5 produced in reaction 26a would not have enough energy to decompose any further. This route could be important only if the absorption cross section of Te_2Et_2 far exceeded that of TeEt. At present, this mechanism is speculative.

A different mechanism of DETe decomposition has been proposed for CdTe epitaxy by photolysis of

DMCd/DETe mixtures in H_2 carrier gas.[283] In this case, methyl radicals from DMCd photolysis (reactions 4 and 25) lead to the production of H atoms by

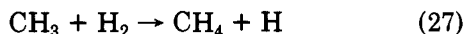

$$CH_3 + H_2 \rightarrow CH_4 + H \quad (27)$$

which then may catalyze the DETe decomposition:

$$Te(C_2H_5)_2 + H \rightarrow Te + C_2H_5 + C_2H_6 \quad (28)$$

Again, this possible mechanism is still speculative.

Parallel to these investigations of photon-assisted, low-temperature deposition of CdTe, HgTe, and HgCdTe are several efforts trying to lower the temperature needed for conventional CVD by using alternative precursors. For example, tellurium precursors such as $Te_2(CH_3)_2$, which are less stable than the more commonly used DMTe and DETe, have been used.[283] These alternative precursors are also candidates for photodeposition.

Most studies of II–VI semiconductor deposition, including all the examples cited here so far, proceed by the dissociation of gas-phase species. Recently, the surface chemistry[289] and photolytic decomposition[290] of adsorbed layers of DMCd and DMTe at 295 K in UHV have been studied. ArF laser (193 nm) irradiation photolyzes DMTe adsorbed at submonolayer coverages on gold to form metallic Te with negligible carbon contamination. In contrast, DMCd adsorbed on amorphous SiO_2 desorbs (~80%) and decomposes (~20%) upon 193-nm irradiation, forming adsorbed Cd and carbon as hydrocarbon and carbidic impurities.[290] The resulting chemisorbed methyl radicals desorb and do not decompose at 193 nm at low fluence (0.25 J/cm^2).

C. Compound Insulators

Several oxide and nitride insulator films have been grown using a semiconductor or metal precursor and N_2O for oxygen or NH_3 for nitrogen. Laser pyrolytic deposition follows the analogous thermal CVD reaction closely. In photolysis, usually one of the two reactants absorbs strongly, while the other absorbs relatively weakly. The strongly absorbing species dissociates and controls the reaction chemistry. Many studies of insulator deposition have been conducted using ultraviolet lamps by direct excitation of the reactants or by mercury sensitization. These topics have been reviewed recently,[1] and are not covered here.

Silicon Dioxide Deposition. In analogy with conventional CVD, lasers have been used to heat surfaces locally to assist the deposition of silicon dioxide using buffered silane/nitrous oxide mixtures, with the probable overall reaction

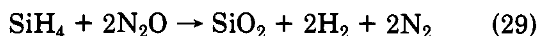

$$SiH_4 + 2N_2O \rightarrow SiO_2 + 2H_2 + 2N_2 \quad (29)$$

Using this mixture silicon dioxide rods have been grown pyrolytically with a focused krypton ion laser at 530.9 nm,[291] and silicon dioxide microlenses have been grown pyrolytically with a focused CO_2 laser on a quartz substrate and an argon ion laser on a Si substrate.[292,293]

Large-area stoichiometric SiO_2 films have been grown photolytically with a 193-nm ArF laser focused to a line above and parallel to the substrate in the presence of SiH_4/N_2O mixtures.[294-296] SiO_x has also been deposited by using KrF laser (248 nm) photolysis of $SiH_4/O_2/N_2$ mixtures[297] and by ArF laser photolysis of Si_2H_6/N_2O mixtures.[298]

The exact steps in photolytic deposition of SiO_2 films are not known. However, in SiO_2 deposition from 193-nm photolysis of SiH_4/N_2O mixtures, the production of oxygen atoms from nitrous oxide photolysis

$$N_2O + h\nu \xrightarrow{\lambda < 260 \text{ nm}} N_2 + O(^1D) \quad (30)$$

is probably the first step, since the absorption cross section of N_2O at 193 nm (8×10^{-20} cm^2)[299] is much larger than that of SiH_4. The following general steps in SiO_2 deposition have been hypothesized recently.[1] $O(^1D)$ is probably relaxed rapidly by collisions to form $O(^3P)$, which reacts with SiH_4

$$O(^3P) + SiH_4 \rightarrow SiH_3 + OH \quad (31)$$

to produce SiH_3, which may also be formed in the subsequent reaction

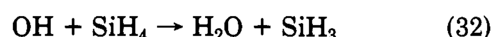

$$OH + SiH_4 \rightarrow H_2O + SiH_3 \quad (32)$$

SiH_3 can undergo disproportionation to produce SiH_2 radicals:

$$SiH_3 + SiH_3 \rightarrow SiH_2 + SiH_4 \quad (33)$$

Reactions of N_2O with SiH_2, or less likely with SiH_3, will form SiO_mH_n products. After further reaction of these intermediates with SiH_2, SiH_3, and O, more complex species are produced, $(SiO_xH_y)_z$, which migrate to the heated substrate surface and decompose to form the SiO_2 film. The last steps are very complex and have not been investigated yet.

GeO_2–SiO_2 glass has been photodeposited by 193-nm photolysis of $GeH_4/SiH_4/N_2O$ mixtures.[300] Though the absorption cross section of germane (3×10^{-20} cm^2)[237] is much greater than that of silane at this wavelength and is, in fact, comparable to that of nitrous oxide, the Ge/(Ge + Si) fraction in these films is close to the $GeH_4/(GeH_4 + SiH_4)$ fraction in the reactant mixture. Oxygen atoms from nitrous oxide photolysis react with both the silane and germane and control the rate of reaction.

Silicon Nitride Deposition. As in conventional CVD, silicon nitride films have been grown by using buffered SiH_4/NH_3 gas mixtures, with ammonia replacing the nitrous oxide used in silicon dioxide film growth. Localized deposits have been formed by using localized heating of the substrate with this mixture.[292,293] Large-area films have been grown by CO_2 laser gas-phase heating and homogeneous decomposition[301] and by photolysis of this mixture with an ArF laser parallel to the substrate.[302-304] Silicon nitride films have also been deposited by ArF laser photolysis of disilane/ammonia mixtures.[221,304-306]

The net kinetics of silicon nitride deposition by CW CO_2 laser heating of gas-phase SiH_4 in the presence of NH_3 have been investigated by measuring the individual Si and N deposition rates as a function of gas and surface temperature.[301] The gas temperature was determined from steady-state energy balance between laser absorption and heat flow, while the substrate temperature was controlled directly. Up to a gas-phase temperature of 750 °C, the effective E_{act} for the silicon deposition rate was ~44 kcal/mol, which is nearly the value that was obtained in the absence of NH_3.[201] At higher temperatures, the rate of silicon deposition was limited by the flow rate of silane. The ratio of the deposition rates of N atoms to that of Si atoms de-

pended weakly on the substrate temperature, with an effective $E_{act} \sim 4.5$ kcal/mol. Consequently, the rate of deposition of the silicon nitride film is controlled essentially by the gas temperature, while the relative Si/N stoichiometry is controlled by the substrate temperature.

The individual steps of this process are not well understood, but some things are clear.[301] Since the activation energies for the initial step in thermal decomposition of silane and ammonia are ~52 and ~91 kcal/mol, respectively, laser heating initially decomposes SiH_4 (to $SiH_2 + H_2$). NH_3 does not decompose unimolecularly but instead reacts with products, such as SiH_2, in the gas and on the surface to form $Si_xN_yH_z$ intermediates that decompose further on the surface. Because the substrate temperature affects the Si/N ratio in the film, some of these intermediates must be formed on the surface.

In silicon nitride deposition by 193-nm photolysis of SiH_4/NH_3 mixtures, the first step is probably photodissociation of ammonia:

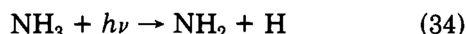

$$NH_3 + h\nu \rightarrow NH_2 + H \quad (34)$$

where the NH_2 is formed in its ground state with nearly unity efficiency.[307] The low-intensity absorption cross section of ammonia at 193 nm is 1×10^{-17} cm^2.[302] At high intensities, a second photon may be absorbed by the NH_2[1] to form NH + H. Silane, which absorbs very weakly at this wavelength, probably reacts with the ammonia photolysis products in a sequence similar to that in SiO_2 deposition, though the exact pathway is not known. Two-photon dissociation of silane is probably unimportant here.

Apparently, the only study of the gas-phase kinetics during photolytic silicon nitride film formation is the recent work[304b] in which steady-state and time-resolved molecular beam sampling mass spectrometry was used to examine products of 193-nm photolysis of silane/ammonia mixtures. All possible aminosilanes, SiH_3NH_2, $SiH_2(NH_2)_2$, $SiH(NH_2)_3$, and $Si(NH_2)_4$, were found in steady state, in addition to the higher order silanes Si_2H_6 and Si_3H_8. Surprisingly, time-resolved analysis showed that each of these gas-phase products is formed <0.1 s after the laser pulse and that secondary photolysis is not needed to form each of the observed products. The authors hypothesize that after reaction 34, SiH_3 is promptly formed by

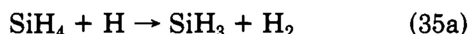

$$SiH_4 + H \rightarrow SiH_3 + H_2 \quad (35a)$$

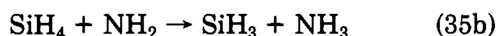

$$SiH_4 + NH_2 \rightarrow SiH_3 + NH_3 \quad (35b)$$

SiH_2 can form by SiH_3 disproportionation, reaction 33, and higher order silanes can be produced by SiH_3/SiH_3 and by SiH_2/SiH_4 recombination, reaction 14. Aminosilanes are initially formed by reactions such as

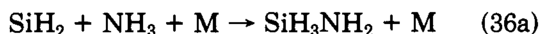

$$SiH_2 + NH_3 + M \rightarrow SiH_3NH_2 + M \quad (36a)$$

$$SiH_3 + NH_2 \rightarrow SiH_2NH_2 + H \quad (36b)$$

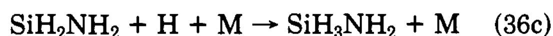

$$SiH_2NH_2 + H + M \rightarrow SiH_3NH_2 + M \quad (36c)$$

where M is any third body, followed by reactions such as

$$SiH_n(NH_2)_m + NH_2 \rightarrow SiH_{n-1}(NH_2)_{m+1} + H \quad (37a)$$

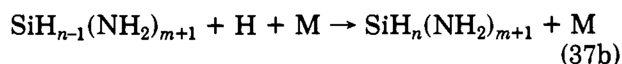

$$SiH_{n-1}(NH_2)_{m+1} + H + M \rightarrow SiH_n(NH_2)_{m+1} + M \quad (37b)$$

Presumably, these aminosilanes decompose on the heated substrate to form the silicon nitride film, as in plasma CVD. The details of this mechanism are still very uncertain.

In silicon nitride film deposition by ArF laser (193 nm) irradiation of Si_2H_6/NH_3 mixtures,[221,304-306] photolysis of the silicon-bearing reactant, disilane, is probably very important in the deposition kinetics, as is the photolysis of NH_3, because of the large absorption cross section of Si_2H_6 at 193 nm. This has yet to be studied in detail.

Aluminum Oxide and Nitride Film Deposition. Aluminum oxide films have been deposited by ArF laser (193 nm) photolysis of TMAl/N_2O gas mixtures.[53,308-310] The absorption cross sections of the two reactants are comparable at 193 nm, on the order of 10^{-19} cm^2. After the first 193-nm photon is absorbed by the TMAl dimer, TMAl is produced with what appears to be almost (but not) enough energy to break one Al–CH_3 bond. Subsequent absorption of photons can break up to two Al–CH_3 bonds per 193-nm photon. The resulting Al atom or $Al(CH_3)_x$ radical probably reacts with $O(^1D)$ from N_2O photolysis (reaction 30). In the presence of small amounts of oxygen (due to imperfect vacuum conditions in the chamber), aluminum oxynitride films are formed as the result of 193-nm photolysis of TMAl/NH_3 mixtures.[311] Both TMAl and NH_3 absorb at 193 nm strongly, and Al or $Al(CH_3)_x$ reacts with NH_2 (reaction 34) and residual oxygen. The mechanistic details of aluminum oxide and nitride photodeposition still need further study.

Other Insulators. Several other oxides have been deposited by using laser-assisted deposition. Some of these are insulators, while others are large-band-gap semiconductors; they are included here because of similarities to the deposition of SiO_2 and Al_2O_3. The large-band-gap II–VI semiconductor ZnO has been photodeposited by 193- and 248-nm photolysis of DMZn/N_2O mixtures.[312] Both reactants are photodissociated in this case. TiO_2 films have been formed by CW CO_2 laser heating of quartz substrates in the presence of $TiCl_4/H_2/CO_2$ mixtures.[80]

Tin oxide has been deposited on GaAs with a focused scanning argon ion laser by pyrolytic deposition of tin from $SnCl_4$ in the presence of residual oxygen.[313] Large-area SnO_2 films have also been grown by 193-nm photolysis of $SnCl_4/N_2O$ mixtures.[314a] In this case, both reactants are photolyzed:

$$SnCl_4 + h\nu \rightarrow SnCl_3 + Cl \quad (38)$$

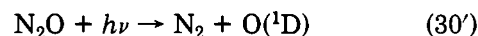

$$N_2O + h\nu \rightarrow N_2 + O(^1D) \quad (30')$$

with absorption cross sections 3.8×10^{-17} and 7.9×10^{-20} cm^2, respectively. When the ArF laser photolyzes the gas but does not impinge on the SiO_2 substrate, a white powdery deposit forms, which is presumably $SnOCl_2$, due to

$$SnCl_3 + O(^1D) \rightarrow SnOCl_2 + Cl \quad (39)$$

When the laser is incident on the substrate, this $SnOCl_2$ intermediate is apparently converted to a conductive SnO_2 film, possibly by a thermally induced reaction. The exact mechanism is not clear.

Mixed Cr_2O_3/CrO_2 thin films and Cr_2O_3 single crystals have been directly written from CrO_2Cl_2 vapor by

using an argon ion laser operating with the 488- and 514.5-nm lines.[314b] The deposition is initially photolytic, and after some deposition the laser can heat the surface and induce pyrolytic deposition. CrO_2 is first formed, possibly by the sequential elimination of Cl from CrO_2Cl_2. Laser heating of the deposited film not only helps induce further decomposition but also helps transform the deposited CrO_2 into Cr_2O_3 by oxygen elimination.

Other insulators have also been deposited by using laser chemical processing. TiC has been deposited on CO_2 laser heated quartz and stainless steel in contact with $TiCl_4/CH_4$ gas mixtures.[80] PN films have been deposited on InP at relatively low temperatures (300 °C) by ArF laser (193 nm) photolysis of PH_3/NH_3 mixtures in parallel geometry.[315]

In limited studies, insulating polymer films have also been formed by using laser-assisted deposition. A solid polymer with poly(dimethylsiloxane) structure has been deposited by using a TEA CO_2 laser to irradiate a methyl methacrylate (MMA)/SiH_4 mixture.[316] Collisionally assisted infrared laser multiple-photon dissociation of the silane produces SiH_2 radicals that add to the carbon double bonds in MMA to form three-membered rings, which then decompose into a siloxane polymer. Also, 1-methyl-1-silacyclobutane has been decomposed by CW CO_2 laser heating of an SF_6 sensitizer to form an organosilicon polymer.[317]

IV. Growth Models

In section III, different examples of laser-assisted deposition were presented and were analyzed in terms of basic dissociation steps and, when known, subsequent chemical steps. Other factors, such as gas transport, can be equally important in the overall deposition process for both pyrolytic and photolytic growth from gas-phase and adsorbed reactants; this is also true for other deposition methods, such as CVD. Several groups have modeled the overall process chemistry for laser-assisted growth with the hope of explaining and predicting deposition rates, deposit morphology, and deposit localization.

Laser deposition can be conceptually described by a six-step model of basic steps that occur simultaneously during thin film growth:[81,193] (1) basic interaction of the laser with the medium, (2) transport of reactant gas to the laser interaction region, (3) primary decomposition step, (4) secondary decomposition of intermediates and transport to the film, (5) incorporation of deposit atoms into the film, and (6) transport of product gas from the film and the laser interaction region. Each of these "steps" may be complex and may vary in time, even with CW laser irradiation. These steps are currently not well characterized for many processes. Because of the complexity of modeling, the reported studies have usually treated only a few of these steps in detail, while treating the others only approximately. Furthermore, these studies have usually been applied to systems with fairly simple chemical kinetics, such as the thermal decomposition of $Ni(CO)_4$.

In step 1 the laser is absorbed by the substrate in heterogeneous pyrolytic deposition, and after rapid energy equilibration in the solid, the substrate and the surrounding gas are heated. The temperature rise can be calculated by using the time-dependent or steady-state form of the heat flow equation, as needed. Steady-state analysis suffices in many process regimes if the laser irradiation is CW. In direct laser writing with a laser of spot size w scanning relative to the surface at a speed v, steady-state analysis demands that the dwell time of the laser at that spot w/v and the pulse length of the laser (if it is indeed pulsed) greatly exceed the characteristic thermal diffusion time w^2/D, where D is the thermal diffusivity; otherwise, time-dependent analysis is required.[318] Time-dependent analysis may also be needed if the thermal properties or optical properties of the substrate change as a result of deposition.[319] In homogeneous pyrolytic deposition, the laser is absorbed in the gas by the deposit-containing reactant or by another absorber. After energy relaxation, the heat flow equation can again be used to determine the temperature profile in the gas. Homogeneous pyrolysis can also occur in cases of laser substrate heating. In photodeposition, step 1 describes photon absorption by gas-phase or surface-adsorbed reactants containing the deposit atoms. Furthermore, electron–hole pairs can be formed as a result of laser absorption in semiconductors which can affect both pyrolytic and photolytic deposition. The electron–hole pair density can be calculated by balancing photocreation of the pairs, with diffusion and losses, such as those due to direct recombination and Auger processes.

Step 2 describes the gas transport of reactants to the site of laser excitation near or at the substrate surface. As in CVD, this can be a rate-limiting step. In pyrolytic and photolytic deposition in which heterogeneous chemistry of the reactants is important, this step also includes the adsorption of reactants on the surface. Large-area and direct laser-assisted deposition differ in that in the former case transport is essentially a one-dimensional problem to or from the surface, whereas in localized processing, transport can be considered to be a three-dimensional problem. Consequently, in localized deposition, transport of reactant gas to the reaction site and of product gas from the site of deposition are less likely to be rate-limiting steps than in large-area deposition, and the local deposition rates can be much faster in direct laser writing. In localized laser deposition, the nature of gas transport depends on the Knudsen number $K_n = l/\rho$, where l is the mean free path and ρ is the characteristic size of the deposit region.[81,193] If $K_n \gg 1$, transport is in the molecular flow regime where collisions near the irradiation site are unimportant. The impingement flux of reactants incident on the laser-irradiated region is $n_g v_g/4$, where n_g and v_g are the reactant concentration and average speed, respectively. For $K_n \lesssim 1$, diffusion and, at times, also convective flow and turbulence are important if the reactive sticking coefficient is $\sim$1. When deposition rates are fast and when more than one volatile molecule is released per reactant in decomposition (as in $Ni(CO)_4$ pyrolysis where four CO molecules are released for each $Ni(CO)_4$ molecule consumed), replenishment of reactants at the deposition site can be hindered due to convection of gas products at high velocities from the reaction site. At slow deposition rates and when only one product molecule is released per reactant molecule, transport is diffusion limited for $K_n \lesssim 1$. The transport of reactants into the microreaction zone surrounding the laser focus can help ex-

plain the dependence of the deposition rate on reactant pressure, laser beam radius, and irradiation time,[17,158,320] as is discussed below in more detail.

The primary decomposition step 3 has been given for many precursors in section III. As also seen in section III, step 4, which involves possible secondary reactions and transport to the surface, can be equally important. These secondary reactions can be very complex and are usually poorly characterized; this is true for laser-assisted deposition and for non-laser methods such as CVD. When binary compounds are deposited with laser-assisted decomposition of only one of the two precursors, these secondary reactions involve the decomposition of the second reactant.

In many of the examples discussed in section III, particularly those of photodecomposition, the primary interaction of the laser produces a molecular fragment that includes the deposit atom and undesired atomic impurities such as C, O, and H. In some cases of photolytic deposition, only modest heating of the substrate is needed to decompose these intermediates into the deposit atoms and volatile products. Furthermore, when deposit atoms or intermediates are generated in the gas, they must be transported to the surface. Sometimes important chemical or physical interactions occur during this transport, at times with undesirable effects resulting from this chemistry or transport. For example, when metal atoms are generated by photolysis of gas-phase molecules, clusters of atoms can form during transport to the surface. This produces films with low adhesion that are full of voids. Moreover, any spatial selectivity derived by local laser excitation in the gas can be lost due to lateral diffusion of products during transport to the surface.

In step 5 the deposit atoms are incorporated into the film. Sometimes, this is very sensitive to surface conditions, depending on the nature of the initial substrate surface or the film already deposited, as during the epitaxial growth of thin films. Initial nucleation of the thin film from deposit atoms can be very important.

Transport of product molecules from the deposition site in step 6 can also include the desorption of volatile molecules from the surface. Many of the modeling considerations in this step are similar to and are linked to those for reactant transport to the reaction site, described by step 2.

A. Pyrolytic Deposition

Models of heterogeneous pyrolytic reactions utilize the temperature distribution produced by laser heating of the substrate. Several analytic solutions of the steady-state heat flow equation for simple cases, such as laser beam heating of a semiinfinite substrate, have been obtained[2,318,321,322] and are used in some of these models. In the simple case of a laser beam with a Gaussian profile (eq 2) of power P and beam size w, incident on a substrate with reflectivity R, absorption coefficient α, and thermal conductivity K, the temperature rise is given by[321,322]

$$\Delta T(r,z,W) = \frac{P(1-R)}{2\pi^{1/2}Kw}N(r,z,W) \qquad (40)$$

where $W = \alpha w$ and $N(r,z,W)$ is a single integral expression. All optical and thermal parameters have been assumed to be independent of temperature in eq 40. In the limit that the laser spot size w is much greater than the absorption depth $1/\alpha$

$$N(0,0,W) \rightarrow 1 - \frac{2}{\pi^{1/2}}\frac{1}{W} \quad \text{as } W \rightarrow \infty \qquad (41a)$$

N decreases parabolically near the center, and far from the center it decreases as

$$N(r,z,W) \rightarrow \frac{1}{\pi^{1/2}}\frac{1}{(r^2+z^2)^{1/2}} \quad \text{as } r/w \text{ or } z/w \rightarrow \infty \qquad (41b)$$

If the thermal conductivity is a function of temperature, the form of eq 40 is slightly different.[318,322]

When the substrate geometry or other deposition conditions are more complex, numerical analysis of the heat flow equation using finite difference or finite element analysis is needed, such as when there are multiple films on the substrate. This is particularly true when the optical and thermal properties of the substrate depend on temperature in a complex manner or when the effect of the deposit on the process must be considered. Laser heating has been examined for several cases of specific interest to localized laser CVD, such as laser absorption by (deposit-like) disks on substrates.[25,323,324a] If the laser of power P is totally absorbed near the surface of a disk of diameter d with reflectivity R and thermal conductivity K_d and if the thermal conductivity of the substrate is K_s, then the temperature rise at the edge of the disk is approximately given by[324a]

$$\Delta T(r = d/2) = \frac{P(1-R)}{2dK_s} \qquad (42)$$

If the deposit has much higher thermal conductivity than the substrate ($K_d \gg K_s$), then this expression also gives the approximate temperature rise throughout the disk. If $K_d \sim K_s$, then the temperature rise is much larger near the center of the disk than at its circumference. For $K_d = K_s$ the temperature profile resembles that of a uniform semiinfinite substrate. Figure 7 shows the temperature profiles of laser-heated Si disks on fused silica and sapphire substrates calculated by finite difference solution of the steady-state heat flow equation.[25]

These results can give some insight into the deposition process in localized CVD in which the laser focus is fixed at one spot (static conditions), by assuming these disks are the actual laser deposits.[323,324a] If the deposited material and substrate have roughly the same thermal conductivity, $K_d \sim K_s$, then as the deposit grows, the temperature distribution on the deposit surface does not change very much and deposition continues with an approximately constant growth rate as long as the laser irradiates the deposit. However, if the deposit has much higher thermal conductivity than the substrate, $K_d \gg K_s$, then as the diameter of the deposit grows, the temperature rise throughout the deposit decreases, as shown by eq 42. Therefore, the growth rate decreases with deposit size in this case and the deposit will grow to a certain size and then grow no more, even with continued laser irradiation.

The time dependence of the flux of reactants, j, to a hemispherical deposit of radius R was calculated in ref 17 and 320 to examine transport limitations during

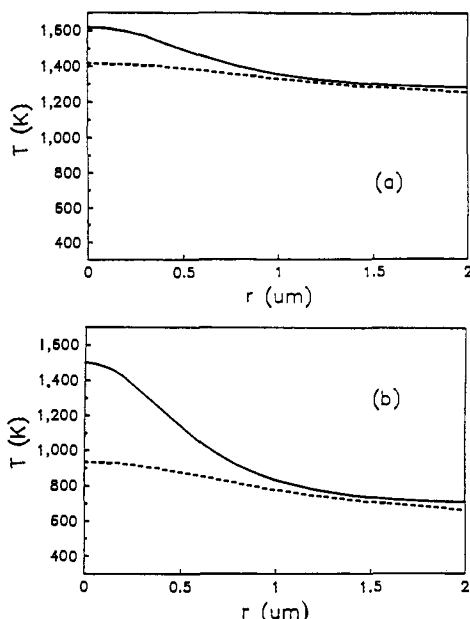

Figure 7. Calculated temperature profiles vs radial displacement (μm) for 4-μm-diameter, 0.62-μm-thick polysilicon disks for the top of the disk (solid line) and bottom of the disk (dashed line) for CW laser heating of (a) a fused-silica substrate (488 nm, 24 mW) and (b) a sapphire substrate (514.5 nm, 100 mW). (From ref 25.)

heterogeneous laser-assisted microreactions. In steady state this flux is

$$j = \frac{Dp_1}{k_B T(2D/\alpha u + R)} \quad (43a)$$

where D is the diffusion coefficient, p_1 is the reactant pressure, k_B is Boltzmann's constant, T is the temperature, α is the reactive sticking coefficient, and u is the reactant velocity. If the atomic or molecular volume of the deposit is v_1, then the steady-state rate of change of the hemisphere volume V is

$$\frac{dV}{dt} = \frac{2\pi R^2 v_1 D p_1}{k_B T(2D/\alpha u + R)} \quad (43b)$$

and the rate of change of the deposit radius is

$$\frac{dR}{dt} = \frac{v_1 D p_1}{k_B T(2D/\alpha u + R)} \quad (43c)$$

which is also the vertical deposition rate.[158] These expressions ignore transport of the product gas away from the site of deposition, convection, and thermal diffusion into the gas.

In the limit of high pressure the vertical deposition rate varies inversely as R, becoming very large for small deposits and, in fact, much larger than the deposition rates possible in large-area CVD.[17,320] (Remember that the diffusion coefficient varies inversely with pressure.) Though the local vertical deposition rate is large for small R, the rate of increase of the total deposit volume is still larger for large R and for conventional large-area CVD than for small-radius deposits.

In ref 158 the expression for the vertical deposition rate eq 43c was generalized to include buffer gas added to the reactant gas to obtain

$$\frac{dR}{dt} = \frac{\alpha v_1 p_1}{(2\pi m k_B T)^{1/2}}\left(\frac{4K_n/3\alpha}{1 + (4K_n/3\alpha)}\right) \quad (44a)$$

where $K_n = 3D_{12}/[R(8k_BT/\pi m)^{1/2}]$ and D_{12} is the binary diffusion coefficient for the reactant/buffer combination. Again, deposition is assumed to be in steady state and diffusion of products from the surface, convection, and thermal diffusion are neglected. When the Knudsen number $K_n \gg \alpha$ (the reactive sticking coefficient), eq 44a simplifies to

$$\frac{dR}{dt} = \frac{\alpha v_1 p_1}{(2\pi m k_B T)^{1/2}} \quad (44b)$$

This condition ($K_n \gg \alpha$) refers to two commonly encountered experimental conditions: (1) the free or molecular flow regime where the mean free path $l \gg R$ and (2) the regime where surface processes, such as precursor reactivity and product adsorption, are rate limiting, so $\alpha \ll 1$ (for any l and R as long as $\alpha \ll K_n$ also). In this study eq 44b was used to model one regime of local laser CVD of gold from $Me_2Au(HFAc)$.[158] Comparison of eq 44b with the measured deposition rate gave $\alpha = 0.60$. Since the deposition rate in this experiment did not depend strongly on the temperature induced by the laser, growth appeared to be limited by mass transport after a deposit was initially formed on the substrate.

When $K_n \ll \alpha$, eq 44a becomes

$$\frac{dR}{dt} = \frac{D_{12} v_1 p_1}{R k_B T} \quad (44c)$$

For $\alpha \sim 1$, this expression is valid for $l \ll R$. If there is no buffer eq 44c predicts that the growth rate is independent of the reactant pressure p_1 in this regime. If the pressure of the buffer gas $p_2 \gg p_1$, then the deposition rate increases linearly with the reactant pressure p_1 and decreases inversely with the buffer pressure p_2.[158]

More refined models of laser pyrolytic deposition include the interplay of laser heating, mass transport, surface kinetics, and surface reactivity. As mentioned earlier, even these models entail many approximations and have usually been applied to relatively simple systems. Heterogeneous decomposition of $Ni(CO)_4$ to produce Ni films has been analyzed most frequently.

One early model of localized laser CVD was applied to the growth of Ni from $Ni(CO)_4$ on silicon substrates, using a Gaussian-profiled laser for substrate heating.[81] In this quasi-steady-state analysis, closed-form numerical solutions of the heat flow equation were used to determine the temperature profile. Gas diffusion was handled by using a Green's function method. The heterogeneous reaction rate for CVD of Ni from the carbonyl, characterized in ref 107 by a Langmuir–Hinshelwood adsorption–surface reaction mechanism, was used to determine the steady-state local deposition rate. This reaction rate expression is a function of the local partial pressures of the $Ni(CO)_4$ reactant and the CO product and the local temperature. Closed-form limiting expressions for the initial deposition rate at the center of the laser spot were obtained by using the reactant pressure and the ratio of laser power P and beam radius w as parameters. In the limit low laser-induced temperature rises (small P/w), the deposition rates are surface-reaction limited and increase exponentially with P/w. For high laser-induced temperature rises (large P/w), growth is limited by gas-phase diffusion. The magnitude of this maximum, transport-lim-

ited deposition rate increases with reactant pressure. The experimental studies of local laser CVD of nickel conducted as part of this study showed saturation of the deposition rate with increasing laser power (at constant beam radius), in qualitative agreement with the model predictions.

A more recent study[319] examined laser CVD of Ni on fused quartz with $Ni(CO)_4$. The local temperature was obtained by time-dependent finite difference analysis of laser heating of the substrate and was used in the same expression for Ni CVD cited above;[107] the local $Ni(CO)_4$ and CO pressures used in this expression were obtained only approximately.[320] Notably, this investigation included variations in the deposit-related and temperature-dependent thermal and optical parameters during the course of deposition, which are extremely important for this process. Experimental deposition rates measured in this study were within a factor of ~ 2 of theory, which is quite good considering the large changes in optical and thermal parameters during deposition.

In a related, purely theoretical study, mass transport during laser CVD, in general, and laser-assisted Ni deposition from $Ni(CO)_4$, in particular, were examined.[325] Perhaps the most important contribution of this study was the inclusion of convection in mass transport, in addition to diffusion. It was found that the local reactant partial pressure near the laser microreaction site and the deposition rate are both lower when convection of the CO products from the deposition site is included in the mass transport analysis, because this convection hinders diffusion of reactants to the reaction zone.

Another totally theoretical study of heterogeneous local laser CVD was conducted recently to analyze how the deposit shape and deposition rates depend on gas transport and kinetic effects; finite element analysis was used in this study.[326] As in the other studies, nickel deposition was used as the main example in this treatment. A transient analysis of localized laser heating of the substrate was employed, along with quasi-steady-state heating of the surrounding gas region and mass transfer. In the parameterization, reaction rates were assumed to follow either Arrhenius-type of Langmuir–Hinshelwood kinetics. One important conclusion of this study is that the localized depression sometimes observed in deposits grown by static laser CVD can be attributed to two effects: to the depletion of gas and reactants at the center of the laser beam and to adsorption/desorption effects; the latter was manifest only when using Langmuir–Hinshelwood-type kinetics instead of Arrhenius-type kinetics. Furthermore, only this latter mechanism produced very deeply depressed volcanos, while both factors decreased the overall deposition rate. Two other mechanisms were found to decrease overall deposition rates without producing volcano-type structures: net convection of products from the deposition site (Stefan flow effect) and fast thermal diffusion of reactants away from the hot center of the laser-heated deposition region. No specific comparison of model predictions with published experimental data was made.

The morphology and structure of deposition features during localized surface heating have also been analyzed by using a detailed Green's function analysis to follow diffusion and kinetics.[327] Reactions of the type A + B $\rightleftarrows$ 2C and B $\rightleftarrows$ A + 2C, where A is a surface species, B is the reactant molecule, and C is the product molecule, were analyzed, which can serve as a prototype of the coupled etching and deposition reactions: $Si(s) + SiH_4(g) \rightarrow 2SiH_2(g)$ and $SiH_4(g) \rightarrow Si(s) + 2H_2(g)$. This theoretical study demonstrates why deposition rates can be much faster in localized deposition vis-à-vis large-area deposition. Furthermore, this kinetic treatment explains why attempts to deposit silicon from silane on Si surfaces can instead etch the surface in some experimental regimes.

These models qualitatively account for many of the features observed in heterogeneous, localized laser CVD. Few attempts have been made to check for quantitative agreement with experiment. Furthermore, these studies have concentrated on simple systems, where the chemical steps could be lumped into a single expression for the deposition rate. Consequently, the general value of these models for quantitative prediction of growth rates is limited. It should be remembered, however, that this complexity and lack of characterization of kinetics that affects laser CVD modeling, also plague attempts to model conventional CVD and lamp-assisted deposition.

Models of large-area pyrolytic growth by laser heating of the gas have also been developed, which include details of laser absorption, gas-phase thermalization, heat transfer to the surface, simplified reaction kinetics, and gas transport of reactant and intermediates to the surface.[201,301,328,329] These models have been applied to the deposition of amorphous silicon and silicon nitride; the results were briefly mentioned in section III.

B. Photolytic Deposition

Several models of deposition have been developed to predict growth rates from local photolysis of gas-phase and surface-adsorbed reactants. These models include only the initial photolysis event and ignore the possibility of subsequent chemistry such as recombination.

One aim of these studies has been to determine whether gas-phase or surface decomposition dominates growth in a given experimental regime. An early simple model predicted that at the center of the deposit the growth rate is proportional to $1/w$ if gas-phase photolysis dominates, where w is the laser beam radius, while the deposition rate is proportional to $1/w^2$ if surface photolysis dominates.[68] In this same study, the experimental photodeposition rate of DMCd was found to vary as $1/w^{0.73\pm0.15}$, suggesting that deposition was apparently due to gas-phase photolysis in the particular experimental regime examined. This model has been refined and used in other experimental studies to determine the relative importance of gas-phase and surface photodecomposition.[20,41]

A quite comprehensive treatment of photodeposition by a Gaussian-profiled laser has been published recently which treats gas-phase deposition in the molecular flow (free flow or "ballistic") regime and in the diffusion regime and treats surface-controlled photodeposition as photolysis of either physisorbed or chemisorbed species.[330] This study neglects chemical processes other than initial photolysis. The deposition rate at the center of the deposit was found to have the same dependence on the beam radius as determined in ref 68.

Moreover, a simple approximate expression for the deposition rate $k_{\text{photolysis}}$ as a function of radius r was obtained for gas-phase photolysis under molecular flow conditions:

$$k_{\text{photolysis}} = \frac{fn\phi_t\sigma_d(\lambda)}{2[\pi(w^2 + r^2)]^{1/2}} \frac{8w^4 + r^4}{8w^4 + \pi^{1/2}r^4} \quad (45)$$

where n is the gas density, ϕ_t is the photon flux, σ_d is the photodissociation cross section, r is the radial coordinate, w is the laser half-width at $1/e$ intensity (as in eq 2), and f is $\alpha_p/2$, where α_p is the sticking coefficient of the deposit atom on the surface. Equation 45 predicts a growth rate that decreases as $1 - (r/w)^2/2$ for $r/w \ll 1$ and decreases as $1/r$ for $r/w \gg 1$. Therefore, the photodeposit is expected to be much less localized than the Gaussian profile of the laser beam because of this very slow decrease at large r/w.

Exactly the same profile of growth rate vs r was calculated for gas-phase photodeposition in the diffusion-limited regime as in the molecular flow regime (eq 45), but the overall rate is faster (for equivalent parameters), because $f = 1$ in this case. When the sticking coefficient $\alpha_p = 1$, the deposition rate in the diffusion regime is predicted to be twice that in the free flow regime. This is reasonable because in the diffusion regime every atom produced near the surface will eventually stick to it (in fact, this is true for any nonzero sticking coefficient when there is no recombination), while in the molecular flow regime, half of the photoproduced atoms head toward the surface and half head away.

Growth rates for surface-controlled deposition were also obtained[330] and were found to have the same Gaussian spatial profile as the photolysis laser. As mentioned earlier, the growth rate for surface-controlled deposition in this model was found to vary as $1/w^2$ at the center of the spot, while for gas-phase deposition, it varied as $1/w$ (eq 45). Moreover, the ratio of the growth rate from photolysis of chemisorbed or physisorbed molecules to that from gas-phase molecules at the center of the laser spot, G, was also derived:

$$G = \frac{2\eta k_B T A(\lambda)}{\pi^{1/2} p w \sigma_d(\lambda)} \quad (46a)$$

where η is the quantum yield for dissociation of the adsorbed molecule, k_B is Boltzmann's constant, T is the temperature, $A(\lambda)$ is the absorption coefficient of a single physisorbed or chemisorbed monolayer, and p is the precursor vapor pressure for physisorbed layers and the precursor partial pressure for chemisorbed layers. This expression for G can be cast into a more useful form:

$$G = \frac{120\eta E}{w(\mu\text{m})p(\text{Torr})} \quad (46b)$$

This assumes a surface site density of $4 \times 10^{16}/\text{cm}^2$ (which is probably too high). E is the ratio of absorption coefficients for one (chemisorbed or physisorbed) monolayer to one monolayer equivalent of the gas. For DEZn, $E \sim 7$ for chemisorption and $E \sim 4.7$ for physisorption. This result suggests that for a DEZn precursor at a partial pressure of 1.5 Torr, deposition from the chemisorbed layers exceeds that from the gas for spot size $w < 0.5$ mm and that deposition from the physisorbed layers is faster than that from gas-phase photolysis for $T < 70$ °C when $w = 1$ μm.

The net photodeposition rate in this model[330] is the sum of the rates derived from gas-phase, chemisorbed layer, and physisorbed layer photodecomposition. This model showed very good agreement with the dependence of deposition rate with spot size, partial pressure, and temperature obtained in the photodeposition experiments in ref 41 and 68 using DEZn and DMCd, respectively. In particular, the deviation of the $1/w^{0.73}$ dependence of the deposition rate observed in ref 68 from the $1/w$ or $1/w^2$ model predictions made in that reference was attributed to the simplifying assumptions made in that study.

Apparently, no experiments have been conducted to compare the different model predictions obtained for the molecular flow and diffusion-limited regimes of gas transport in photodeposition. At partial pressures of added buffer gas high enough that gas-phase transport is diffusive, this model predicts no change in the photodeposition rate with buffer pressure. However, there is experimental evidence for a slow decrease of the deposition rate with added pressure,[46,90] possibly due to recombination in the gas phase.

Very recent finite difference calculations of laser-induced photochemical gas-phase processing[324b] have shown that a simple $1/w^n$ model for the deposition rate is inadequate, even when surface dissociation is neglected, because of recombination, reactions with the deposition chamber walls, and variations in the reactivity of gas-phase-generated species at different locations on the surface. These effects were not included in ref 330.

In closing this section about modeling photodeposition, we briefly note the work on surface diffusion of physisorbed reactants. In this study, surface diffusion was analyzed theoretically by using a Green's function integral technique and experimentally by examining the surface migration of tetraethyllead adsorbed on sapphire.[331] This is potentially important in the photodeposition of surface-adsorbed molecules.

C. Nucleation and Other Surface Effects

Nucleation effects can be important in many forms of thin-film growth. In a narrow sense, nucleation entails the physical processes of adatom surface adsorption, migration, desorption, formation of nuclei, and incorporation into the deposited film through either two-dimensional growth (Frank–van de Merwe), three-dimensional growth (Volmer–Weber), or a mixed-growth mechanism (Stanski–Kranstanov).[332] The sticking coefficient of adatoms formed in the gas phase or on the surface may be much greater on an predeposited film than on the initial substrate surface, so nucleation sites can accelerate physical or chemical vapor deposition. More broadly speaking, nucleation can also include chemical reactivity effects. For instance, a particular reactant containing a given deposit atom may react slowly with the initial surface and therefore decompose slowly but may react much faster with an already deposited film containing the same atom or even a different atom. In this case, chemical vapor deposition can occur much faster at nucleation (or "prenucleation") sites. Another example of this expanded concept of nucleation occurs in hybrid photolytic/pyrolytic laser-assisted deposition, in which the

substrate is initially transparent and pyrolytic deposition occurs only at nucleation regions preseeded by photolysis where the laser can be absorbed. These nucleation effects have been observed in several examples of photolytic and pyrolytic laser-assisted deposition.

Several examples of patterned growth of metals have been demonstrated by using both focused beam deposition[42,45,163,333-335] and excimer laser projection printing[26,61,62,336] to form angstrom-dimension-thick localized prenucleation sites. Growth of selective-area thin films was subsequently continued by a large-area (non spatially selective) process. Most of these studies demonstrated the deposition of patterned aluminum films.

The importance of using only surface processes in the prenucleation of large-area patterns was demonstrated in ref 336. TIBA gas was photolyzed by either 193- or 248-nm light projected through a mask to nucleate selected regions on glass (250 °C); growth was then continued by conventional CVD on these nucleated regions. Because 248-nm radiation induces only surface photochemistry, the laser-activated pattern was sharply defined in the areas irradiated by laser projection through the mask, as demonstrated in Figure 3. However, at 193 nm both gas-phase and surface photochemistry occur, so the nucleated regions and subsequently grown film included scattered contributions outside the areas defined by the mask, which were formed by the lateral diffusion of gas-phase photoproducts before they impinged on the surface.

Some of these nucleation effects in laser-assisted deposition have been treated theoretically. One study examined the physical and chemical nucleation barriers to growth using a kinetic approach,[335] while another investigation employed similar arguments from classical nucleation theory to examine physical hindrances to nucleation.[336] Yet another theoretical study utilized Monte Carlo simulation of adatom surface adsorption, migration, desorption, and nucleation coupled with adatom production by CVD to examine nucleation effects during localized laser CVD.[193,337] One conclusion of this study was that for static laser heating to temperatures below a given critical temperature, nucleation occurs at the center of the spot, while for temperatures above this critical temperature nucleation occurs initially in an annulus symmetrically placed about the center. Nucleation does not occur first at the center of the laser-heated region in this latter case because adatoms desorb faster than they can nucleate on the surface, even though the adatom formation rate is greatest at the center since the temperature is higher there than elsewhere. Under these conditions subsequent film growth at the center can begin either from nucleation sites that are later produced there or by deposition on the inside of the initially nucleated annulus. It is possible that this nucleation effect is an additional factor in the growth of the volcano-like deposits sometimes observed in local laser CVD. Though these nucleation models give results in qualitative agreement with observations, no quantitative comparison with experiment has been made.

V. Spatial Localization of Deposits

Two types of spatial localization are of potential interest in laser-assisted deposition. Both the lateral localization of the deposit and the control of deposit thickness are important in the fabrication of localized dots (static laser) and narrow lines (scanning laser) in direct writing and in projection printing.

The laser spot size is the crucial parameter in lateral localization during direct writing. As is clear from eq 3, submicron spot sizes are readily attainable with focused visible light. The discussion in section IV.B shows that in photolytic deposition the size of the deposit will equal roughly the laser spot size if surface photochemistry is dominant, while it can be significantly larger than the spot size if gas-phase photochemistry is dominant because of the long radial wings in the growth rate (eq 45). Clearly other effects can be important. Surface migration of product atoms can broaden the deposits, while the addition of inert buffers can narrow the features slightly when gas-phase photochemistry is important; this would also decrease the deposition rate slighlty. Furthermore, if the sticking coefficient of the deposit atoms is high on the deposited structure and very low on the initial substrate, the deposited structure can be even smaller than the laser spot size because of this nucleation effect.

In pyrolytic direct deposition, the net deposition rate constant can sometimes be modeled by an Arrhenius form:

$$k_{\text{photolysis}} = \frac{fn\phi_t\sigma_d(\lambda)}{2[\pi(w^2 + r^2)]^{1/2}} \frac{8w^4 + r^4}{8w^4 + \pi^{1/2}r^4} \quad (47)$$

where E_{act} is the effective activation energy. Since the temperature profile is sharply peaked at the center of the laser spot (in laser heating of a uniform substrate), $k_{\text{deposition}}$ will be even more sharply peaked, especially for large E_{act}. Consequently, deposits much smaller than the laser spot size can be formed, particularly during the initial stages of deposition. Since deposition occurs isotropically in later stages of growth, the feature can broaden with continued deposition. Also, as discussed in section IV.A, the temperature profile can broaden radially as a result of deposition, thereby limiting the localization tendency of $k_{\text{deposition}}$.[22] As in photolytic deposition, nucleation effects can also affect deposit size. Examples of submicron growth from pyrolytic direct laser deposition may be found in ref 17 and 22, which also give examples of highly localized photolytic growth.

As described earlier, submicron feature sizes are achievable in large-area deposition by projection printing only if surface photochemistry determines growth, at least during the nucleation phase.[26] If gas-phase photochemistry were important, the localization provided by the laser would be lost because of the large volumes of excited gas. This point is not applicable to focused laser photodeposition.

Thickness control is sometimes important as well in laser deposition. Laser-assisted atomic layer epitaxy[256-258] can provide very fine control of deposit thickness, in fact, to monolayer accuracy. Similarly, in excimer-laser-assisted deposition, control of the number of laser pulses irradiating the system can finely control layer thickness, as was shown in the growth of superlattices.[221] Even without these features, reasonable thickness control can often be achieved in deposition. However, in many cases of local laser CVD the growth

rate is quite sensitive to the exact surface conditions, and adequate thickness control can be difficult.

Closely linked to the issues of lateral and thickness control is the exact morphology of the deposited structure. In some cases localized deposits are flat or concave down on top. In other examples, depressions are observed at the center; volcanos in static deposition[80,150] and double-humped ridged structures in scanned lines.[324a] Locally, the deposits can be smooth, clumpy, or grainy, i.e., exhibiting grain structure. In some cases fringe patterns have been observed in the deposits, superimposed on larger morphological features.[249,338-340] In photodeposition, this has been explained by the coupling of the laser with surface plasmons.[338,339,341] Resonance effects have been observed in the photodeposition growth of dots[39] and gratings.[342]

VI. Optical Spectroscopy

A. Reactant Absorption

The gas-phase absorption spectroscopy of most of the metal precursors cited in section III was investigated in some detail long before the initiation of work on laser-assisted photodeposition; for example, the ultraviolet absorption spectra of many of the metal alkyls[343] and metal carbonyls[344] were examined years ago. Still, there have been several recent spectroscopic studies specifically motivated by photodeposition. Many absorption spectra have been reanalyzed more carefully, sometimes as part of the photodeposition studies cited above. Spectroscopy has been performed for the first time on relatively newly synthesized species such as DMAH[29] and DVHg.[31]

The ultraviolet absorption spectra of several dimethylmetals, DMZn, DMCd, and DMHg, were recently investigated in great detail.[35,65] The observed vibrational structure of the spectrum was explained in terms of a direct, asymmetric dissociation that results in a methyl radical and a metal monomethyl molecule, which itself apparently decomposes rapidly as in reaction 4e. Spectra of trimethylmetals have also been investigated.[345] In another study, the UV absorption spectra of several of the metal alkyls used in photodeposition of HgCdTe films, DMHg, DMCd, and DETe, were examined.[346a,347] The spectra of other potential II–VI semiconductor precursors have also been measured recently, including those of the Te precursors,[346b] DMTe, $Te_2(CH_3)_2$, Te(isopropyl)$_2$, and Te(allyl)$_2$, the Hg precursor DVHg,[31] and the dimethyl and diethyl precursors for sulfur and selenium.[347] Finally, the vacuum-ultraviolet absorption spectra of several of the group IV hydrides have been investigated recently, some for the first time: SiH_4,[210] Si_2H_6,[210] Si_3H_8,[210] and GeH_4.[210,237]

Several surface-sensitive spectroscopic methods have been applied to the identification of adsorbed reactants and products to aid the study of photodeposition from adsorbed molecules. Ultraviolet absorption spectroscopy and infrared total internal reflection spectroscopy of chemisorbed and physisorbed layers of dimethylmetals have been performed both before and after excimer laser irradiation to determine the bonding of adsorbates and the nature of the photolytically produced film. DMCd[40,69] and DEZn[41] on fused silica have been studied in the ultraviolet in this manner, while DMCd on passivated Si and both DMCd[348,349] and DMZn on quartz have been investigated in the infrared.[350] Optoacoustic surface infrared spectroscopy has been used to monitor C–H bonds on TMAl adsorbed on hydroxylated oxide surfaces.[75-77,351] These experiments employed a frequency-doubled Nd^{3+}:YAG laser-pumped dye laser that was Raman shifted in H_2 to produce tunable radiation near 3 μm for adsorbate absorption.

B. Optical Diagnostics of Deposition

Several in situ optical probes have been developed for use in studies of laser-assisted deposition to help characterize process conditions and to monitor film growth.[2] When used in large-area deposition only modest optical probe spatial resolution is needed ($\sim$1 mm), while in direct writing microprobes are needed with much finer transverse resolution ($\sim$1 μm).

The local temperature during focused laser beam heating and CVD has been monitored by Raman scattering,[25,182,352] photoluminescence,[353] blackbody radiation,[179,242] and nonoptical techniques as well, including microthermocouple analysis[354] and phase transition identification.[355]

Laser transmission[32,83,233,356] and reflectivity[31,221,267] have been used as in situ probes of deposit thickness in several laser-assisted deposition experiments, particularly in those involving large-area deposition. Transmission is sensitive to the absorption coefficient of the deposit and must be used with transparent substrates, while reflectivity can be used with absorbing substrates as well and is sensitive to the index of refraction of the deposit (leading to interference effects that depend on thickness) and is sensitive to a lesser degree to the absorption coefficient of the deposit. For thicker deposits, the film absorption eventually washes away the fringe pattern.

Other optical probes have been used to monitor the composition of deposited films and to identify the volatile product gases produced during deposition. The progress of local laser CVD has been monitored by Raman microprobe methods to determine the crystallinity of Si deposits[182] and the stoichiometry of Ge–Si alloy films,[229,240] while laser-induced fluorescence has been used during deposition to probe gas-phase product Cu atoms from the photolysis of Cu(HFAc)$_2$,[151] SiHCl radicals from laser CVD of SiH_2Cl_2,[227] Te atoms from the photolysis of DMTe and DETe,[288,357] and Ga atoms from the photolysis of gas-phase and surface-adsorbed TMGa.[358] Fluorescence from Ge and GeH and absorption by Ge have been monitored during the growth of Ge films by laser-assisted deposition,[232] as was the fluorescence of Ga atoms during photolytic GaAs growth.[267] Optoacoustic infrared absorption spectroscopy of surface adsorbates described above[351] has been used to monitor the disappearance of C–H stretching modes during the photolysis of adsorbed TMAl.[75-77] Other relevant spectroscopic studies may be found in the cited references.[359-363]

VII. Applications

Use of laser-assisted deposition, etching, and doping in microelectronics has been reviewed by several authors.[14,364] Of particular interest here are the several laser deposition techniques that have been implemented

in the fabrication of integrated circuits and related optoelectronic components. In several studies to date, direct writing methods have been used to fix or modify microelectronic circuits, to fabricate prototype integrated circuits, or to produce semicustomized circuits. Specifically, laser-assisted deposition has been used to repair masks,[365-367] help make active electronic devices,[23,368] interconnect or restructure gate arrays on a given chip,[369-372] interconnect chips,[373] and produce optical wave guides.[143] High-conductivity materials such as highly doped polysilicon, metal silicides, or, preferably, metals such as copper, aluminum, gold, or tungsten are most desirable for use as interconnects and have been deposited using lasers. Use of the large-area epitaxial films grown with lasers, such as those of the II–VI semiconductors, will be tested in detectors and devices in the near future.

In assessing the success of these applications of laser deposition, one must consider several issues. The deposition rate must be fast, the deposit must have suitable electrical and material properties as well as good adhesion to the substrate, and the overall process must be compatible with preexisting structures; i.e., it should not modify doping profiles, introduce defects, etc. The importance of the thermally induced stresses and strains that occur during pyrolytic direct laser writing, which can produce defects, has been addressed recently.[21,374] Of course, a necessary requirement for the application of any laser-based process is that it improves a current method or creates a new fabrication capability.

VIII. Conclusions

This review has shown that many electronic materials can be deposited by using lasers, having suitable purity and morphology for use in the manufacture of integrated circuits. In many cases, the practical advantages of laser-assisted methods vis-à-vis more conventional methods are still under debate. For instance, in some cases, lasers and (the much cheaper) UV lamps are equally useful for inducing a given photolytic deposition, while in others, processing with lasers has definite advantages, such as in those applications dependent on laser intensity and the ability to focus a laser to a small spot. It has also been seen that in several cases very impure deposits are formed by laser-assisted deposition, which are of no practical interest.

The fundamental dynamics and kinetics of several laser processes have been investigated in some detail, yet much still remains to be learned about thermal and photolytic processes on surfaces and in the gas phase. For instance, little is still known about the relative rates of reaction and relaxation during photolysis of surface-adsorbed molecules.

The close analogy between laser CVD and conventional CVD means that basic research in either area will provide much understanding in the other; this is also true for laser photodeposition and UV lamp assisted deposition. Questions regarding the relative merits of pyrolytic vs photolytic growth and surface- vs gas-phase-dominated growth are common to both laser and non-laser types of processing. For example, in general, surface-controlled growth produces deposits with better properties and with a more controllable growth rate than does gas-phase-controlled growth. This is usually true for both laser and non-laser deposition processes. Though monolayer control of growth is more easily achieved by heterogeneous deposition processes, such as in atomic layer epitaxy, it has also been demonstrated during homogeneous deposition by careful experimental control of the growth rate, such as by controlling the number of laser pulses during each growth cycle.

The spatial localization provided by direct laser writing and large-area projection printing are unique features of laser-assisted deposition. In some cases, it has been seen that the best overall process is provided by laser-assisted deposition of spatially patterned nucleation features, followed by conventional, large-area, surface-sensitive growth of the required thicker patterns. Several examples of surface-sensitive thermal growth have been shown to be important in laser, as well as non-laser, deposition. These include the growth of Al with TIBA on surfaces such as Al, Ge, from GeH_4 on Ge surfaces, and the growth of W using WF_6, which is selective on Si without H_2 added and is also selective with added H_2 on substrates that dissociate hydrogen.

Synthesis of better precursors for both laser and non-laser deposition is very important, and many groups are now actively testing new potential precursors.[375] As has been seen in this review, the same precursors frequently find use in many different approaches to deposition, by both laser and non-laser techniques.

Research into the diverse aspects of laser-assisted deposition[376] and the closely related disciplines of thermal CVD,[375] UV lamp assisted deposition, surface chemistry, and surface spectroscopy is continuing at a rapid pace. There is particular interest in identifying the mechanisms involved in the photolysis and pyrolysis of surface-adsorbed species, in implementing laser-assisted deposition in multistep in situ processing, and in other aspects of fabricating, restructuring, and repairing integrated circuits. Work on other laser-assisted processes,[376] such as laser etching and doping and deposition by laser-induced evaporation, is also very active.

Acknowledgments. This work was supported by the Office of Naval Research. The author thanks V. M. Donnelly for providing a prepublication version of ref 1.

References

(1) McCrary, V. R.; Donnelly, V. M. In *Chemical Vapor Deposition*; Jensen, K. F., Ed.; Academic: New York, in press.
(2) Herman, I. P. In *Laser Chemical Processing for Microelectronics*; Ibbs, K. G., Osgood, R. M., Eds.; Cambridge University Press: Cambridge, 1989; p 61.
(3) Osgood, R. M., Jr.; Deutsch, T. F. In *Laser Chemical Processing for Microelectronics*; Ibbs, K. G., Osgood, R. M., Eds.; Cambridge University Press: Cambridge, 1989; p 146.
(4) Houle, F. A. *Appl. Phys. A* **1986**, *41*, 315.
(5) (a) *Laser Microfabrication: Thin Film Processes and Lithography*; Ehrlich, D. J., Tsao, J. Y., Eds.; Academic: New York, 1989. (b) Boyd, I. W. *Laser Processing of Thin Films and Microstructures: Oxidation, Deposition and Etching of Insulators*; Springer: Berlin, 1987. (c) Bäuerle, D. *Chemical Processing with Lasers, Materials Science Vol. 1*; Springer: Berlin, 1986.
(6) Mayo, M. J. *Solid State Technol.* April 1986, 141.
(7) Rytz-Froidevaux, Y.; Salathe, R. P.; Gilgen, H. H. *Appl. Phys. A* **1985**, *37*, 121.
(8) Jones, K. A. *Solid State Technol.* Oct 1985, 151.
(9) Osgood, R. M.; Gilgen, H. H. *Annu. Rev. Mater. Sci.* **1985**, *15*, 549.

(10) Osgood, R. M.; Deutsch, T. F. *Science* **1985**, *227*, 709.
(11) Solanki, R.; Moore, C. A.; Collins, G. J. *Solid State Technol.* June 1985, 220.
(12) Ehrlich, D. J.; Tsao, J. Y. In *VLSI Electronics: Microstructure Science*; Einspruch, N., Ed.; Academic: New York, 1984; Vol. 7, p 129.
(13) Deutsch, T. F. In *Laser Processing and Diagnostics, Chemical Physics Vol. 39*; Bäuerle, D., Ed.; Springer: New York 1984; p 239.
(14) Herman, I. P. In *Laser Processing and Diagnostics, Chemical Physics Vol. 39*; Bäuerle, D., Ed.; Springer: New York, 1984; p 396.
(15) von Gutfeld, R. J. In *Laser Applications*; Academic: New York, 1984; Vol. 5, p 1.
(16) Chuang, T. J. *Surf. Sci. Rep.* **1983**, *3*, 1.
(17) Ehrlich, D. J.; Tsao, J. Y. *J. Vac. Sci. Technol. B* **1983**, *1*, 969.
(18) Osgood, R. M., Jr. *Annu. Rev. Phys. Chem.* **1983**, *34*, 77.
(19) Gilgen, H. H.; Cacouris, T.; Shaw, P. S.; Krchnavek, R. R.; Osgood, R. M. *Appl. Phys. B* **1987**, *42*, 55.
(20) Braichotte, D.; van den Bergh, H. *Appl. Phys. A* **1988**, *45*, 337.
(21) Welsh, L. P.; Tuchman, J. A.; Herman, I. P. *J. Appl. Phys.* **1988**, *64*, 6274.
(22) Ehrlich, D. J.; Tsao, J. Y. *Appl. Phys. Lett.* **1984**, *44*, 267.
(23) McWilliams, B. M.; Herman, I. P.; Mitlitsky, F.; Hyde, R. A.; Wood, L. L. *Appl. Phys. Lett.* **1983**, *43*, 946.
(24) Bernhardt, A. F.; McWilliams, B. M.; Mitlitsky, F.; Whitehead, J. C. *Mater. Res. Soc. Symp. Proc.* **1987**, *75*, 633.
(25) Pazionis, G. D.; Tang, H.; Herman, I. P. *IEEE J. Quantum Electron.* **1989**, *25*, 976.
(26) Higashi, G. S.; Fleming, C. G. *Appl. Phys. Lett.* **1986**, *48*, 1051.
(27) Higashi, G. S.; Blonder, G. E.; Fleming, C. G., unpublished; the author thanks G. Higashi for supplying this figure.
(28) Ehrlich, D. J.; Tsao, J. Y. *Appl. Phys. Lett.* **1985**, *46*, 198.
(29) Cacouris, T.; Scelsi, G.; Shaw, P.; Scarmozzino, R.; Osgood, R. M.; Krchnavek, R. R. *Appl. Phys. Lett.* **1988**, *52*, 1865.
(30) Baum, T. H.; Larson, C. E.; Jackson, R. L. *Mater. Res. Soc. Symp. Proc.* **1989**, *129*, in press.
(31) Jensen, J. E.; Brewer, P. D.; Olson, G. L.; Tutt, L. W.; Zinck, J. J. *J. Vac. Sci. Technol. A* **1988**, *6*, 2808.
(32) Deutsch, T. F.; Ehrlich, D. J.; Osgood, R. M., Jr. *Appl. Phys. Lett.* **1979**, *35*, 175.
(33) Ehrlich, D. J.; Osgood, R. M., Jr.; Deutsch, T. F. *IEEE J. Quantum Electron.* **1980**, *QE-16*, 1233.
(34) Ehrlich, D. J.; Osgood, R. M., Jr.; Deutsch, T. F. *J. Vac. Sci. Technol.* **1982**, *21*, 23.
(35) Chen, C. J.; Osgood, R. M. *J. Chem. Phys.* **1984**, *81*, 327. The spectroscopic notation for linear $M(CH_3)_2$ and MCH_3 molecules discussed in this cited article used the electronic-state notation of the linear MH_2 and MH model molecules. In eq 4, this notation has been revised to reflect the true symmetry of these molecules.
(36) Ehrlich, D. J.; Osgood, R. M., Jr. *Chem. Phys. Lett.* **1981**, *79*, 381.
(37) Rytz-Froidevaux, Y.; Salathe, R. P.; Gilgen, H. H. *Phys. Lett.* **1981**, *84A*, 216.
(38) Rytz-Froidevaux, Y.; Salathe, R. P.; Gilgen, H. H.; Weber, H. P. *Appl. Phys. A* **1982**, *27*, 133.
(39) Chen, C. J.; Osgood, R. M. *Phys. Rev. Lett.* **1983**, *50*, 1705.
(40) Chen, C. J.; Osgood, R. M., Jr. *Appl. Phys. A* **1983**, *31*, 171.
(41) (a) Krchnavek, R. R.; Gilgen, H. H.; Chen, J. C.; Shaw, P. S.; Licata, T. J.; Osgood, R. M., Jr. *J. Vac. Sci. Technol. B* **1987**, *5*, 20. (b) Licata, T. J.; Podlesnik, D. V.; Colbeth, R. E.; Osgood, R. M., Jr. *Deposition and Growth Limits for Microelectronics*; Rubloff, G. W., Ed.; *Am. Inst. Phys. Conf. Proc. 167*, **1988**, 250.
(42) Oprysko, M. M.; Beranek, M. W. *J. Vac. Sci. Technol. B* **1987**, *5*, 496.
(43) Flicstein, J.; Bouree, J. E.; Bresse, J. F.; Pougnet, A. M. *Mater. Res. Soc. Symp. Proc.* **1988**, *101*, 49. Bouree, J. E.; Flicstein, J. *Mater. Res. Soc. Symp. Proc.* **1988**, *101*, 55.
(44) Flicstein, J.; Bouree, J. E. *Appl. Surf. Sci.* **1989**, *36*, in press.
(45) Tsao, J. Y.; Ehrlich, D. J. *Appl. Phys. Lett.* **1984**, *45*, 617.
(46) Chiu, M. S.; Shen, K. P.; Ku, Y. K. *Appl. Phys. B* **1985**, *37*, 63.
(47) Rytz-Froidevaux, Y.; Salathe, R. P.; Gilgen, H. H. *Mater. Res. Soc. Symp. Proc.* **1983**, *17*, 29.
(48) Braichotte, D.; van den Bergh, H. *Fruhjahrstagun der Schweiz. Physikalischen Gesellschaft* **1986**, *59*, 1014.
(49) Aylett, M. R.; Haigh, J. *Mater. Res. Soc. Symp. Proc.* **1983**, *17*, 177.
(50) Braichotte, D.; van den Bergh, H. In *Laser Processing and Diagnostics, Chemical Physics Vol. 39*; Bäuerle, D., Ed.; Springer: New York, 1984; p 183.
(51) Mingxin, Q.; Monot, R.; van den Bergh, H. *Sci. Sin. A* **1984**, *27*, 531.
(52) Petzold, H.-C.; Putzar, R.; Weigmann, U.; Wilke, I. *Mater. Res. Soc. Symp. Proc.* **1988**, *101*, 75.
(53) Solanki, R.; Ritchie, W. H.; Collins, G. J. *Appl. Phys. Lett.* **1983**, *43*, 454.
(54) Motooka, T.; Gorbatkin, S.; Lubben, D.; Greene, J. E. *J. Appl. Phys.* **1985**, *58*, 4397.
(55) Motooka, T.; Gorbatkin, S.; Lubben, D.; Eres, D.; Greene, J. E. *J. Vac. Sci. Technol. A* **1986**, *4*, 3146.
(56) Eres, D.; Motooka, T.; Gorbatkin, S.; Lubben, D.; Greene, J. E. *J. Vac. Sci. Technol. B* **1987**, *5*, 848.
(57) Arai, Y.; Yamaguchi, S.; Ohsaki, T. *Appl. Phys. Lett.* **1988**, *52*, 2083.
(58) Higashi, G. S. *J. Chem. Phys.* **1988**, *88*, 422.
(59) Higashi, G. S.; Steigerwald, M. L. *Appl. Phys. Lett.* **1989**, *54*, 81.
(60) Hanabusa, M.; Oikawa, A.; Cai, P. Y.; Furuno, S.; Iguchi, S. *Mater. Res. Soc. Symp. Proc.* **1989**, *129*, in press.
(61) Blonder, G. E.; Higashi, G. S.; Fleming, C. G. *Appl. Phys. Lett.* **1987**, *50*, 766. Fleming, C. G.; Blonder, G. E.; Higashi, G. S. *Mater. Res. Soc. Symp. Proc.* **1988**, *101*, 183.
(62) Mantell, D. A. *Appl. Phys. Lett.* **1988**, *53*, 1387; *J. Vac. Sci. Technol. A* **1989**, *7*, 630.
(63) Yu, C. F.; Youngs, F.; Tsukiyama, K.; Bersohn, R.; Preses, J. *J. Chem. Phys.* **1986**, *85*, 1382. Note that the fluorescence observed in this study, identified as $CdCH_3$ A → X and which is evidence for reactions 4b and 4d, was not observed in: Suto, M.; Ye, C.; Lee, L. C. *J. Chem. Phys.* **1988**, *89*, 160.
(64) (a) Smith, G. P.; Patrick, R. J. *Int. J. Chem. Kinet.* **1983**, *15*, 167. (b) McMillen, D. F.; Golden, D. M. *Annu. Rev. Phys. Chem.* **1982**, *33*, 493. (c) Cox, J. D.; Pilcher, G. *Thermochemistry of Organic and Organometallic Compounds*; Academic: New York, 1970. (d) Kochi, J. K. *Organometallic Mechanisms and Catalysis*; Academic: New York, 1978. (e) *Comprehensive Organometallic Chemistry*; Wilkinson, G., Ed.; Pergamon: Oxford, 1982; Vol. 1. (f) Mole, T., Jeffery, E. A. *Organoaluminium Compounds*, Elsevier: Amsterdam, 1972. (g) Price, S. J. W. In *Comprehensive Chemical Kinetics. Decomposition of Inorganic and Organometallic Compounds*; Bamford, C. H., Tipper, C. F. H., Eds.; Elsevier: Amsterdam, 1972; Vol. 4, p 197. Also see references cited therein.
(65) Chen, C. J.; Osgood, R. M. *J. Chem. Phys.* **1984**, *81*, 318.
(66) Jonah, C.; Chandra, P.; Bersohn, R. *J. Chem. Phys.* **1971**, *55*, 1903.
(67) Baughcum, S. I.; Leone, S. R. *Chem. Phys. Lett.* **1982**, *89*, 183.
(68) Wood, T. H.; White, J. C.; Thacker, B. A. *Appl. Phys. Lett.* **1983**, *42*, 408.
(69) Chen, C. J.; Osgood, R. M. *Chem. Phys. Lett.* **1983**, *98*, 363.
(70) Shaw, P.; O'Neill, J.; Sanchez, E.; Wu, Z.; Osgood, R. M., Jr. *Mater. Res. Soc. Symp. Proc.* **1989**, *129*, in press.
(71) (a) Stuke, M.; Zhang, Y.; Küper, S. *Mater. Res. Soc. Symp. Proc.* **1988**, *101*, 139. (b) Zhang, Y.; Stuke, M. *J. Cryst. Growth* **1988**, *93*, 143. (c) Zhang, Y.; Stuke, M. *Mater. Res. Soc. Symp. Proc.* **1989**, *131*, 375. *Chem. Phys. Lett.* **1988**, *149*, 310. (d) Zhang, Y.; Beuermann, Th.; Stuke, M. *Appl. Phys. B* **1989**, *48*, 97.
(72) Orlowski, T. E.; Mantell, D. A. *J. Vac. Sci. Technol. A* **1989**, *7*, 2598; *Mater. Res. Soc. Symp. Proc.* **1989**, *131*, 369.
(73) Lubben, D.; Motooka, T.; Greene, J. E.; Wendelken, J. F.; Sundgren, J.-E.; Salaneck, W. R. *Mater. Res. Soc. Symp. Proc.* **1988**, *101*, 151.
(74) Orlowski, T. E.; Mantell, D. A. *Mater. Res. Soc. Symp. Proc.* **1988**, *101*, 165. Mantell, D. A.; Orlowski, T. E. *Mater. Res. Soc. Symp. Proc.* **1988**, *101*, 171.
(75) Higashi, G. S.; Rothberg, L. J. *Appl. Phys. Lett.* **1985**, *47*, 1288.
(76) Higashi, G. S.; Rothberg, L. J.; Fleming, C. G. *Chem. Phys. Lett.* **1985**, *115*, 167.
(77) Higashi, G. S.; Rothberg, L. J. *J. Vac. Sci. Technol. B* **1985**, *3*, 1460.
(78) (a) Ziegler, K.; Nagel, K.; Pfohl, W. *Justus Liebigs Ann. Chem.* **1960**, *629*, 210. (b) Green, M. L.; Levy, R. A.; Nuzzo, R. G.; Coleman, E. *Thin Solid Films* **1984**, *114*, 367. Cooke, M. J.; Heinecke, R. A.; Stern, R. C.; Maes, J. W. C. *Solid State Technol.* Dec 1982, p 62. (c) For example, see: Squire, D. W.; Dulcey, C. S.; Lin, M. C. *J. Vac. Sci. Technol. B* **1985**, *3*, 1513.
(79) Bent, B. E.; Nuzzo, R. G.; Dubois, L. H. *Mater. Res. Soc. Symp. Proc.* **1988**, *101*, 177; *J. Vac. Sci. Technol. A* **1988**, *6*, 1920, and submitted for publication.
(80) Allen, S. D. *J. Appl. Phys.* **1981**, *52*, 6501.
(81) Herman, I. P.; Hyde, R. A.; McWilliams, B. M.; Weisberg, A. H.; Wood, L. L. *Mater. Res. Soc. Symp. Proc.* **1983**, *17*, 9.
(82) Krauter, W.; Bäuerle, D.; Fimberger, F. *Appl. Phys. A* **1983**, *31*, 13.
(83) Allen, S. D.; Jan, R. Y.; Mazuk, S. M.; Vernon, S. D. *J. Appl. Phys.* **1985**, *58*, 327.
(84) Petzoldt, F.; Piglmayer, K.; Krauter, W.; Bäuerle, D. *Appl. Phys. A* **1984**, *35*, 155.
(85) Bezuk, S. J.; Baseman, R. J.; Kryzak, C.; Warner, K.; Thomes, G. *Mater. Res. Soc. Symp. Proc.* **1987**, *75*, 75.

(86) Allen, S. D.; Tringubo, A. B. *J. Appl. Phys.* **1983**, *54*, 1641.
(87) Jackman, R. B.; Foord, J. S.; Adams, A. E.; Lloyd, M. L. *J. Appl. Phys.* **1986**, *59*, 2031.
(88) Ehrlich, D. J.; Osgood, R. M., Jr.; Deutsch, T. F. *J. Electrochem. Soc.* **1981**, *128*, 2039.
(89) Solanki, R.; Boyer, P. K.; Mahan, J. E.; Collins, G. J. *Appl. Phys. Lett.* **1981**, *38*, 572.
(90) Chiu, M. S.; Tseng, Y. G.; Ku, Y. K. *Opt. Lett.* **1985**, *10*, 113.
(91) Gluck, N. S.; Wolga, G. J.; Bartosch, C. E.; Ho, W.; Ying, Z. *J. Appl. Phys.* **1987**, *61*, 998.
(92) Jackson, R. L.; Tyndall, G. W. *J. Appl. Phys.* **1987**, *62*, 315.
(93) Jackson, R. L.; Tyndall, G. W. *J. Appl. Phys.* **1988**, *64*, 2092.
(94) Mayer, T. M.; Fisanik, G. J.; Eichelberger, T. S., IV. *J. Appl. Phys.* **1982**, *53*, 8462.
(95) Natzle, W. C. *Mater. Res. Soc. Symp. Proc.* **1988**, *101*, 213.
(96) (a) Singmaster, K. A.; Houle, F. A.; Wilson, R. J. *Appl. Phys. Lett.* **1988**, *53*, 1048. (b) Singmaster, K. A.; Houle, F. A., to be published, and personal communication.
(97) Uesugi, F.; Morishige, Y.; Shinzawa, T.; Kishida, S.; Hirata, M.; Yamada, H.; Matsumoto, K. *Mater. Res. Soc. Symp. Proc.* **1988**, *101*, 61.
(98) Bottka, N.; Walsh, P. J.; Dalbey, R. Z. *J. Appl. Phys.* **1983**, *54*, 1104. A UV lamp was used in this study.
(99) Love, P. J.; Loda, R. T.; La Roe, P. R.; Green, A. K.; Rehn, V. *Mater. Res. Soc. Symp. Proc.* **1984**, *29*, 101.
(100) Solanki, R.; Boyer, P. K.; Collins, G. J. *Appl. Phys. Lett.* **1982**, *41*, 1048.
(101) Flynn, D. K.; Steinfeld, J. I.; Sethi, D. S. *J. Appl. Phys.* **1986**, *59*, 3914.
(102) Yokoyama, H.; Uesugi, F.; Kishida, S.; Washio, K. *Appl. Phys. A* **1985**, *37*, 25.
(103) Konstantinov, L.; Nowak, R.; Hess, P. *Appl. Phys. A* **1988**, *47*, 171.
(104) Jervis, T. R. *J. Appl. Phys.* **1985**, *58*, 1400.
(105) Gray, H. B.; Beach, N. A. *J. Am. Chem. Soc.* **1963**, *85*, 2922.
(106) Whetten, R. L.; Fu, K.-J.; Grant, E. R. *J. Chem. Phys.* **1983**, *79*, 4899.
(107) Carlton, H. E.; Oxley, J. H. *AIChE J.* **1967**, *13*, 86.
(108) Carlton, H. E.; Oxley, J. H. *AIChE J.* **1965**, *11*, 79.
(109) Lewis, K. E.; Golden, D. M.; Smith, G. P. *J. Am. Chem. Soc.* **1984**, *106*, 3905 and references cited therein. Also see: Fletcher, T. R.; Rosenfeld, R. N. *J. Am. Chem. Soc.* **1988**, *110*, 2097.
(110) Nathanson, G.; Gitlin, B.; Rosan, A. M.; Yardley, J. T. *J. Chem. Phys.* **1981**, *74*, 361.
(111) Yardley, J. T.; Gitlin, B.; Nathanson, G.; Rosan, A. M. *J. Chem. Phys.* **1981**, *74*, 370.
(112) Tumas, W.; Gitlin, B.; Rosan, A. M.; Yardley, J. T. *J. Am. Chem. Soc.* **1982**, *104*, 55.
(113) (a) Seder, T. A.; Church, S. P.; Weitz, E. *J. Am. Chem. Soc.* **1986**, *108*, 4721. (b) Seder, T. A.; Ouderkirk, A. J.; Weitz, E. *J. Chem. Phys.* **1986**, *85*, 1977. (c) Weitz, E. *J. Phys. Chem.* **1987**, *91*, 3945. (d) Ganske, J. A.; Rosenfeld, R. N. *J. Phys. Chem.* **1989**, *93*, 1959. (e) Fletcher, T. R.; Rosenfeld, R. N. *J. Am. Chem. Soc.* **1985**, *107*, 2203. (f) Holland, J. P.; Rosenfeld, R. N. *Chem. Phys. Lett.* **1988**, *145*, 481; *J. Chem. Phys.* **1988**, *89*, 7217.
(114) Waller, I. M.; Hepburn, J. W. *J. Chem. Phys.* **1988**, *88*, 6658. Waller, I. M.; Davis, H. F.; Hepburn, J. W. *J. Phys. Chem.* **1987**, *91*, 506.
(115) (a) Ray, U.; Brandow, S. L.; Bandukwalla, G.; Venkataraman, B. K.; Zhang, Z.; Vernon, M. *J. Chem. Phys.* **1988**, *89*, 4092. (b) Venkataraman, B. K.; Bandukwalla, G.; Zhang, Z.; Vernon, M. *J. Chem. Phys.* **1989**, *90*, 5510. (c) Venkataraman, B. K. "Photodissociation Dynamics of Transition Metal Carbonyls", Ph.D. Dissertation, Columbia University, 1989. Venkataraman, B. K.; Hou, H.; Zhang, Z.; Chen, S.; Bandukwalla, G.; Vernon, M., to be published.
(116) At shorter wavelengths all CO ligands can be removed from the carbonyl after the absorption of a single photon, such as for $Ni(CO)_4$ and $Fe(CO)_5$ at 104.8 and 106.7 nm in: Hellner, L.; Masanet, J.; Vermeil, C. *Chem. Phys. Lett.* **1981**, *83*, 474.
(117) Creighton, J. R. *J. Vac. Sci. Technol. A* **1986**, *4*, 669; *J. Appl. Phys.* **1986**, *59*, 410.
(118) Bartosch, C. E.; Gluck, N. S.; Ho, W.; Ying, Z. *Phys. Rev. Lett.* **1986**, *57*, 1425.
(119) Gluck, N. S.; Ying, Z.; Bartosch, C. E.; Ho, W. *J. Chem. Phys.* **1987**, *86*, 4957.
(120) Ho, W. *Comments Condens. Matter Phys.* **1988**, *13*, 293.
(121) Swanson, J. R.; Friend, C. M. *J. Vac. Sci. Technol. A* **1988**, *6*, 770.
(122) Friend, C. M.; Swanson, J. R.; Flitsch, F. A. *Proc. NATO Workshop—Surface Reactions of Organometallic Compounds*, in press; *Mater. Res. Soc. Symp. Proc.* **1989**, *131*, 461.
(123) Ying, Z.; Ho, W. *J. Vac. Sci. Technol. A* **1988**, *6*, 834.
(124) Swanson, J. R.; Friend, C. M.; Chabal, Y. J. *J. Chem. Phys.* **1987**, *87*, 5028; **1988**, *89*, 2593.
(125) Andreoni, W.; Varma, C. M. *Phys., Rev. B* **1981**, *23*, 437.
(126) Morosanu, C.-E.; Soltuz, V. *Thin Solid Films* **1978**, *52*, 181.
(127) (a) Broadbent, E. K.; Ramiller, C. L. *J. Electrochem. Soc.* **1984**, *131*, 1427. (b) Tsao, K. Y.; Busta, H. H. *J. Electrochem. Soc.* **1984**, *131*, 2702. (c) Bryant, W. A. *J. Electrochem. Soc.* **1978**, *125*, 1534.
(128) Yu, M. L.; Eldridge, B. N.; Joshi, R. V. *Workshop on Tungsten and Other Refractory Metals for VLSI Applications IV*, Mater. Res. Soc. Proc., Pittsburgh, PA, in press. Yu, M. L.; Eldridge, B. N.; Joshi, R. V. *Deposition and Growth: Limits for Microelectronics*; Rubloff, G. W., Ed.; *Am. Inst. Phys. Conf. Proc. 167* **1988**, 202. *Workshop on Tungsten and Other Refractory Metals for VLSI Applications III*; Wells, V. A., Ed.; Mater. Res. Soc. Proc., Pittsburgh, PA, 1988; p 75.
(129) Jackman, R. B.; Foord, J. S. *Surf. Sci.* **1988**, *201*, 47.
(130) Yu, M. L.; Eldridge, B. N. *J. Vac. Sci. Technol. A* **1989**, *7*, 625.
(131) Berg, R. S.; Mattox, D. M. *Proceedings of the Fourth International Conference on Chemical Vapor Deposition*; Wakefield, G. F., Blocher, J. M, Jr., Eds.; Electrochemical Society: Princeton, NJ, 1973; p 196.
(132) Zhang, G. Q.; Szörényi, T.; Bäuerle, D. *J. Appl. Phys.* **1987**, *62*, 673.
(133) Grossman, W. M.; Karnezos, M. *J. Vac. Sci. Technol. B* **1987**, *5*, 843.
(134) Gottsleben, O.; Stuke, M. *Appl. Phys. Lett.* **1988**, *52*, 2230.
(135) Lin, J. Y.; Allen, S. D., to be published, and personal communication.
(136) Herman, I. P.; McWilliams, B. M.; Mitlitsky, F.; Chin, H. W.; Hyde, R. A.; Wood, L. L. *Mater. Res. Soc. Symp. Proc.* **1984**, *29*, 29.
(137) Liu, Y. S.; Yakymyshyn, C. P.; Philipp, H. R.; Cole, H. S.; Levinson, L. M. *J. Vac. Sci. Technol. B* **1985**, *3*, 1441.
(138) Black, J. G.; Ehrlich, D. J.; Sedlacek, J. H. C.; Feinerman, A. D.; Busta, H. H. *IEEE Electron Dev. Lett.* **1986**, *EDL-7*, 422.
(139) Black, J. G.; Doran, S. P.; Rothschild, M.; Ehrlich, D. J., presented at the National Meeting of the American Vacuum Society, October 1988, Atlanta, GA, and *Appl. Phys. Lett.*, to be published.
(140) Deutsch, T. F.; Rathman, D. D. *Appl. Phys. Lett.* **1984**, *45*, 623.
(141) Adams, A. E.; Lloyd, M. L.; Morgan, S. L.; Davis, N. G. In *Laser Processing and Diagnostics. Chemical Physics Vol. 39*; Bäuerle, D., Ed.; Springer: New York, 1984; p 269.
(142) Shintani, A.; Tsuzuku, S.; Nishitani, E.; Nakatani, M. *J. Appl. Phys.* **1987**, *61*, 2365.
(143) Tsao, J. Y.; Becker, R. A.; Ehrlich, D. J.; Leonberger, F. J. *Appl. Phys. Lett.* **1983**, *42*, 559.
(144) Tsao, J. Y.; Ehrlich, D. J. *J. Chem. Phys.* **1984**, *81*, 4620.
(145) Geohegan, D. B.; McCown, A. W.; Eden, J. G. *Mater. Res. Soc. Symp. Proc.* **1984**, *29*, 93.
(146) Geohegan, D. B.; Eden, J. G. *Appl. Phys. Lett.* **1984**, *45*, 1146.
(147) Houle, F. A.; Baum, T. H.; Moylan, C. R. In *Laser Chemical Processing for Microelectronics*; Ibbs, K. G., Osgood, R. M., Eds.; Cambridge University Press: Cambridge, 1989; p 25 and references therein.
(148) Baum, T. H. *J. Electrochem. Soc.* **1987**, *134*, 2616.
(149) Houle, F. A.; Jones, C. R.; Baum, T.; Pico, C.; Kovac, C. A. *Appl. Phys. Lett.* **1985**, *46*, 204. Jones, C. R.; Houle, F. A.; Kovac, C. A.; Baum, T. H. *Appl. Phys. Lett.* **1985**, *46*, 97.
(150) Moylan, C. R.; Baum, T. H.; Jones, C. R. *Appl. Phys. A* **1986**, *40*, 1.
(151) Marinero, E. E.; Jones, C. R. *J. Chem. Phys.* **1985**, *82*, 1608.
(152) Wilson, R. J.; Houle, F. A. *Phys. Rev. Lett.* **1985**, *55*, 2184.
(153) Markwalder, B.; Widmer, M.; Braichotte, D.; van den Bergh, H. *J. Appl. Phys.* **1989**, *65*, 2470.
(154) Baum, T. H.; Jones, C. R. *Appl. Phys. Lett.* **1985**, *47*, 538.
(155) Baum, T. H.; Jones, C. R. *J. Vac. Sci. Technol. B* **1986**, *4*, 1187.
(156) Baum, T. H.; Marinero, E. E.; Jones, C. R. *Appl. Phys. Lett.* **1986**, *49*, 1213.
(157) Comita, P. B.; Kodas, T. T. *Appl. Phys. Lett.* **1987**, *51*, 2059.
(158) Kodas, T. T.; Baum, T. H.; Comita, P. B. *J. Appl. Phys.* **1987**, *62*, 281.
(159) Kodas, T. T.; Baum, T. H.; Comita, P. B. *J. Cryst. Growth* **1988**, *87*, 378.
(160) Heidberg, J.; Daghighi-Ruhi, R.; von Weyssenhoff, H.; Habekost, A. *Mater. Res. Soc. Symp. Proc.* **1988**, *101*, 221.
(161) Braichotte, D.; van den Bergh, H. *Appl. Phys. A* **1987**, *44*, 353.
(162) (a) Garrido-Suarez, C.; Braichotte, D.; van den Bergh, H. *Appl. Phys. A* **1988**, *46*, 285. (b) Braichotte, D.; van den Bergh, H. *Appl. Phys. A* **1989**, *49*, 189.
(163) Cole, H. S.; Liu, Y. S.; Rose, J. W.; Guida, R. *Appl. Phys. Lett.* **1988**, *53*, 2111.
(164) Buono-Core, G.; Iwai, K.; Chow, Y. L.; Koyanagi, T.; Kaji, A.; Hayami, J.-I. *Can. J. Chem.* **1979**, *57*, 8.
(165) Dupuy, C. G.; Beach, D. B.; Hurst, J. E., Jr.; Jasinski, J. M. *Chem. Mater.* **1989**, *1*, 16.
(166) Schröder, H.; Kompa, K. L.; Masci, D.; Gianinoni, I. *Appl. Phys. A* **1985**, *38*, 227.

(167) Koplitz, L. V.; Shuh, D. K.; Chen, Y.-J.; Williams, R. S.; Zink, J. I. *Appl. Phys. Lett.* **1988**, *53*, 1705.
(168) Gozum, J. E.; Pollina, D. M.; Jensen, J. A.; Girolami, G. S. *J. Am. Chem. Soc.* **1988**, *110*, 2688.
(169) Chen, Y.-J.; Kaesz, H. D.; Thridandam, H.; Hicks, R. F. *Appl. Phys. Lett.* **1988**, *53*, 1591.
(170) Stauf, G. T.; Dowben, P. A. *Thin Solid Films* **1988**, *156*, L31.
(171) Armstrong, J. V.; Burk, A. A., Jr.; Coey, J. M. D.; Moorjani, K. *Appl. Phys. Lett.* **1987**, *50*, 1231.
(172) Liu, Y. S.; Yakymyshyn, C. P.; Philipp, H. R.; Cole, H. S.; Levinson, L. M. *Mater. Res. Soc. Ext. Abstr.* **1984**, *EA-1*, 73.
(173) Codella, P. J.; Adar, F.; Liu, Y. S. *Appl. Phys. Lett.* **1985**, *46*, 1076.
(174) West, G. A.; Gupta, A.; Beeson, K. W. *Appl. Phys. Lett.* **1985**, *47*, 476.
(175) West, G. A.; Beeson, K. W.; Gupta, A. *J. Vac. Sci. Technol. A* **1985**, *3*, 2278.
(176) Gupta, A.; West, G. A.; Beeson, K. W. *J. Appl. Phys.* **1985**, *58*, 3573.
(177) Christensen, C. P.; Laiken, K. M. *Appl. Phys. Lett.* **1978**, *32*, 254.
(178) Ehrlich, D. J.; Osgood, R. M., Jr.; Deutsch, T. F. *Appl. Phys. Lett.* **1981**, *39*, 957.
(179) Bäuerle, D.; Irsigler, P.; Leyendecker, G.; Noll, H.; Wagner, D. *Appl. Phys. Lett.* **1982**, *40*, 819.
(180) Bäuerle, D.; Leyendecker, G.; Wagner, D.; Bauser, E.; Lu, Y. C. *Appl. Phys. A* **1983**, *30*, 147.
(181) Binnie, T. D.; Wilson, J. I. B.; Colles, M. J.; West, J. L. *J. Appl. Phys.* **1985**, *58*, 4446.
(182) Magnotta, F.; Herman, I. P. *Appl. Phys. Lett.* **1986**, *48*, 195.
(183) Ishizu, A.; Inoue, Y.; Nishimura, T.; Akasaka, Y.; Miki, H. *Jpn. J. Appl. Phys.* **1986**, *25*, 1830.
(184) Roy, S. K.; Vengurlekar, A. S.; Karulkar, V. T.; Joshi, A. V.; Chandrasekhar, S. *J. Electron. Mater.* **1987**, *16*, 211.
(185) Milne, D.; Black, A.; Wilson, J. I. B.; John, P. *Electron. Lett.* **1988**, *24*, 19.
(186) Tonneau, D.; Auvert, G.; Pauleau, Y. *Thin Solid Films* **1987**, *155*, 75.
(187) Kotecki, D. E.; Herman, I. P., unpublished.
(188) Auvert, G.; Tonneau, D.; Pauleau, Y. *Appl. Phys. Lett.* **1988**, *52*, 1062.
(189) Kotecki, D. E.; Herman, I. P. *Mater. Res. Soc. Symp. Proc.* **1988**, *101*, 119.
(190) Buss, R. J.; Ho, P.; Breiland, G.; Coltrin, M. E. *J. Appl. Phys.* **1988**, *63*, 2808. Robbins, D. J.; Young, I. M. *Appl. Phys. Lett.* **1987**, *50*, 1575. Farnaam, M. K.; Olander, D. R. *Surf. Sci.* **1984**, *145*, 390.
(191) (a) Beers, A. M.; Bloem, J. *Appl. Phys. Lett.* **1982**, *41*, 153. (b) Scott, B. A.; Estes, R. D.; Jasinski, J. M. *J. Chem. Phys.* **1988**, *89*, 2544.
(192) For example, see: Jasinski, J. M.; Estes, R. D. *Chem. Phys. Lett.* **1985**, *117*, 495. Jasinski, J. M.; Meyerson, B. S.; Scott, B. A. *Annu. Rev. Phys. Chem.* **1987**, *38*, 109 and references cited therein.
(193) Kotecki, D. E.; Herman, I. P. *J. Appl. Phys.* **1988**, *64*, 4920.
(194) Hanabusa, M.; Namiki, A.; Yoshihara, K. *Appl. Phys. Lett.* **1979**, *35*, 626.
(195) Hanabusa, M.; Moriyama, S.; Kikuchi, H. *Thin Solid Films* **1983**, *107*, 227.
(196) Bilenchi, R.; Gianinoni, I.; Musci, M.; Murri, R.; Tacchetti, S. *Appl. Phys. Lett.* **1985**, *47*, 279.
(197) Meguro, T.; Ishihara, Y.; Itoh, T.; Tashiro, H. *Jpn. J. Appl. Phys.* **1986**, *25*, 524.
(198) Hanabusa, M.; Kikuchi, H. *Jpn. J. Appl. Phys.* **1983**, *22*, L712.
(199) Meunier, M.; Gattuso, T. R.; Adler, D.; Haggerty, J. S. *Appl. Phys. Lett.* **1983**, *43*, 273.
(200) Branz, H. M.; Fan, S.; Flint, J. H.; Fiske, B. T.; Adler, D.; Haggerty, J. S. *Appl. Phys. Lett.* **1986**, *48*, 171.
(201) Meunier, M.; Flint, J. H.; Haggerty, J. S.; Adler, D. *J. Appl. Phys.* **1987**, *62*, 2812, 2822.
(202) Branz, H. M.; Flint, J. H.; Harris, C. J.; Haggerty, J. S.; Adler, D. *Appl. Phys. Lett.* **1987**, *51*, 922.
(203) Metzger, D.; Hesch, K.; Hess, P. *Appl. Phys. A* **1988**, *45*, 345. Hesch, K.; Hess, P.; Oetzmann, H.; Schmidt, C. *Mater. Res. Soc. Symp. Proc.* **1989**, *131*, 495.
(204) Deutsch, T. F.; Ehrlich, D. J.; Rathman, D. D.; Silversmith, D. J.; Osgood, R. M., Jr. *Appl. Phys. Lett.* **1981**, *39*, 825.
(205) Suzuki, K.; Lubben, D.; Greene, J. E. *J. Appl. Phys.* **1985**, *58*, 979. See also: Motooka, T.; Greene, J. E. *J. Appl. Phys.* **1986**, *59*, 2015, and ref 230.
(206) Bayer, E.; Kusian, W.; Schneider, G. *Seimens Forsch-u. Entwickl.-Ber. Bd.* **1988**, *17*, 190.
(207) Toyoshima, Y.; Kumata, K.; Itoh, U.; Matsuda, A. *Appl. Phys. Lett.* **1987**, *51*, 1925.
(208) Clark, J. H.; Anderson, R. G. *Appl. Phys. Lett.* **1978**, *32*, 46.
(209) Fuchs, C.; Boch, E.; Fogarassy, E.; Aka, B.; Siffert, P. *Mater. Res. Soc. Symp. Proc.* **1988**, *101*, 361.
(210) Itoh, U.; Toyoshima, Y.; Onuki, H.; Washida, N.; Ibuki, T. *J. Chem. Phys.* **1986**, *85*, 4867. Dillon, M. A.; Spence, D.; Boesten, L.; Tanaka, H. *J. Chem. Phys.* **1988**, *88*, 4320.
(211) Stafast, H. *Appl. Phys. A* **1989**, *45*, 93.
(212) Perkins, G. G. A.; Austin, E. R.; Lampe, F. W. *J. Am. Chem. Soc.* **1979**, *101*, 1109.
(213) Farrow, R. F. C. *J. Electrochem. Soc.* **1974**, *121*, 899. Eversteyn, F. C.; Put, B. H. *J. Electrochem. Soc.* **1973**, *120*, 106.
(214) Adams, A. C. "Dielectric and Polysilicon Film Deposition". In *VLSI Technology*; Sze, S. M., Ed.; McGraw-Hill: New York, 1983; p 93.
(215) Yamada, A.; Konagai, M.; Takahashi, K. *Jpn. J. Appl. Phys.* **1985**, *24*, 1586.
(216) Taguchi, T.; Morikawa, M.; Hiratsuka, Y.; Toyoda, K. *Appl. Phys. Lett.* **1986**, *49*, 971.
(217) Tanaka, T.; Deguchi, K.; Hirose, M. *Jpn. J. Appl. Phys.* **1987**, *26*, 2057.
(218) Iwanaga, T.; Hanabusa, M. *Jpn. J. Appl. Phys.* **1984**, *23*, L473.
(219) Zarnani, H.; Demiryont, H.; Collins, G. J. *J. Appl. Phys.* **1986**, *60*, 2523.
(220) Eres, D.; Lowndes, D. H.; Geohegan, D. B.; Mashburn, D. N. *Mater. Res. Soc. Symp. Proc.* **1988**, *101*, 355.
(221) Lowndes, D. H.; Geohegan, D. B.; Eres, D.; Pennycook, S. J.; Mashburn, D. N.; Jellison, G. E., Jr. *Appl. Phys. Lett.* **1988**, *52*, 1868.
(222) Ishida, M.; Tanaka, H.; Sawada, K.; Namiki, A.; Nakamura, T.; Ohtake, N. *J. Appl. Phys.* **1988**, *64*, 2087.
(223) Gau, S. C.; Weinberger, B. R.; Akhtar, M.; Kiss, Z.; MacDiarmid, A. G. *Appl. Phys. Lett.* **1981**, *39*, 436.
(224) Jasinski, J. M.; Chu, J. O.; Begemann, M. H. *Mater. Res. Soc. Symp. Proc.* **1989**, *131*, 487. Chu, J. O.; Begemann, M. H.; McKillop, J. S.; Jasinski, J. M. *Chem. Phys. Lett.* **1989**, *155*, 576.
(225) Perkins, G. G. A.; Lampe, F. W. *J. Am. Chem. Soc.* **1980**, *102*, 3764.
(226) Winstel, M.; Krimmel, E. F.; Weiss, A. *Siemens Forsch.-u. Entwickl.-Ber. Bd.* **1988**, *17*, 6.
(227) Magnotta, F. *Microbeam Analysis—1987*; Geiss, R. H., Ed.; San Francisco Press: San Francisco, CA, 1987; p 153.
(228) Baranauskas, V.; Mammana, C. I. Z.; Klinger, R. E.; Greene, J. E. *Appl. Phys. Lett.* **1980**, *36*, 930.
(229) Herman, I. P.; Magnotta, F. *J. Appl. Phys.* **1987**, *61*, 5118.
(230) Hall, L. H. *J. Electrochem. Soc.* **1972**, *119*, 1593 and references cited therein.
(231) (a) Andreatta, R. W.; Abele, C. C.; Osmundsen, J. F.; Eden, J. G.; Lubben, D.; Greene, J. E. *Appl. Phys. Lett.* **1982**, *40*, 183. (b) Eden, J. G.; Greene, J. E.; Osmundsen, J. F.; Lubben, D.; Abele, C. C.; Gorbatkin, S.; Desai, H. D. *Mater. Res. Soc. Symp. Proc.* **1983**, *17*, 185.
(232) Osmundsen, J. F.; Abele, C. C.; Eden, J. G. *J. Appl. Phys.* **1985**, *57*, 2921.
(233) King, K. K.; Tavitian, V.; Geohegan, D. B.; Cheng, E. A. P.; Piette, S. A.; Scheltens, F. J.; Eden, J. G. *Mater. Res. Soc. Symp. Proc.* **1987**, *75*, 189.
(234) (a) Tavitian, V.; Kiely, C. J.; Geohegan, D. B.; Eden, J. G. *Appl. Phys. Lett.* **1988**, *52*, 1710. (b) Tavitian, V.; Kiely, C. J.; Eden, J. G. *Mater. Res. Soc. Symp. Proc.* **1988**, *101*, 349. (c) Kiely, C. J.; Tavitian, V.; Eden, J. G. *J. Appl. Phys.* **1989**, *65*, 3883.
(235) Kiely, C. J.; Tavitian, V.; Jones, C.; Eden, J. G. *Appl. Phys. Lett.* **1989**, *55*, 65.
(236) Gow, T. R.; Coronell, D. G.; Masel, R. I. *J. Mater. Res.* **1989**, *4*, 634.
(237) Mitchell, M. J.; Wang, X.; Chin, C. T.; Suto, M.; Lee, L. C. *J. Phys. B: At. Mol. Phys.* **1987**, *20*, 5451.
(238) Eres, D.; Lowndes, D. H.; Tischler, J. Z.; Sharp, J. W.; Geohegan, D. B.; Pennycook, S. J. *Mater. Res. Soc. Symp. Proc.* **1989**, *131*, 517. International Laser Science Conference, Atlanta, GA, October 1988.
(239) Stanley, A. E.; Johnson, R. A.; Turner, J. B.; Roberts, A. H. *Appl. Spectrosc.* **1986**, *40*, 374.
(240) Burke, H. H.; Herman, I. P.; Tavitian, V.; Eden, J. G. *Appl. Phys. Lett.* **1989**, *55*, 253.
(241) Leyendecker, G.; Bäuerle, D.; Geittner, P.; Lydtin, H. *Appl. Phys. Lett.* **1981**, *39*, 921.
(242) Leyendecker, G.; Noll, H.; Bäuerle, D.; Geittner, P.; Lydtin, H. *J. Electrochem. Soc.* **1983**, *130*, 157.
(243) Lyons, A. M.; Wilkins, C. W., Jr.; Mendenhall, F. T. *Mater. Res. Soc. Symp. Proc.* **1988**, *101*, 67.
(244) Tokuda, J.; Takai, M.; Nakai, H.; Gamo, K.; Namba, S. J. *J. Opt. Soc. Am. B* **1987**, *4*, 267.
(245) Radloff, W.; Hohmann, H.; Albrecht, H.; Freudenberg, T. *Spectrochim. Acta* **1987**, *43A*, 225.
(246) Tachibana, H.; Nakaue, A.; Kawate, Y. *Mater. Res. Soc. Symp. Proc.* **1988**, *101*, 367.
(247) Kitahama, K.; Hirata, K.; Nakamatsu, H.; Kawai, S.; Fujimori, N.; Imai, T.; Yoshino, H.; Doi, A. *Appl. Phys. Lett.* **1986**, *49*, 634. Kitahama, K.; Hirata, K.; Nakamatsu, H.; Kawai, S.; Fujimori, N.; Imai, Y. *Mater. Res. Soc. Symp. Proc.* **1987**, *75*, 309.

(248) Kitahama, K. *Appl. Phys. Lett.* **1988**, *53*, 1812. Kitahama, K.; Hirata, K.; Nakamatsu, H.; Kawai, S.; Fujimori, N.; Imai, T.; Yoshino, H.; Doi, A. *Appl. Phys. Lett.* **1989**, *54*, 968.
(249) Shaapur, F.; Allen, S. D. *J. Appl. Phys.* **1986**, *60*, 470.
(250) Nakamatsu, H.; Hirata, K.; Kawai, S. *Mater. Res. Soc. Symp. Proc.* **1988**, *101*, 397.
(251) (a) Mountziaris, T. J.; Jensen, K. F. *Mater. Res. Soc. Symp. Proc.* **1989**, *131*, 117. (b) Kuech, T. F.; Veuhoff, E.; Kuan, T. S.; Deline, V.; Potemski, R. *J. Cryst. Growth* **1986**, *77*, 257. (c) Lee, P. W.; Omstead, T. R.; McKenna, D. R.; Jensen, K. F. *J. Cryst. Growth* **1988**, *93*, 134; **1987**, *85*, 165. (d) Omstead, T. R.; van Sickle, P. M.; Lee, P. W.; Jensen, K. F. *J. Cryst. Growth* **1988**, *93*, 20. Also see: Lüth, H. *J. Vac. Sci. Technol. A* **1989**, *7*, 696.
(252) Aoyagi, Y.; Masuda, S.; Namba, S.; Doi, A. *Appl. Phys. Lett.* **1985**, *47*, 95.
(253) Bedair, S. M.; Whisnant, J. K.; Karam, N. H.; Tischler, M. A.; Katsuyama, T. *Appl. Phys. Lett.* **1986**, *48*, 174.
(254) Karam, N. H.; El-Masry, N. A.; Bedair, S. M. *Appl. Phys. Lett.* **1986**, *49*, 880.
(255) Bedair, S. M.; Whisnant, J. K.; Karam, N. H.; Griffis, D.; El-Masry, N. A.; Stadelmaier, H. H. *J. Cryst. Growth* **1986**, *77*, 229.
(256) Doi, A.; Aoyagi, Y.; Namba, S. *Appl. Phys. Lett.* **1986**, *49*, 785.
(257) Aoyagi, Y.; Doi, A.; Iwai, S.; Namba, S. *J. Vac. Sci. Technol. B* **1987**, *5*, 1460.
(258) Karam, N. H.; Liu, H.; Yoshida, I.; Bedair, S. M. *Appl. Phys. Lett.* **1988**, *52*, 1144.
(259) Epler, J. E.; Chung, H. F.; Treat, D. W.; Paoli, T. L. *Appl. Phys. Lett.* **1988**, *52*, 1499.
(260) Karam, N. H.; Liu, H.; Yoshida, I.; Bedair, S. M. *Appl. Phys. Lett.* **1988**, *53*, 767.
(261) Solanki, R.; Sudarsan, U.; Johnson, J. C. *Appl. Phys. Lett.* **1988**, *52*, 919. For an extension of this work to GaP homoepitaxy using ArF lasers, see: Sudarsan, U.; Cody, N. W.; Dosluoglu, T.; Solanki, R. *Appl. Phys. Lett.* **1989**, *55*, 738.
(262) Roth, W.; Krautle, H.; Krings, A.; Beneking, H. *Mater. Res. Soc. Symp. Proc.* **1983**, *17*, 193.
(263) Kukimoto, H.; Ban, Y.; Komatsu, H.; Takechi, M.; Ishizaki, M. *J. Cryst. Growth* **1986**, *77*, 223.
(264) Nishizawa, J.; Abe, H.; Kurabayashi, T.; Sakurai, N. *J. Vac. Sci. Technol. A* **1986**, *4*, 706.
(265) Nishizawa, J.; Kurabayashi, T.; Hoshina, J. *J. Electrochem. Soc.* **1987**, *134*, 502.
(266) Nishizawa, J.; Kurabayashi, T.; Abe, H.; Sakurai, N. *J. Vac. Sci. Technol. A* **1987**, *5*, 1572.
(267) Donnelly, V. M.; McCrary, V. R.; Appelbaum, A.; Brasen, D.; Lowe, W. P. *J. Appl. Phys.* **1987**, *61*, 1410.
(268) Balk, P.; Fischer, M.; Grundmann, D.; Lückerath, R.; Lüth, H.; Richter, W. *J. Vac. Sci. Technol. B* **1987**, *5*, 1453.
(269) McCrary, V. R.; Donnelly, V. M.; Brasen, D.; Appelbaum, A.; Farrow, R. C. *Mater. Res. Soc. Symp. Proc.* **1987**, *75*, 223.
(270) Nishizawa, J.; Kurabayashi, T. *Mater. Res. Soc. Symp. Proc.* **1988**, *101*, 275.
(271) Chu, S. S.; Chu, T. L.; Chang, C. L.; Firouzi, H. *Appl. Phys. Lett.* **1988**, *52*, 1243.
(272) Juang, C.; Dubey, S. K.; Wiseman, T. M.; Jones, K. A. *J. Vac. Sci. Technol. A* **1986**, *4*, 728.
(273) Zinck, J. J.; Brewer, P. D.; Jensen, J. E.; Olson, G. L.; Tutt, L. W. *Mater. Res. Soc. Symp. Proc.* **1987**, *75*, 233.
(274) Mitchell, S. A.; Hackett, P. A.; Rayner, D. M.; Humphries, M. R. *J. Chem. Phys.* **1985**, *83*, 5028.
(275) Tu, C. W.; Donnelly, V. M.; Beggy, J. C.; Baiocchi, F. A.; McCrary, V. R.; Harris, T. D.; Lamont, M. G. *Appl. Phys. Lett.* **1988**, *52*, 966. Donnelly, V. M.; Tu, C. W.; Beggy, J. C.; McCrary, V. R.; Lamont, M. G.; Harris, T. D.; Baiocchi, F. A.; Farrow, R. C. *Appl. Phys. Lett.* **1988**, *52*, 1065.
(276) McCaulley, J. A.; McCrary, V. R.; Donnelly, V. M. *J. Phys. Chem.* **1989**, *93*, 1148.
(277) Tokumitsu, E.; Yamada, T.; Konagai, M.; Takahashi, K. *Mater. Res. Soc. Symp. Proc.* **1988**, *101*, 307.
(278) Nishizawa, J.; Kokubun, Y.; Shimawaki, H.; Koike, M. *J. Electrochem. Soc.* **1985**, *132*, 1939.
(279) Donnelly, V. M.; Geva, M.; Long, J.; Karlicek, R. F. *Appl. Phys. Lett.* **1984**, *44*, 951.
(280) Donnelly, V. M.; Brasen, D.; Appelbaum, A.; Geva, M. *J. Appl. Phys.* **1985**, *58*, 2022.
(281) Donnelly, V. M.; Brasen, D.; Appelbaum, A.; Geva, M. *J. Vac. Sci. Technol. A* **1986**, *4*, 716.
(282) Zuhoski, S. P.; Killeen, K. P.; Biefeld, R. M. *Mater. Res. Soc. Symp. Proc.* **1988**, *101*, 313.
(283) (a) Irvine, S. J. C.; Mullin, J. B.; Giess, J.; Gough, J. S.; Royle, A.; Crimes, G. *J. Cryst. Growth* **1988**, *93*, 732. (b) Irvine, S. J. C.; Mullin, J. B. *J. Vac. Sci. Technol. A* **1987**, *5*, 2100. (c) Irvine, S. J. C. *CRC Crit. Rev. Solid State Mater. Sci.* **1987**, *13*, 279. (d) Mullin, J. B. *J. Vac. Sci. Technol. A* **1986**, *4*, 700. (e) Note that in (d), 115 kcal/mol is given as an estimate for the average DMTe bond energy. This estimate is very high; perhaps, this value represents the total bond energy, with 58 kcal/mol being the actual estimated average bond energy.
(284) Morris, B. J. *Appl. Phys. Lett.* **1986**, *48*, 867.
(285) Tutt, L. W., submitted for publication, and personal communication.
(286) Zinck, J. J.; Brewer, P. D.; Jensen, J. E.; Olson, G. L.; Tutt, L. W. *Appl. Phys. Lett.* **1988**, *52*, 1434; *Mater. Res. Soc. Symp. Proc.* **1988**, *101*, 319. Brewer, P. D., personal communication.
(287) Fujii, S.; Fujita, Y.; Iuchi, T. *J. Cryst. Growth* **1988**, *93*, 750.
(288) Brewer, P. D.; Jensen, J. E.; Olson, G. L.; Tutt, L. W.; Zinck, J. J. *Mater. Res. Soc. Symp. Proc.* **1988**, *101*, 327.
(289) Stinespring, C. D.; Freedman, A. *Chem. Phys. Lett.* **1988**, *143*, 584.
(290) Stinespring, C. D.; Freedman, A. *Appl. Phys. Lett.* **1988**, *52*, 1959.
(291) Szikora, S.; Kräuter, W.; Bäuerle, D. *Mater. Lett.* **1984**, 2, 263.
(292) Sugimura, A.; Hanabusa, M. *Jpn. J. Appl. Phys.* **1987**, *26*, L56.
(293) Sugimura, A.; Fukuda, Y.; Hanabusa, M. *J. Appl. Phys.* **1987**, *62*, 3222.
(294) Boyer, P. K.; Roche, G. A.; Ritchie, W. H.; Collins, G. J. *Appl. Phys. Lett.* **1982**, *40*, 716.
(295) Boyer, P. K.; Emery, K. A.; Zarnani, H.; Collins, G. J. *Appl. Phys. Lett.* **1984**, *45*, 979.
(296) Tate, A.; Jinguji, K.; Yamada, T.; Takato, N. *Appl. Phys. A* **1985**, *38*, 221.
(297) Nishino, S.; Honda, H.; Matsunami, H. *Jpn. J. Appl. Phys.* **1986**, *25*, L87.
(298) Shirafuji, J.; Miyoshi, S.; Aoki, H. *Thin Solid Films* **1988**, *157*, 105.
(299) Hudson, R. D. *Can. J. Chem.* **1974**, *52*, 1465.
(300) Tate, A.; Jinguji, K.; Yamada, T.; Takato, N. *J. Appl. Phys.* **1986**, *59*, 932.
(301) Pan, E. T.-S.; Flint, J. H.; Adler, D.; Haggerty, J. S. *J. Appl. Phys.* **1987**, *61*, 4535.
(302) Deutsch, T. F.; Silversmith, D. J.; Mountain, R. W. *Mater. Res. Soc. Symp. Proc.* **1983**, *17*, 129.
(303) Boyer, P. K.; Moore, C. A.; Solanki, R.; Ritchie, W. K.; Roche, G. A.; Collins, G. J. *Mater. Res. Soc. Symp. Proc.* **1983**, *17*, 119.
(304) (a) Jasinksi, J. M.; Meyerson, B. S.; Nguyen, T. N. *J. Appl. Phys.* **1987**, *61*, 431. (b) Jasinski, J. M.; Beach, D. B.; Estes, R. D. *Mater. Res. Soc. Symp. Proc.* **1989**, *131*, 501.
(305) West, G. A.; Gupta, A. *Mater. Res. Soc. Symp. Proc.* **1984**, *29*, 61.
(306) Sugii, T.; Ito, T.; Ishikawa, H. *Appl. Phys. A* **1988**, *46*, 249.
(307) Donnelly, V. M.; Baronauski, A. P.; McDonald, J. R. *Chem. Phys.* **1979**, *43*, 271.
(308) Deutsch, T. F.; Silversmith, D. J.; Mountain, R. W. *Mater. Res. Soc. Symp. Proc.* **1984**, *29*, 67.
(309) Minakata, M.; Furukawa, Y. *J. Electron. Mater.* **1986**, *15*, 159.
(310) Sawada, K.; Ishida, M.; Nakamura, T.; Suzaki, T. *J. Cryst. Growth* **1989**, *95*, 494.
(311) Demiryont, H.; Thompson, L. R.; Collins, G. J. *J. Appl. Phys.* **1986**, *59*, 3235; *Appl. Opt.* **1986**, *25*, 1311.
(312) Solanki, R.; Collins, G. J. *Appl. Phys. Lett.* **1983**, *42*, 662. Shimizu, M.; Monma, A.; Shiosaki, T.; Kawabata, A.; Yamamoto, Y. *J. Cryst. Growth* **1989**, *94*, 895.
(313) Tokuda, J.; Takai, M.; Gamo, K.; Namba, S. *Mater. Res. Soc. Symp. Proc.* **1988**, *101*, 261.
(314) (a) Kunz, R. R.; Rothschild, M.; Ehrlich, D. J. *Appl. Phys. Lett.* **1989**, *54*, 1631. (b) Arnone, C.; Rothschild, M.; Black, J. G.; Ehrlich, D. J. *Appl. Phys. Lett.* **1986**, *48*, 1018.
(315) Hirota, Y.; Mikami, O. *Electron. Lett.* **1985**, *21*, 77.
(316) Alexandrescu, R.; Morjan, J.; Grigoriu, C.; Mihailescu, I. N.; Bastl, Z.; Tlaskal, J.; Mayer, R.; Pola, J. *Appl. Phys. A* **1988**, *46*, 275.
(317) Pola, J.; Chvalovsky, V.; Volnina, E. A.; Guselnikov, L. E. *J. Organomet. Chem.* **1988**, *341*, C13.
(318) Moody, J. E.; Hendel, R. H. *J. Appl. Phys.* **1982**, *53*, 4364.
(319) Allen, S. D.; Goldstone, J. A.; Stone, J. P.; Jan, R. Y. *J. Appl. Phys.* **1986**, *59*, 1653.
(320) Ehrlich, D. J.; Tsao, J. Y. *Mater. Res. Soc. Symp. Proc.* **1983**, *17*, 3.
(321) Lax, M. *J. Appl. Phys.* **1977**, *48*, 3919.
(322) Lax, M. *Appl. Phys. Lett.* **1978**, *33*, 786.
(323) Piglmayer, K.; Doppelbauer, J.; Bäuerle, D. *Mater. Res. Soc. Symp. Proc.* **1984**, *29*, 47.
(324) (a) Bäuerle, D. In *Laser Processing and Diagnostics, Chemical Physics Vol. 39*; Bäuerle, D., Ed.; Springer: Berlin, 1984; p 166. (b) Piglmayer, K.; Bäuerle, D. *Appl. Phys. B* **1989**, *48*, 453.
(325) Copley, S. M. *J. Appl. Phys.* **1988**, *64*, 2064.
(326) Skouby, D. C.; Jensen, K. F. *J. Appl. Phys.* **1988**, *63*, 198.
(327) Zieger, H. J.; Ehrlich, D. J. *J. Vac. Sci. Technol. B* **1989**, *7*, 466.

(328) Pan, E. T.-S.; Flint, J. H.; Liang, J. M.; Adler, D.; Haggerty, J. S. *Appl. Opt.* **1987**, *26*, 70.
(329) Patnaik, S.; Brown, R. A. *J. Electrochem. Soc.* **1988**, *135*, 697.
(330) Chen, C. J. *J. Vac. Sci. Technol. A* **1987**, *5*, 3386.
(331) Tsao, J. Y.; Zeiger, H. J.; Ehrlich, D. J. *Surf. Sci.* **1985**, *160*, 419.
(332) Venables, J. A.; Spiller, G. D. T.; Hanbucken, M. *Rep. Prog. Phys.* **1984**, *47*, 399.
(333) Ehrlich, D. J.; Osgood, R. M., Jr.; Deutsch, T. F. *Appl. Phys. Lett.* **1981**, *38*, 946.
(334) Ehrlich, D. J.; Osgood, R. M., Jr. *Thin Solid Films* **1982**, *90*, 287.
(335) Tsao, J. Y.; Ehrlich, D. J. *J. Cryst. Growth* **1984**, *68*, 176.
(336) Higashi, G. S.; Blonder, G. E.; Fleming, C. G.; McCrary, V. R.; Donnelly, V. M. *J. Vac. Sci. Technol. B* **1987**, *5*, 1441.
(337) Herman, I. P.; Magnotta, F.; Kotecki, D. E. *J. Vac. Sci. Technol. A* **1986**, *4*, 659.
(338) Brueck, S. R. J.; Ehrlich, D. J. *Phys. Rev. Lett.* **1982**, *48*, 1678.
(339) Ehrlich, D. J.; Brueck, S. R. J. *Appl. Phys. Lett.* **1985**, *47*, 216.
(340) Du, Y. C.; Kempfer, U.; Piglmayer, K.; Bäuerle, D.; Titulaer, U. M. *Appl. Phys. A* **1986**, *39*, 167.
(341) Jelski, D. A.; George, T. F. *J. Appl. Phys.* **1987**, *61*, 2353.
(342) Chen, C. J.; Gilgen, H. H.; Osgood, R. M. *Opt. Lett.* **1985**, *10*, 173.
(343) Thompson, H. W.; Linnett, J. W. *Proc. R. Soc. London* **1936**, *A156*, 108.
(344) Lundquist, R. T.; Cais, M. *J. Org. Chem.* **1962**, *27*, 1167.
(345) (a) Gilgen, H. H.; Chen, C. J.; Krchnavek, R.; Osgood, R. M., Jr. In *Laser Processing and Diagnostics, Chemical Physics Vol. 39*; Bäuerle, D., Ed.; Springer: Berlin, 1984; p 225. (b) Itoh, H.; Watanabe, M; Mukai, S.; Yajima, H. *J. Cryst. Growth* **1988**, *93*, 165.
(346) (a) Irvine, S. J. C.; Mullin, J. B.; Robbins, D. J.; Glasper, J. L. *J. Electrochem. Soc.* **1985**, *132*, 968. (b) Hails, J. E.; Irvine, S. J. C.; Mullin, J. B.; Shenai-Khatkhate, D. V.; Cole-Hamilton, D. *Mater. Res. Soc. Symp. Proc.* **1989**, *131*, 75.
(347) Fujita, Y.; Fujii, S.; Iuchi, T. *J. Vac. Sci. Technol. A* **1989**, *7*, 276.
(348) Sanchez, E.; Shaw, P. S.; O'Neill, J. A.; Osgood, R. M., Jr. *J. Vac. Sci. Technol. A* **1988**, *6*, 765; *Chem. Phys. Lett.* **1988**, *147*, 153.
(349) O'Neill, J. A.; Sanchez, E.; Osgood, R. M., Jr. *J. Vac. Sci. Technol. A* **1989**, *7*, 2110.
(350) Shaw, P. S.; Sanchez, E.; Wu, Z.; Osgood, R. M., Jr. *Chem. Phys. Lett.* **1988**, *151*, 449.
(351) Rothberg, L. *J. Phys. Chem.* **1987**, *91*, 3467.
(352) Pazionis, G. D.; Tang, H.; Ge, L.; Herman, I. P. *Mater. Res. Soc. Symp. Proc.* **1988**, *101*, 113.
(353) Takai, M.; Nakai, H.; Tsuchimoto, J.; Gamo, K.; Namba, S. *Jpn. J. Appl. Phys.* **1985**, *24*, L705. Also see: Kirillov, D.; Merz, J. L. *J. Appl. Phys.* **1983**, *54*, 4104.
(354) Kodas, T. T.; Baum, T. H.; Comita, P. B. *J. Appl. Phys.* **1987**, *61*, 2749.
(355) Shaapur, F.; Allen, S. D. *Appl. Phys. Lett.* **1987**, *50*, 723.
(356) Comita, P. B.; Kodas, T. T. *J. Appl. Phys.* **1987**, *62*, 2280.
(357) Brewer, P. D. *Chem. Phys. Lett.* **1987**, *141*, 301.
(358) Suzuki, H.; Mori, K.; Kawasaki, M.; Sato, H. *J. Appl. Phys.* **1988**, *64*, 371; *Mater. Res. Soc. Symp. Proc.* **1988**, *101*, 217.
(359) Karny, Z.; Naaman, R.; Zare, R. N. *Chem. Phys. Lett.* **1978**, *59*, 33.
(360) Hackett, P. A.; John, P. *J. Chem. Phys.* **1983**, *79*, 3593.
(361) Mitchell, S. A.; Hackett, P. A. *J. Chem. Phys.* **1983**, *79*, 4815.
(362) Chu, J. O.; Flynn, G. W.; Chen, C. J.; Osgood, R. M., Jr. *Chem. Phys. Lett.* **1985**, *119*, 206.
(363) Larciprete, R.; Stuke, M. *J. Cryst. Growth* **1986**, *77*, 235.
(364) Ibbs, K. G.; Osgood, R. M. In *Laser Chemical Processing for Microelectronics*; Ibbs, K. G., Osgood, R. M., Eds.; Cambridge University Press: Cambridge, 1989; p 1.
(365) Ehrlich, D. J.; Osgood, R. M., Jr.; Silversmith, D. J.; Deutsch, T. F. *IEEE Electron. Dev. Lett.* **1980**, *EDL-1*, 101.
(366) Randall, J. N.; Ehrlich, D. J.; Tsao, J. Y. *J. Vac. Sci. Technol. B* **1985**, *3*, 262.
(367) Oprysko, M. M.; Beranek, M. W.; Young, P. L. *IEEE Electron Dev. Lett.* **1985**, *EDL-6*, 344.
(368) Tsao, J. Y.; Ehrlich, D. J.; Silversmith, D. J.; Mountain, R. W. *IEEE Electron Dev. Lett.* **1982**, *EDL-3*, 164.
(369) Ehrlich, D. J.; Tsao, J. Y.; Silversmith, D. J.; Sedlacek, J. H. C.; Mountain, R. W.; Graber, W. S. *IEEE Electron Dev. Lett.* **1984**, *EDL-5*, 32.
(370) Whitehead, J. C.; Mitlitsky, F.; Ashkenas, D. J.; Bernhardt, A. F.; Farmwald, S. E.; Kaschmitter, J. L.; McWilliams, B. M. *SPIE* **1986**, *621*, 62.
(371) Black, J. G.; Ehrlich, D. J.; Rothschild, M.; Doran, S. P.; Sedlacek, J. H. C. *J. Vac. Sci. Technol. B* **1987**, *5*, 419.
(372) Black, J. G.; Scott, P. D.; Rothschild, M.; Ehrlich, D. J. *Appl. Phys. Lett.* **1987**, *50*, 1016.
(373) Liu, Y. S., presented at the National Meeting of the American Vacuum Society, October 1988, Atlanta, GA.
(374) Tuchman, J. A.; Welsh, L. P.; Herman, I. P. *Mater. Res. Soc. Symp. Proc.* **1989**, *130*, 333.
(375) For example, see: *Mater. Res. Soc. Symp. Proc.* **1989**, *131*.
(376) For example, see: *Mater. Res. Soc. Symp. Proc.* **1989**, 129.